COMPARISON OF EXPERIMENTAL STUDY AND FINITE ELEMENT ANALYSIS OF BOLTED FLANGE CONNECTIONS

A THESIS SUBMITTED TO
THE GRADUATE SCHOOL OF NATURAL AND APPLIED SCIENCES
OF
MIDDLE EAST TECHNICAL UNIVERSITY

BY

SAMET EMRE YILMAZ

IN PARTIAL FULFILLMENT OF THE REQUIREMENTS
FOR
THE DEGREE OF MASTER OF SCIENCE
IN
AEROSPACE ENGINEERING

SEPTEMBER 2015

Approval of the thesis:

COMPARISON OF EXPERIMENTAL STUDY AND FINITE ELEMENT ANALYSIS OF BOLTED FLANGE CONNECTIONS

submitted by **SAMET EMRE YILMAZ** in partial fulfillment of the requirements for the degree of **Master of Science in Aerospace Engineering, Middle East Technical University** by,

Prof. Dr. Gülbin Dural Ünver _____
Dean, Graduate School of **Natural and Applied Sciences**

Prof. Dr. Ozan Tekinalp _____
Head of Department, **Aerospace Engineering**

Prof. Dr. Altan Kayran _____
Supervisor, **Aerospace Engineering Dept., METU**

Examining Committee Members

Asst. Prof. Dr. Ercan Gürses _____
Aerospace Engineering Dept., METU

Prof. Dr. Altan Kayran _____
Aerospace Engineering Dept., METU

Assoc. Prof. Dr. Demirkan Çöker _____
Aerospace Engineering Dept., METU

Asst. Prof. Dr. Tuncay Yalçınkaya _____
Aerospace Engineering Dept., METU

Asst. Prof. Dr. Cihan Tekoğlu _____
Mechanical Engineering Dept., TOBB ETÜ

Date: 03.09.2015

I hereby declare that all information in this document has been obtained and presented in accordance with academic rules and ethical conduct. I also declare that, as required by these rules and conduct, I have fully cited and referenced all material and results that are not original to this work.

Name, Last name :Samet Emre YILMAZ

Signature :

ABSTRACT

COMPARISON OF EXPERIMENTAL STUDY AND FINITE ELEMENT ANALYSIS OF BOLTED FLANGE CONNECTIONS

Yılmaz, Samet Emre

M.S., Department of Aerospace Engineering

Supervisor: Prof. Dr. Altan Kayran

September 2015, 132 Pages

Design and analysis of bolted flange connections is challenging because of the nonlinear nature of contact mechanics involved in the analysis of bolted flange connections. Aerospace industry requires faster design with least number of tests because testing is costly and time consuming. Bolted flange connections are subject to variety of load cases that includes thermal, centrifugal and contact loads and it is not practical to consider all of the load cases during tests. As a result, finite element method is considered to be the fastest and most reliable tool during the design and the analysis phases of the bolted flange connections. Finite element method takes contact and material nonlinearities into account and simulates the problems more realistically. However, high level of expertise is required during the analysis, because there are many contact parameters that should be chosen by the user and accuracy and convergence of the bolted flange connection solution are affected by these parameters. There are also linear tools to determine structural

integrity of the bolted joints but these tools result in either conservative or non-conservative solutions. In the thesis, the effect of main contact parameters on the accuracy and solution time of the finite element analysis of the bolted flange connection is investigated. Main contact parameters that are considered are the contact stiffness factor, penetration tolerance factor the contact algorithm. Both elastic and plastic analyses are performed for a bolted flange connection for which experimental data is available in the literature. The results of finite element analysis for varying main contact parameters are compared with the experimental data of the bolted flange connection, and conclusions are inferred with regard to the effect of main contact parameters on the accuracy and computational time of the finite element analysis. Experiments are also performed for tensile loading of a bolted L-bracket, and strain gage and digital image correlation results are compared with the finite element analysis results of the bolted L-bracket. Results show that with the proper choice of the contact parameters, close agreement can be obtained between the experimental results and finite element analysis results of the bolted L-bracket.

Keywords: Contact Stiffness, Penetration Tolerance, Finite Element Method

ÖZ

CIVATALI FLANŞ BAĞLANTILARININ DENEYSEL ÇALIŞMALAR VE SONLU ELEMANLAR ANALİZLERİ İLE KIYASLANMASI

Yılmaz, Samet Emre

Yüksek Lisans, Havacılık ve Uzay Mühendisliği Bölümü

Tez Töneticisi: Prof. Dr. Altan Kayran

Eylül 2015, 132 Sayfa

Cıvatalı flanş bağlantılarının tasarım ve analizi kontak mekaniğinin sahip olduğu doğrusal olmayan yapıdan dolayı zorlu bir süreçtir. Havacılık endüstrisinde testlerin pahalı olması ve uzun zaman alması sebebiyle, testlerin dahil edilmediği daha hızlı bir tasarım süreci gerekliliği vardır. Cıvatalı flanş bağlantıları termal, merkezkaç ve kontak yükleri gibi çok çeşitli yüklere mağruz kalmaktadır ve bu yüklerin tamamının test sürecine dahil edilmesi uygulanabilir değildir. Sonuç olarak, sonlu elemanlar metodu cıvatalı flanş bağlantılarının tasarım ve analiz safhalarındaki en hızlı ve güvenilir araç olarak öne çıkmaktadır. Sonlu elemanlar metodu kontak ve malzemeden kaynaklanan doğrusal olmayan özellikleri de hesaba katarak problemleri daha gerçekçi bir şekilde simüle etmektedir. Ancak kontak analizleri sırasında kullanıcın uzmanlık derecesi oldukça önemlidir, çünkü analizlerde kullanıcı tarafından seçilmesi gereken bir çok kontak parametresi vardır ve bu parametrelerin çözümün doğruluğunda ve yakınsamasında büyük bir

etkisi vardır. Cıvatalı flanş bağlantılarının yapısal bütünlüğünü sağlayabilmek adına oluşturulmuş doğrusal bir takım araçlar da bulunmaktadır fakat bu araçlar yapının gerilme değerlerini daha yüksek ya da daha düşük tahmin etmektedirler. Bu tezde, başlıca kontak parametrelerinin teorik altyapısı ve uygulanışı sonuçların doğruluğu ve çözüm süresi açısından incelenmektedir. Çalışma kapsamında değerlendirilen ana parametreler, kontak katılık faktörü, penetrasyon faktörü ve algoritmadır.

Liteartürde deney verileri bulunan bir cıvatalı flanş bağlantısı için elastik ve plastik analizler gerçekleştirilmiştir. Değişken kontak parametreleriyle çözümü sağlanan sonlu elemanlar analizlerinin sonuçları kontak parametrelerinin etkileri dikkate alınarak doğruluk ve çözüm süresi açısından değerlendirilmiştir. Buna ek olarak, cıvatalı L-braket yapılarının çekme testleri gerçekleştirilmiştir ve elde edilen gerinim ölçer ve sayısal imge korelasyon verileri sonlu elemanlar analiz sonuçlarıyla kıyaslanmıştır. Sonuç olarak, uygun kontak parametreleri seçildiğinde, sonlu elemanlar ve deney verilerinin uyuştuğu görülmüştür.

Anahtar Kelimeler: Kontak Katılığı, Penetrasyon Toleransı, Sonlu Elemanlar Yöntemi

To Loved Ones…

Mom, Dad and Sister

ACKNOWLEDGMENTS

First of all, I would like to give my deepest gratitude to my family, especially to my mother who has always been there for me.

I would like thank to Prof. Dr. Altan Kayran for his guidance and his affords throughout the study. It was a pleasure and honor to work with him.

I would also like to Asst. Prof. Dr. Ercan Gürses and Assoc. Prof. Dr. Demirkan Çöker for their guidance and suggestions.

Support of the Scientific and Technological Research Council of Turkey (TUBİTAK) should be acknowledged for funding me with National Scholarship Programme for MSc Students.

Support of TUSAŞ Engine Industries Inc. (TEI) is also acknowledged.

TABLE OF CONTENTS

APPENDICES

LIST OF TABLES

TABLES

LIST OF FIGURES

FIGURES

CHAPTER 1

INTRODUCTION

1.1 Objective of the Thesis

Finite element method is an essential tool that is used for almost every part of gas turbine engines. Over the past decades, there are enhancements on the finite element method but studies show that finite element method can lead to incorrect solutions when used by an inexperienced analyzer. Bolted joint analysis with nonlinear contact mechanics is an advanced topic of finite element method and the level of expertise is crucial in order to acquire accurate solutions. It is not possible to perform tests at each design point of bolted joints considering financial and time issues and finite element method is implemented. Finite element analyses are supposed to give closest results to reality but to achieve that contact parameters of finite element method should be chosen carefully during each finite element run. Main contact parameters that are considered during the analyses are the contact stiffness factor, the penetration tolerance factor and the contact algorithm. Considering all the geometrical and loading variations that a bolted flange connection has, it is known that some of these parameters may have an influence on the accuracy and run time of the analyses.

Main purpose of the thesis is to determine the contact parameters that are most suitable for bolted flange connections. In order to validate the results of finite element method experimental data of a bolted flange connection which is available in the literature is used. In addition, tests are performed for two L-

bracket geometries and results are compared with finite element analyses with varying contact parameters.

1.2 Literature Review

Solution of nonlinear contact problems is still a difficult issue when finite element method is used considering both mathematical and engineering aspects [1]. Practical and theoretical aspects of this topic have been researched for past decades but there is not a single method that can be used for every engineering problem. There are some commercially available standards and some commercially unavailable tools for the design of bolted flanges. Bolted joint connections are of great concern for civil engineering application and most of the research is done on civil engineering applications. However, importance of bolted joint connections cannot be omitted for aerospace engineering applications. Especially for gas turbine engines, bolted joint connections are used at the critical parts that are exposed to variety of load cases such as centrifugal and thermal loads.

There are some studies that compare ASME codes with finite element solution in terms of tangential, axial and radial stress results. Abid and Nash performed a parametric study for variable geometrical specifications of metal to metal bolted flanges for stress safe designs [2]. They used both finite element method and ASME codes to determine the flange stress and made a comparison. Vishwanath et al. also investigated some geometrical parameters like flange thickness, bolt number and bolt preload and compared ASME codes with finite element results [3]. In both of the studies, for some cases finite element method is more conservative when compared to the ASME standards and vice versa. Baker, on the other hand, investigated the plastic behavior of bolts using the ASME codes and the finite element method [4]. Finally, it is stated that finite element method can be inadequate for accuracy for such a detailed study as it is not possible to model every detail with finite elements.

Leakage is another design requirement that the bolted flanges should satisfy especially when they are used for connecting piping systems and there are some studies that investigate the leakage rates of bolted flange connections with gasket. Guizzo, for example, investigated the leakage rate of bolted flange connections using the gasket constants theory developed by Pressure Vessels Research Committee (PVRC) and compared the results with the experimental data [5]. It is concluded that PVRC method is not applicable for the calculation of leak rate and a new methodology is required.

Finite element method is a fast and a reliable tool in most of the cases. However, there are certain numbers of input parameters that are used in the nonlinear contact analysis using the finite element method. There are numerous studies that use finite element method for the numerical simulation and the importance of these input parameters are acknowledged in almost every study. In these studies, the investigation of the effect of the contact parameters on the results take a minor part and it should be stated that these parameters is mostly problem dependent and affect both accuracy and solution time of the analysis.

Mathematical background of the contact algorithms, which are chosen by the user during the analysis, is also concerned in some studies. There are studies that propose new methods for the solution of contact problems and there are also some studies that investigate the advantages and disadvantages of popular contact algorithms that are used in most of the commercially available finite element software. For example, Auricchio and Sacco propose a new methodology for the solution of plates that does not take frictional effects into account while focusing on two Augmented Lagrange methods available in literature [6] and claim that new methodology is more accurate when compared to the classical methods. Stefancu et al. investigated the Penalty and the Augmented Lagrange methods with a numerical application [7]. It is shown that Penalty method is less sensitive to contact parameters and Augmented Lagrange method can lead to inaccurate

results. Each study has different outcomes and the researchers cannot agree on a specific algorithm.

Abilio and his colleagues conducted a numerical study that investigates the fatigue behavior of a riveted and a bolted joint made of puddle iron [8]. Instead of using the global S-N curve application, the calculations are performed by adaptation of a unique S-N curve. During the calculations, they have performed nonlinear contact analysis in order to determine the stress intensity factor of the structures. Stress intensity factor values are required as input to the adapted S-N curve calculations. In finite element model of bolted flanges, the clamping stresses are included and thermal loading (decreasing the temperature) was applied in order to simulate the clamping stresses. Models were created using 20 node SOLID95 elements of ANSYS. In order to decide the contact stiffness and penetration tolerance factors a sensitivity study is performed. It is seen that variation of penetration tolerance factor when contact stiffness factor is within the range of 0.1 to 1 made no difference on the results. However, when contact stiffness factor is decreased to 0.01, which is not an acceptable value, the change in the penetration tolerance factor is found to have a little effect on the local stress values. It is rather more appropriate to choose a contact stiffness factor value that is higher than the ANSYS default 1 but Abilio and his colleagues made a sensitivity study for lower contact stiffness values and the results are not adequate and satisfactory. Moreover, the contact algorithm Abilio et al. used is the Augmented Lagrange algorithm. Choosing a different contact algorithm in the analysis may lead to a completely different result.

Xiaoyun et al. performed finite element analysis for sheet metal assemblies [9]. Starting with a small contact stiffness factor value and checking the penetration of the system along with number of cumulative iterations, the final values of contact stiffness factor and penetration tolerance factor values are decided. However, the range of the contact stiffness factor is once again chosen between 0.1 and 1, which does not simulate the reality for almost all of the nonlinear contact problems.

Three dimensional finite element analysis of interference fit assembly which is subjected to bending is investigated by Lanoue et al [10]. Solution convergence and contact parameters are changed during the analysis and a sensitivity study is done in order observe the effects of contact parameters on the accuracy and the solution time of the analysis. Penalty, Augmented Lagrange and Pure Lagrange algorithms are used during the study. ANSYS Workbench 11.0 is used during the analyses. Meshing was done with new generation 20 node SOLID186 elements of ANSYS. Four global and five sub-models that take advantage of the symmetry are created in order to investigate the effect of the mesh size on the results. Details about the finite element models and contact settings are given in detail in the paper [10]. Considering the displacement, it is observed that improvement of the mesh does not affect the results and using too fine mesh structures are not required in order to get accurate results. Lanoue et al. made the comparison of contact algorithms for their converged settings but the contact stiffness factor, penetration tolerance factor are different when the comparison of the algorithms is made. It is stated that the results are similar for the converged set of contact settings except the Pure Lagrange algorithm. They used contact stiffness factor values up to 1000, which is extremely high, and for such high contact stiffness factor values convergence is not achieved. Pure Lagrange method is suggested as it does not require supplementary parameters but it is also noted that the solution cost can be high. Augmented Lagrange method is stated to be the best method if the penetration tolerance value is known as the solution time is relatively lower. All the models can be considered as small models, i.e. the biggest model has 22462 elements with 91605 nodes. Even with such small models, convergence is not achieved in some cases and the elapsed time is more than 24 hours. Considering the very large finite element models that are created to simulate the gas turbine engines with lots of contact regions (in this case there is only one contact region), this study does not lead to a real engineering application.

Del Coz Diaz et al. investigated the buckling behavior of unbolted base plates using finite element method and compared the results with the experimental data [11]. Emphasizing the importance of contact parameters, it is claimed that contact stiffness factor value is supposed to be between 0.1 to 1. For the penetration tolerance factor, the default value of ANSYS, 0.1 is chosen for the analysis. Bolts are not modeled as solid but as beams which is available in the ANSYS element database. When the results of numerical and experimental data are compared, it is clear that numerical model gives unsatisfactory results for higher load cases. This might be due to the low contact stiffness factor values used throughout the analyses.

Santos et al. carried out a test campaign of a double-shear single dowel wood connection under quasi-static loading [12]. Experimental stiffness values of the dowel is compared with the finite element results and it is concluded that use of default ANSYS settings for the numerical simulations resulted in better agreement with the experimental data. It should be noted that for the sensitivity analysis, the range for the contact stiffness factor is once again 0.1 to 1. On the other hand, it is said that penetration tolerance factor affects the result only when it is too small. Use of very small penetration tolerance factor results in high number of iterations. There is no comparison of the contact algorithms and the Augmented Lagrange algorithm is used for all of the analyses. As there is only one contact region and the range that is used for contact stiffness factor and penetration tolerance factor values is not reasonable, the application of the outcome of this study to most of the engineering problems is questionable.

Design and analysis of bolted flange connections is a popular topic, because there are lots of unknowns and difficulties from both design and analysis point of view. There are some basic methods for mathematical modeling of contact problems and there are also studies to improve the models as the traditional algorithms are found to have some drawbacks. Design phase is mostly based on standards, however the reliability of these standards are uncertain when compared to the

finite element analysis. In the literature, there is no consensus on the use of the standards of the finite element method. It is noted that Finite element method is also not reliable, because the input parameters relevant for contact have significant effects on the accuracy of the analysis.

1.3 Background

1.3.1 Introduction to Contact Mechanics

Contact mechanics is applied to almost every engineering problem and can be simply defined as the study of the deformation of solids that touch each other at one or more points. No one could ever walk or a car could move if there were no frictional contact [13]. For this reason, contact mechanics has a very long history beginning in ancient Egypt to today's high technology computational methods. In the past, contact problems were modeled with simpler approaches because analytical tools, which can simulate real world problems, were not present. Linear elastic tools can be used to formulate contact problems; however, because of the possible unknown contact areas, all contact problem applications are nonlinear and special solution algorithms are required. Nonlinear continuum mechanics is now used to simulate real world contact problems and it is also possible to analyze the contact problems with finite element method. Contact mechanics is important in the field of mechanical engineering and simulation of mechanical systems without testing is critical both financially and in terms of time consideration.

1.3.2 Mathematical Modeling

Firstly, mathematical modeling of contact mechanics beginning from the basic methodology and difficulties related to contact mechanics are explained with simple contact problems [13].

General formulation of contact without friction

It is possible to define a contact problem by a simple point mass and spring system. In Figure 1.1 point mass m subject to gravitational load and the spring with stiffness k is illustrated [13]. As it is seen in Figure 1.1, maximum deflection of the mass is restricted by the rigid plane [13]

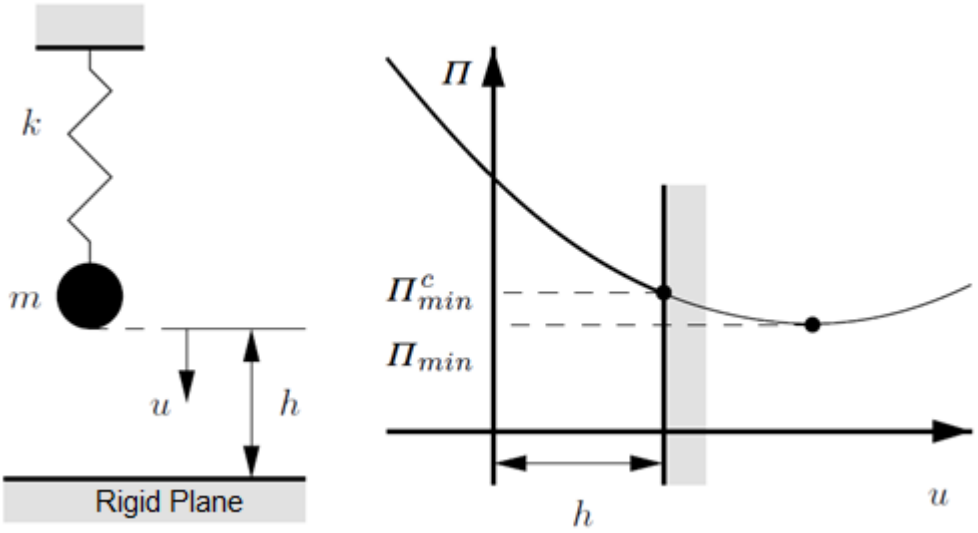

Figure 1.1–Point mass spring system and energy of the system. [13]

The potential energy of the system can be written as:

$$\Pi(u) = \frac{1}{2}ku^2 - mgu \qquad 1.1$$

Assuming there is no restriction on the displacement u, the minimum value of the equation 1.1 can be calculated by taking its variation yielding.

$$\delta\Pi(u) = ku\delta u - mg\delta u = 0 \qquad 1.2$$

The extremum of the equation 1.1 is minimum at $u = \frac{mg}{k}$. The minimum value of the energy of the system is shown in Figure 1.1 assuming there is no restriction to the motion of the mass.

The restriction of the motion of the mass can be described by the following formulation for proper contact definition:

$$c(u) = h - u \geq 0 \tag{1.3}$$

This inequality expression is used to exclude penetration during contact. It should be noted that there is gap the between the point mass and the rigid plane when $c(u) > 0$, and the gap is closed when $c(u) = 0$.

Noting that the term δu is restricted at the surface of contact; from equation 1.3 one can see that $\delta u \leq 0$, which means that the displacement of the mass should meet the restriction condition and the motion can only occur in the upward direction. The inequality of equation 1.2 becomes:

$$ku\delta u - mg\delta u \geq 0 \tag{1.4}$$

Equation 1.4 is called variational inequality [13] and the greater sign in the formulation is due the fact that mg force is greater than the spring force kh when the contact is present, and at the rigid support $\delta u \leq 0$. Due the nature of the problem the solution of equation 1.1 is not minimum at the point which is defined as Π_{min}, but minimum at point Π^{c}_{min}.

In general, the difference between a test function v and the solution u is used instead of the term δu: $\delta u = v - u$. The condition $v - h \leq 0$ should be satisfied by the test function and the solution $u$at the point of contact. The test function can be included in 1.2 as:

$$ku(v - u) - mg(v - u) = 0 \tag{1.5}$$

As $mg > ku$ at the point of contact, including the expression $v - h \leq 0$:

$$ku(v - h) \geq mg(v - h) \tag{1.6}$$

In both of the expression, the inequality 1.3 that constrains the displacement u of the point mass results in variational inequalities to characterize the solution of u. It is not possible to apply these variational inequalities to solve a contact problem and some special methods should be constructed.

When the point mass comes into contact with rigid surface, a reaction force f_R is present. The reaction force between rigid surface and the point mass is taken to be negative in classical contact mechanics [13], and as a conclusion the contact pressure can only be compression. This assumption does not include adhesion forces in the contact leading to restriction:

$$R_N \leq 0 \tag{1.7}$$

This means there is a compression state ($R_N < 0$) or no reaction force ($R_N = 0$) present.

To sum up, two cases of the contact problem should be distinguished considering that the motion is constrained by the equation 1.3.

1. The stiffness of the spring is large enough so that the point mass does not touch the rigid surface and in this case:

$$c(u) > 0 \text{ and } R_N = 0 \tag{1.8}$$

2. The system properties allows point mass to come into contact with rigid surface and the conditions are:

$$c(u) = 0 \text{ and } R_N < 0 \tag{1.9}$$

Two cases can be combined as follows:

$$c(u) \geq 0, R_N \leq 0 \text{ and } R_N c(u) = 0 \tag{1.10}$$

Expressions in equation 1.10 are known as HERTZ-SINORINI-MOREAU conditions in contact mechanics. In optimization theory, these conditions coincide with KUHN-TUCKER complementary conditions [13]. KUHN-TUCKER conditions are first order necessary conditions for a solution in nonlinear problems to be optimal provided that some regularity conditions are satisfied.

Above results can be demonstrated by the reaction force versus the gap plot as shown in Figure 1.2.

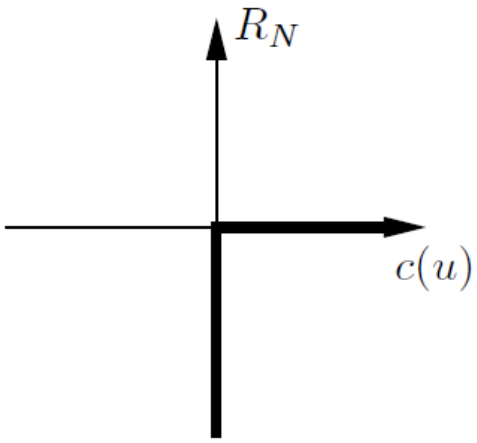

Figure 1.2 – Reaction force versus gap [13]

Load displacement curve has a corner and cannot be differentiated using standard differentiation procedure and contact problems can be solved by applying non-standard mathematical methods for non-smooth curves.

General formulation of contact with friction

Figure 1.1 shows the same system with frictional behavior included. Assuming the mass is in touch with the rigid plane $R_N < 0$ condition holds. It should be noted that in this case, an additional force parallel to the plane is applied to the system as shown in Figure 1.3.

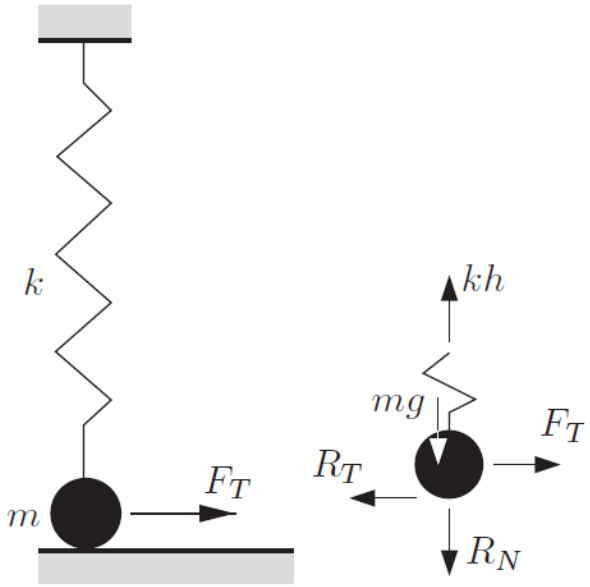

Figure 1.3 – Point mass and spring system including the tangential load [13]

The equations of equilibrium in vertical and tangential directions using the free body diagram given in Figure 1.3 are:

$$R_N + mg - kh = 0 \tag{1.11}$$

$$R_T - F_T = 0 \tag{1.12}$$

A constitutive equation is used to describe the physical process of the friction. Coulomb's law is the widely used model in engineering [13]. Using this constitutive equation, the difference between stick and sliding can be identified. Here, stick means that there is no relative tangential movement when the point mass and the rigid surface are in contact. When sliding occurs, there is a relative displacement u_T between the mass and the rigid surface. With these assumptions, following equations can be written to define the frictional behavior of the system.

1. Following inequality which involves the vertical and tangential reaction forces can be written using Coulomb's law:

$$f(R_N, R_T) = |R_T| + \mu R_N \leq 0 \tag{1.13}$$

Here, μ is the coefficient of friction and absolute value of the tangential reaction force is used because the tangential force F_T can be both positive or negative. Sticking and slip conditions are now be identified using the inequality given in equation 1.13.

2. Sticking is present when:

$$|R_T| < -\mu R_N \tag{1.14}$$

Note that there is no relative tangential motion between the point mass and the rigid support, i.e. $u_T = 0$. In this case, it is possible to determine the tangential reaction force R_T using equation 1.12.

3. Slip is present when:

$$|R_T| = -\mu R_N \tag{1.15}$$

Now, there is relative tangential motion between the point mass and the rigid plane, i.e. $u_T \neq 0$ and R_T can be directly calculated using the above equation. Note that, in this case, the direction of the u_T is opposite to the tangential reaction force R_T.

Combining these formulas in the form of KUHN-TUCKER:

$$|u_T| \geq 0, \qquad f \leq 0 \quad \text{and} \quad |u_T| f = 0 \tag{1.16}$$

Here, absolute value of the tangential displacement term is used because, it can be in either positive or negative directions.

When friction is present, load displacement diagram can be plotted as shown in Figure 1.4 using the above statements for the tangential loading and the tangential displacement.

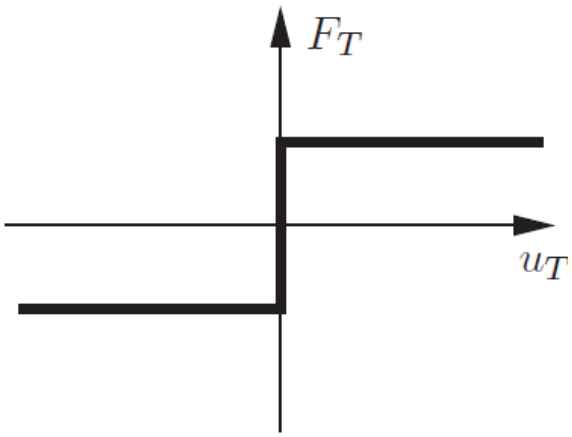

Figure 1.4 – Load-displacement diagram of the frictional contact [13]

For the frictional load-displacement diagram, non-smooth behavior is again present as in no friction case shown in Figure 1.2. As stated before, special mathematical techniques should be implemented for the solution of the frictional contact.

Kinematically Linear Contact Problem

Basics of contact mechanics are explained in previous sections. In this section, equations, assumptions and concepts which are required to build strong form and variational problem definitions which are applicable to contact mechanics of kinematically linear problems are introduced by following the methodology introduced by Laursen [14].

The kinematically linear response of a body Ω which potentially comes into contact with the rigid obstacle Ω^{obs}, is shown in Figure 1.5. This kind of contact problem; in other words, contact with rigid obstacle, is generally called The Signorini problem.

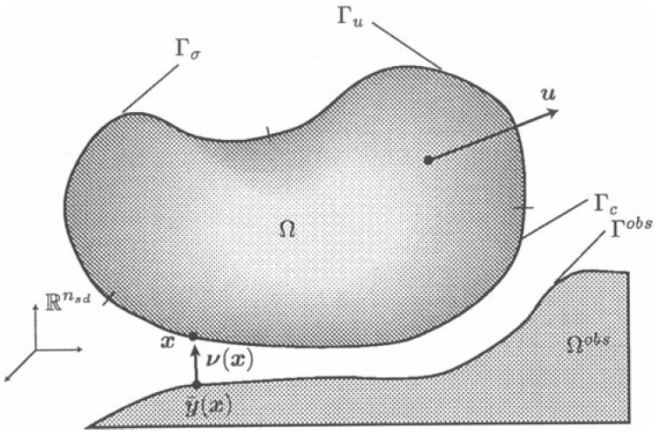

Figure 1.5 - Notation of kinematically linear contact problem [14]

Physically, the points $x \in \Omega$ cannot penetrate the obstacle and it is assumed that there is no friction between contacting bodies. On the other hand, boundary Γ of the body Ω is divided into three sub domains Γ_σ, Γ_u and Γ_c. Γ_σ represents the boundary at which prescribed forces are applied, Γ_u is the boundary on which displacement constraint are defined and finally Γ_c is the boundary that may come into contact with the boundary Γ^{obs} of the rigid body Ω^{obs}. It should be noted that Γ_c and the forces that acts on this region are unknown at first.

In order to define the contact constraints which govern the interaction between the body and the obstacle, any point $\boldsymbol{x} \in \Gamma_c$is considered. It is assumed that, for every possible x there is a corresponding point $\bar{\boldsymbol{y}} \in \Gamma^{obs}$ to define the contact geometry. In this case, $\bar{y}$ is found by minimizing the distance to $\boldsymbol{x}$.

For each point $\boldsymbol{x} \in \Gamma_c$, a local surface normal $\boldsymbol{\nu}(\boldsymbol{x})$ is defined at $\bar{\boldsymbol{y}}(\boldsymbol{x})$, to the surface Γ^{obs} as the unit normal. In the case of kinematically linear contact problem, most crucial assumption is that both the contact point $\bar{\boldsymbol{y}}(\boldsymbol{x})$ and the surface normal $\boldsymbol{\nu}(\boldsymbol{x})$ do not depend on the displacement $\boldsymbol{u}(\boldsymbol{x})$**.** Moreover, $\bar{\boldsymbol{y}}(\boldsymbol{x})$ and $\boldsymbol{\nu}(\boldsymbol{x})$ are defined according to the initial geometrical conditions and kept as fixed throughout the problem.

Then, a gap function $\boldsymbol{g(x)}$, which contains the displacement field $\boldsymbol{u(x)}$ is introduced and the penetration of $\boldsymbol{x}$ into the obstacle Ω^{obs} is prevented by the following inequality:

$$g(\boldsymbol{x}) \leq 0. \tag{1.17}$$

It should be noted that positive values for the gap function $g(x)$ means the penetration of the body into obstacle.

The contact pressure t_N, which is assumed to be positive for compression, is introduced by taking the component of the Cauchy traction $\boldsymbol{t}$ into account at $\boldsymbol{x}$ in the direction of $\boldsymbol{v}$:

$$t_N(x) = \boldsymbol{t}(\boldsymbol{x}) \cdot \boldsymbol{v}(\boldsymbol{x}) = \boldsymbol{v}(\boldsymbol{x}) \cdot \boldsymbol{\sigma}(x)\boldsymbol{n}(x) \tag{1.18}$$

In equation 1.18, the Cauchy traction $\boldsymbol{t}$ is expressed in terms of the famous Cauchy stress $\boldsymbol{\sigma}$ and the outward normal vector $\boldsymbol{n}$ with respect to the surface of the contact region, Γ_c. Note that, there are two surface normal vectors, $\boldsymbol{n(x)}$ and $\boldsymbol{v(x)}$, which are associated with Γ_c and Γ^{obs}, respectively.

Contact equations which relate t_N and g to contact surface Γ can now be written in terms of KUHN-TUCKER conditions as follows:

$$t_N \geq 0 \tag{1.19}$$

$$g(\boldsymbol{x}) \leq 0 \tag{1.20}$$

$$t_N g = 0 \tag{1.21}$$

Above equations hold for all $\boldsymbol{x} \in \Gamma_c$. Considering the sign convention for t_N, equation 1.19 states that the contact interaction is compressive. On the other hand,

equation 1.20 gives the impenetrability condition and equation 1.21 states the so-called complementarity conditions, that compressive stress only occurs when the contact is present, i.e., when $g = 0$. Moreover, when $g < 0$, t_N should be zero.

In Figure 1.6, schematic representation of the equations 1.19 - 1.21 that relate g and t_N is presented. It is clear that the contact stress t_N is a non-smooth and nonlinear function of g. Furthermore, the relation between the variables is multivalued when $g = 0$. It should be noted that $t_N(x)$ is the contact pressure which is required to prevent the interpenetration of x into the obstacle, while satisfying the equilibrium with internal stresses and inertial effects that act on the neighboring material points. Special mathematical techniques are once again required to solve the problem.

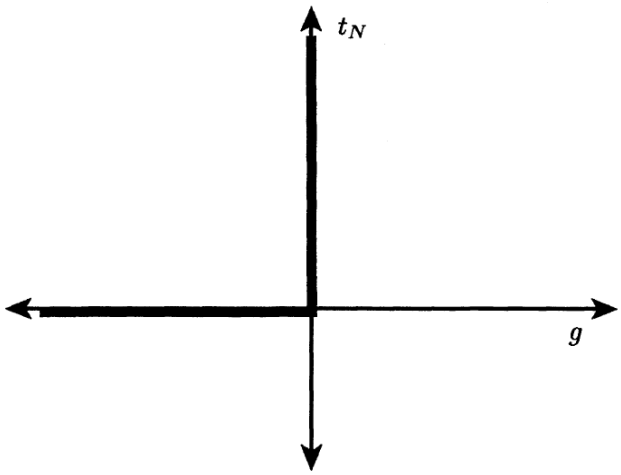

Figure 1.6 – Schematic illustration of the KUHN-TUCKER condition [14]

Beginning from the weak form of contact problems, commonly used contact algorithms can be explained mathematically.

Without the presence of contact the weak form for the stress analysis can be written as:

$$G^{int,ext}(\boldsymbol{u},\boldsymbol{w}) = \int_{\Omega} w_{i,j}\,\sigma_{ij}\,d\Omega - \int_{\Omega} w_i f_i\,d\Omega - \int_{\Gamma_\sigma} w_i \bar{t}_i\,d\Gamma = 0 \qquad 1.22$$

Here, $G^{int,ext}(u,w)$ denotes the sum of internal virtual work and external virtual work due to stresses and applied loadings, respectively. Equation 1.22 is obtained by following the standard procedure explained as:

i) The multiplication of momentum balance with the test functions
ii) Integration of the result of multiplication over the body
iii) Application of integration by parts theorem.

Now, considering the case of a deformable body which is in contact with the rigid body, weak form can be rewritten as:

$$G(\boldsymbol{u},\boldsymbol{w}) = \int_{\Omega} w_{i,j}\,\sigma_{ij}\,d\Omega - \int_{\Omega} w_i f_i\,d\Omega - \int_{\Gamma_\sigma} w_i \bar{t}_i\,d\Gamma - \int_{\Gamma_c} w_i \bar{t}_i\,d\Gamma = 0 \qquad 1.23$$

Here, last term of the equation 1.23 represents the contact virtual work on the bodies that are in contact. Denoting the last term of the above equation as $G^c(\boldsymbol{u},\boldsymbol{w})$ and considering the equation 1.22, the above equation can be rewritten as:

$$G(\boldsymbol{u},\boldsymbol{w}) = G^{int,ext}(\boldsymbol{u},\boldsymbol{w}) + G^c(\boldsymbol{u},\boldsymbol{w}) \qquad 1.24$$

$G^c(\boldsymbol{u}, \boldsymbol{w})$ can be rewritten in terms of the gap function and the contact pressure as following the steps explained in [14]:

$$G^c(\boldsymbol{u}, \boldsymbol{w}) = \int_{\Gamma_c} t_N(x)\delta g d\Gamma \qquad 1.25$$

For body Ω, the total potential energy is given by 1.26, when the contact is not included.

$$\Pi(\boldsymbol{u}) = \int_{\Omega} W(\boldsymbol{\varepsilon}(\boldsymbol{u}))\, d\Omega - \int_{\Omega} \boldsymbol{f} \cdot \boldsymbol{u}\, d\Omega - \int_{\Gamma_\sigma} \bar{\boldsymbol{t}} \cdot \boldsymbol{u} d\Gamma \qquad 1.26$$

In equation 1.26, $W\big(\boldsymbol{\varepsilon}(\boldsymbol{u})\big)$ is the elastic energy per unit volume stored in the body.

Finite element formulations can be constructed by finding the minima of the potential energy function when the contact is not present. As a result, an optimization problem without any constraints is acquired as there is no contact defined. Weak form of the $G^{int,ext}(\boldsymbol{u}, \boldsymbol{w})$ term can be found by taking the drectional derivative of the potential energy function given in equation 1.26 in the direction of $\boldsymbol{w}$. One should also keep in mind that, when the contact is included in the problem contact constraints should also be accounted for and the total potential energy functional is modified as follows:

$$\overline{\Pi}(\boldsymbol{u}, ?) = \Pi(\boldsymbol{u}) + \Pi^c(\boldsymbol{u}, ?) \qquad 1.27$$

Here, Π^c is the contribution of contact to the global potential energy functional and depends on the method that is chosen for the contact constraint formulation. In other words, second variable of the functional Π^c is determined by the contact algorithm.

Hereafter, the methods which are used to enforce contact constraints are explained mathematically. There are varieties of techniques in the optimization literature that are used to solve the contact problem. It is due to the fact that linear elastic case results in a problem of constrained minimization of the total energy Π. The following algorithms are presented by the aid of certain assumptions like dynamics, inelasticity and large deformations are not included.

There are mainly three contact algorithms which are used in the optimization literature:

- Lagrange (multiplier) method
- Penalty Method
- Augmented Lagrange Method

Lagrange Multiplier Method

The following form of the contact contribution Π^c to the global total potential energy functional is included for the frictional contact of the Lagrange multiplier algorithm:

$$\Pi^c(\boldsymbol{u}, \lambda_N) = \int_{\Gamma_c} \lambda_N g d\Gamma \tag{1.28}$$

Then, the global functional takes the following form:

$$\Pi^{lag}(\boldsymbol{u}, \lambda_N) = \Pi(\boldsymbol{u}) + \int_{\Gamma_c} \lambda_N g d\Gamma \tag{1.29}$$

Solution of the equation 1.29 is obtained by making the $\Pi^{lag}(\boldsymbol{u}, \lambda_N)$ term stationary with respect to displacement u and the Lagrange multiplier λ_N. Here, λ_N is the contact pressure. Following the solution steps explained in [14], one gets:

$$\int_{\Omega} w_{i,j}\, \sigma_{ij} d\Omega - \int_{\Omega} w_i f_i d\Omega - \int_{\Gamma_\sigma} w_i \bar{t}_i d\Gamma + \int_{\Gamma_c} \lambda_N \delta g d\Gamma = 0 \qquad 1.30$$

$$\int_{\Gamma_c} (\lambda_N - q_N) g d\Gamma \geq 0 \qquad 1.31$$

Equations are applicable to all $\boldsymbol{w}$ and the admissible variations q_N ($q_N \geq 0$) of λ_N.

Equations 1.30 and 1.31 can be replaced by the KUHN-TUCKER optimality conditions on the multipliers λ_N as:

$$\lambda_N \geq 0 \qquad 1.32$$

$$g(\boldsymbol{x}) \leq 0 \qquad 1.33$$

$$\lambda_N g = 0 \qquad 1.34$$

When the appropriate substitutions of λ_N is made for the contact pressure, t_N, the similarity with the previously given KUHN-TUCKER conditions can be recognized. It should once again be stated that Lagrange multipliers λ_N correspond physically to the contact pressures on the contact region that is necessary to prevent the penetration of the two contacting bodies.

Penalty Methods

Penalty methods have the advantage that they remove the constraints from variational formulation explicitly. Mathematically, the following form for Π^c can be written for the frictionless contact problem:

$$\Pi^c(\boldsymbol{u}) = \int_{\Gamma_c} \epsilon_N \langle g \rangle^2 d\Gamma \qquad 1.35$$

In equation 1.35, ϵ_N is the penalty parameter chosen by the user and $\langle \quad \rangle$ is named as the Macauley bracket and operates as:

$$\langle x \rangle = \begin{cases} x \text{ if } x \geq 0 \\ 0 \text{ if } x < 0 \end{cases} \qquad 1.36$$

Combining equations 1.27 and 1.35, penalized energy functional Π^{pen} can be written as:

$$\Pi^{pen}(\boldsymbol{u}) = \Pi(\boldsymbol{u}) + \int_{\Gamma_c} \epsilon_N \langle g \rangle^2 d\Gamma \qquad 1.37$$

The solution form of the above equation is obtained by minimization; in other words, making it stationary with respect to the variations following the steps explained in [14].

$$\int_{\Omega} w_{i,j}\, \sigma_{ij} d\Omega - \int_{\Omega} w_i f_i d\Omega - \int_{\Gamma_\sigma} w_i \bar{t}_i d\Gamma + \int_{\Gamma_c} \epsilon_N \langle g \rangle \delta g d\Gamma = 0 \qquad 1.38$$

The disadvantage of the penalty methods is clearly obvious in Figure 1.7. In Figure 1.7, pressure-gap relation is given in terms of KUHN-TUCKER conditions by the penalty method and the contact force term t_N is $\epsilon_N\langle g\rangle$. Bold line in the Figure 1.7 represents the admissible combinations of $t_N - g$ pairs and the dashed line is the penalty approximation. Note that, impenetrability condition is satisfied only if $\epsilon_N \to \infty$. This is practically impossible in mathematical calculations because of several reasons and ill-conditioning is the most obvious one among them.

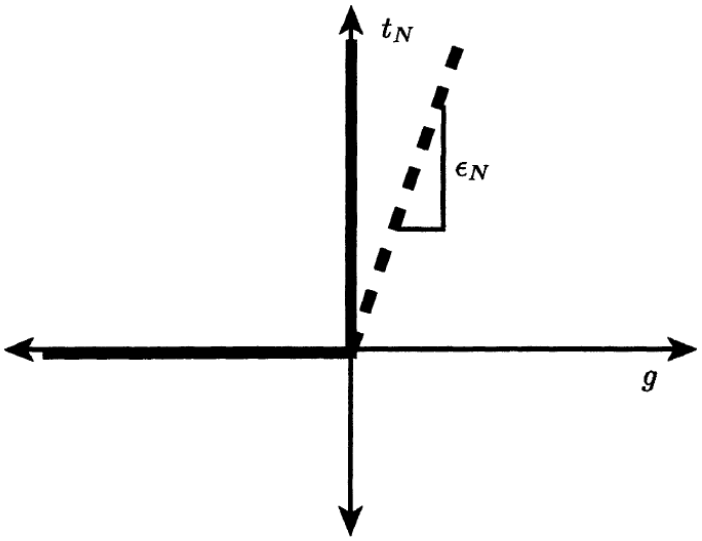

Figure 1.7 - Schematic illustration of penalty method. [14]

Augmented Lagrange Method

The Augmented Lagrange approach can be defined as a compromise between Lagrange multiplier and the Penalty method [14]. In the Augmented Lagrange approach, contact constraints are represented exactly and iterative procedure is performed with the help of penalty method. Π^c for Augmented Lagrangian method is written as:

$$\Pi^{c}(\boldsymbol{u}, \lambda_N) = \int_{\Gamma_c} \left[\frac{1}{2\epsilon_N} \langle \lambda_N + \epsilon_N g \rangle^2 - \frac{1}{2\epsilon_N} {\lambda_N}^2 \right] d\Gamma \qquad 1.39$$

Then, the augmented Lagrangian functional becomes:

$$\Pi^{a.lag}(\boldsymbol{u}, \lambda_N) = \Pi(\boldsymbol{u}) + \int_{\Gamma_c} \left[\frac{1}{2\epsilon_N} \langle \lambda_N + \epsilon_N g \rangle^2 - \frac{1}{2\epsilon_N} {\lambda_N}^2 \right] d\Gamma \qquad 1.40$$

In equation 1.40, $\epsilon_N > 0$ is prescribed by the user as in the penalty method. One should note that, when λ_N is set to 0, the penalty method is recovered. Solution for the Augmented Lagrangian algorithm is obtained by making the augmented Lagrange functional $\Pi^{a.lag}(\boldsymbol{u}, \lambda_N)$ stationary with respect to both $\boldsymbol{u}$ and λ_N. Following the steps explained in [14], the solution point $(\boldsymbol{u}, \lambda_N)$ for the Augmented Lagrangian functional is given by:

$$\int_{\Omega} w_{i,j}\, \sigma_{ij} d\Omega - \int_{\Omega} w_i f_i d\Omega - \int_{\Gamma_\sigma} w_i \bar{t}_i d\Gamma + \int_{\Gamma_c} \langle \lambda_N + \epsilon_N g \rangle \delta g d\Gamma = 0 \qquad 1.41$$

$$\frac{1}{\epsilon_N} \int_{\Gamma_c} [\langle \lambda_N + \epsilon_N g \rangle - \lambda_N] q_N d\Gamma = 0 \qquad 1.42$$

As stated in [14], one should note that augmented Lagrangian algorithm has exactly the same solution as the Lagrange multiplier method. However, numerical treatment of augmented Lagrangian is easier than the Lagrange multiplier method making the former more advantageous.

Difference between the solution techniques are illustrated using the one degree of freedom example given by Laursen [14]. One should note the difficulties that one can face when solving a contact problem using the Lagrange multiplier method. In the particular problem studied, active constraints are easily determined as there is

only one constraint and for most of the real world problems set of active constraints are not known a priori and an iterative solution procedure has to be followed. It is clear for Penalty method that the accuracy of the solution improves with the increase in the penalty parameter and for complicated problems it is not practical to use very high values of penalty parameter. However, for Augmented Lagrange algorithm, the solution is simpler.

Contact problem with Friction

The frictional constitutive description for a contact problem begins with the definition of the kinematic quantities on the contact surface. Because friction is present, tangent vector(s) $\boldsymbol{\tau}_\alpha$ based at point $\bar{\boldsymbol{y}} \in \Gamma^{obs}$, which is assumed to be on the contact surface, can be defined at point $\boldsymbol{x} \in \Gamma_c$. The tangent vector $\boldsymbol{\tau}_1$ can now be related to the surface normal $\boldsymbol{\nu}$, note that $\boldsymbol{\nu}$ has unit length and considering the three dimensional case.The tangent space is shown in Figure 1.8.

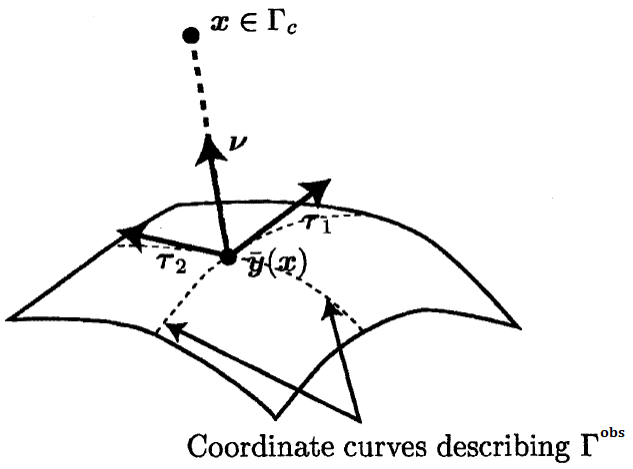

Figure 1.8 - Illustration of the tangent space and the possible contact point $\boldsymbol{x}$ [14]

The tangent vectors $\boldsymbol{\tau}_\alpha$ are assumed to be independent of displacement $\boldsymbol{u}$ as in kinematically linear problem discussed in the previous section. The tangential motion $\boldsymbol{u}_T(\boldsymbol{x})$ of the point $\boldsymbol{x} \in \Gamma_c$, can be written by substracting the normal

component of the displacement vector $[\boldsymbol{u}(\boldsymbol{x}) \cdot \boldsymbol{\nu}]\boldsymbol{\nu}$ from the total displacement vector $\boldsymbol{u}(\boldsymbol{x})$ and it is also possible to write the tangential motion $\boldsymbol{u}_T(\boldsymbol{x})$ in terms of its components and tangent vectors.

Similar approach is used and frictional tractions are defined as:

$$\begin{aligned} \boldsymbol{t}_T(\boldsymbol{x}) &= -(\boldsymbol{t}(\boldsymbol{x}) - [\boldsymbol{t}(\boldsymbol{x}) \cdot \boldsymbol{\nu}]\boldsymbol{\nu}) = -[\boldsymbol{I} - \boldsymbol{\nu}\otimes\boldsymbol{\nu}]\, \boldsymbol{t}(\boldsymbol{x}) \\ &= -\boldsymbol{t}(\boldsymbol{x}) + t_N\boldsymbol{\nu} \end{aligned} \qquad 1.43$$

In equation 1.43, t_N is a scalar and $\boldsymbol{t}_T$ is a vector. Minus sign in the definition of $\boldsymbol{t}_T(\boldsymbol{x})$ represents the frictional traction exerted by the contacting body at $\boldsymbol{x}$ on the contact surface.

Coulomb's law of friction

The conditions described in equations 1.44 and 1.45 should be met for all $\boldsymbol{x} \in \Gamma_c$ along with the KUHN-TUCKER conditions which are given by equations 1.19 - 1.21.

$$\| \boldsymbol{t}_T \| \leq \mu t_N \qquad 1.44$$

$$\boldsymbol{u}_T = \lambda \boldsymbol{t}_T \text{ where } \begin{Bmatrix} \lambda = 0 & \text{if} & \| \boldsymbol{t}_T \| < \mu t_N \\ \lambda \neq 0 & \text{if} & \| \boldsymbol{t}_T \| = \mu t_N \end{Bmatrix} \qquad 1.45$$

Equation 1.44 states that the magnitude of the tangential stress vector $\boldsymbol{t}_T$ should not exceed the value of friction coefficient, μ times the contact pressure value t_N. μt_N term is called the Coulomb limit. On the other hand, equation 1.45 has two physical meanings:

i. The tangential slip vector $\boldsymbol{u}_T$ is equal to zero when the magnitude of tangential stress vector is less than the Coulomb limit.

ii. The tangential slip vector $\boldsymbol{u}_T$ is linearly related to the frictional stress $\boldsymbol{t}_T$ which is due to the sliding of the contact point $\boldsymbol{x}$ on the opposing surface Γ^{obs}.

The graphical illustration of the Coulomb's law of friction is shown in Figure 1.9. It is possible to make analogy between the elastoplasticity formulation and Coulomb's law of friction when the Figure 1.9 is considered and this analogy is used to perform numerical applications of contact problems [14]. It is also possible to express equations 1.44 and 1.45 by:

$$\phi(\boldsymbol{t}_T, t_N) = \| \boldsymbol{t}_T \| - \mu t_N \leq 0 \tag{1.46}$$

$$\dot{\boldsymbol{u}}_T = \dot{\gamma} \frac{\boldsymbol{t}_T}{\| \boldsymbol{t}_T \|} \tag{1.47}$$

$$\dot{\gamma} \geq 0 \tag{1.48}$$

$$\dot{\gamma}\, \phi = 0 \tag{1.49}$$

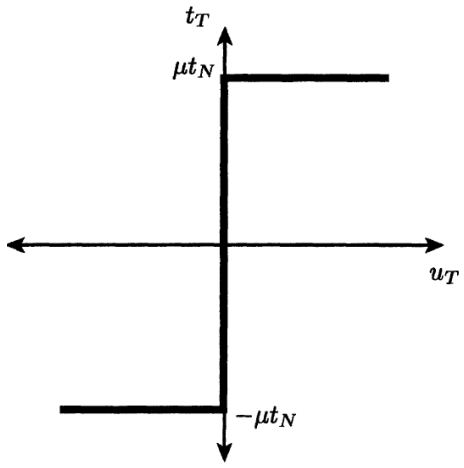

Figure 1.9 – Graphical illustration of Coulomb's law of friction [14]

In equations 1.46 and 1.49 ϕ is named as slip function and is a direct analogue of the yield function of theory of elasticity and $\dot{\gamma}$ is a scalar [15] that satisfies the condition given in equation 1.48.

Regularization of Friction

Figure 1.6 and Figure 1.9 reveal that the constraints of Coulomb's law of friction are indeterminate or multi-valued when the stress is related to deformation [14]. This is similar to the statement which was made previously about the impenetrability constraint. Impenetrability constraint is unknown a priori whether the zero tangential displacement constraint is present or not. Considering computational difficulties, some kind of regularization is utilized to solve problems that involve friction. In the following, Penalty and Augmented Lagrangian approaches are introduced to regularize the Coulomb's law of friction.

- Penalty Approaches

A tangential penalty parameter ϵ_T is introduced for the penalty regularization of the Coulomb frictional problem. One should note that ϵ_T does not have to be equal to the normal penalty parameter ϵ_N which was previously introduced.

Considering equations 1.46 to 1.49, Coulomb's law of friction can be written as:

$$\phi(\boldsymbol{t}_T, t_N) = \| \boldsymbol{t}_T \| - \mu t_N \leq 0 \tag{1.50}$$

$$\dot{\boldsymbol{t}}_T = \epsilon_T \left[\dot{\boldsymbol{u}}_T - \dot{\gamma} \frac{\boldsymbol{t}_T}{\| \boldsymbol{t}_T \|} \right] \tag{1.51}$$

$$\dot{\gamma} \geq 0 \tag{1.52}$$

$$\dot{\gamma}\, \phi = 0 \tag{1.53}$$

$\dot{\gamma}\frac{\boldsymbol{t}_T}{\|\boldsymbol{t}_T\|}$ term in equation 1.51 is called the inelastic slip rate and it is clear that only difference between equations 1.46 to 1.49 and 1.50 to 1.53 is the penalization of the difference between the total slip rate $\dot{\boldsymbol{u}}_T$ and the inelastic slip rate $\dot{\gamma}\frac{\boldsymbol{t}_T}{\|\boldsymbol{t}_T\|}$ with a penalty parameter. Use of above equations removes the indeterminate nature of the Coulombs law of friction and the tangential traction $\boldsymbol{t}_T$ becomes a single valued function of the tangential displacement $\boldsymbol{u}_T$. The regularization idea is illustrated in Figure 1.10 and one can easily notice that exact value of the Coulomb's law of friction is only obtained when the tangential penalty parameter goes to infinity, as before.

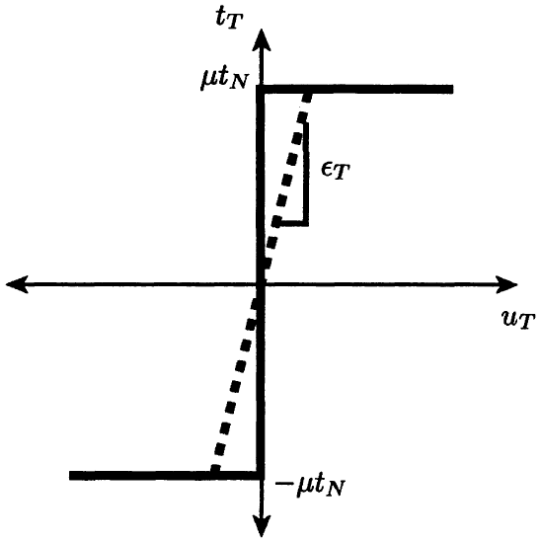

Figure 1.10 – Graphical illustration of the penalty regularization of the Coulomb's law of friction. [14]

- Augmented Lagrangian Approach

Penalty regularization method that is explained in the previous section has the same drawback like the any other penalty method; no slip condition cannot be represented without the use of sufficiently large tangential penalty parameter ϵ_T. On the other hand, use of very large values tangential penalty parameter ϵ_T may

lead to ill-conditioning. At this point, an Augmented Lagrangian regularization method can be introduced as follows:

$$\phi(\boldsymbol{t}_T, t_N) = \| \boldsymbol{t}_T \| - \mu t_N \leq 0 \tag{1.54}$$

$$\dot{\boldsymbol{t}}_T - \dot{\boldsymbol{\lambda}}_T = \epsilon_T \left[\dot{\boldsymbol{u}}_T - \dot{\gamma} \frac{\boldsymbol{t}_T}{\| \boldsymbol{t}_T \|} \right] \tag{1.55}$$

$$\dot{\gamma} \geq 0 \tag{1.56}$$

$$\dot{\gamma}\, \phi = 0 \tag{1.57}$$

In equations 1.54 - 1.57, $\boldsymbol{t}_T$ is the total contribution of both Lagrange multiplier and penalty algorithms to the frictional traction and $t_N = \langle \lambda_N + \epsilon_N g \rangle$ is used in order to indicate the contribution of Lagrange multiplier and penalty algorithms to the pressures. λ_T is the tangential Lagrange parameter.

1.4 Structure of the Thesis

In introduction, brief introduction to the simple mathematical illustrations of the contact problems and the algorithms which are used in the commercial software are explained with examples to illustrate the contact phenomena. Furthermore, studies available in literature and advantages and disadvantages of these studies are explained by giving the sufficiency and applicability.

In Chapter 2, main contact parameters, which are the contact stiffness factor and the penetration tolerance factor, are explained physically and a case study is performed for bolted joint structure. Experimental results available in literature are compared with the finite element analyses with varying contact parameters in elastic limits and effects of the contact parameters on the accuracy and the solution time of the analysis are explained.

In Chapter 3, experimental data of the bolted joint structure in Chapter 2 is compared with the finite element analysis in plastic limits. Drawbacks and limitations of the finite element method are shown and the results are compared for varying contact parameters.

Experimental study of two L-bracket structures is given in Chapter 4. Experimental results of the L-brackets are compared with the varying contact parameters and favorable contact parameters are offered.

In the conclusion chapter, whole study is summarized briefly and the positive aspects of the finite element solution are given. Effects of the contact parameters on the results are explained and suggestions about choosing the correct parameters are made.

CHAPTER 2

FINITE ELEMENT ANALYSES OF THE BOLTED FLANGE STRUCTURE IN ELASTIC LIMITS

Industry requires faster design with the least number of test validations because of the high cost of the tests and there are many loading conditions to consider for bolted-flange connections including thermal, centrifugal loadings and contact forces. Finite element method has gained importance for the analyses of bolted flange connections and there are many contact regions in gas turbine engines. These are bolted flange connections, lug joints and dovetails. Finite element analysis of contact regions requires high level experience and knowledge in order to acquire better results. Because of the nonlinear nature of the contact phenomenon, analyses of bolted flange connections may also be challenging depending on the flange configuration which has many geometrical variables. In the literature, there are analytical methods that are used to analyze bolted flange connections. When linear models are used in the finite element analysis of bolted flange connections, results are either not accurate or over conservative. Finite element models that take plastic deformation and frictional effects at the contact zone into account are known to give more accurate results for the strain and stress distribution in bolted flange connections. Commercially available finite element software has certain input parameters that are used to model the contact behavior and to define the contact algorithm and these parameters are known to have an effect upon the speed, convergence and accuracy of the solution; however, any of this commercial software is not specialized for the gas turbine industry. In this chapter, ANSYS APDL 12.1 is used to perform the parametric study to study the

effect of contact stiffness and penetration tolerance values utilizing different contact algorithms for the three dimensional finite element model of an eight-bolt unstiffened flange-plate steel connection splicing two circular hollow sections. Piecewise linear elastic constitutive models are used for both bolts and flange-plates in the finite element model. Results of the contact analysis of the bolted flange connection of circular hollow sections are compared for different choices of major input parameters of the contact definition in terms of accuracy, convergence and speed for each combination. Finally, results are validated with available experimental results in the literature for a component under pure bending [17]. The input parameter set that produces the closest finite element result to the experimental result is identified.

2.1 Main Parameters of Nonlinear Contact Analysis

Finite element simulation of nonlinear contact analysis requires a number of input parameters that should be chosen by the user. These parameters influence both convergence and accuracy of the analysis and should be chosen carefully because these parameters are problem dependent. These parameters are contact algorithm, contact stiffness factor and penetration tolerance factor. General formulation of the mainly used algorithms and their advantages/disadvantages are explained in the introduction. Here, two other important parameters which are contact stiffness and penetration tolerance parameters are explained in detail. Equation 2.1 [18] is the simple representation of the contact problems:

$$p = k_n x_n \tag{2.1}$$

In equation 2.1, p is the contact pressure, k_n is contact stiffness and x_n is the contact penetration. Assuming a finite amount of contact pressure p, increase in contact stiffness results in decrease in the penetration and vice versa.

In Figure 2.1, mathematical simulation of contact problem is illustrated. Two bodies which are in contact exhibit a certain amount of penetration and contact stiffness resists the penetration. F is external force that acts on the deformable body, ε_N is the contact stiffness and g_N is amount of penetration.

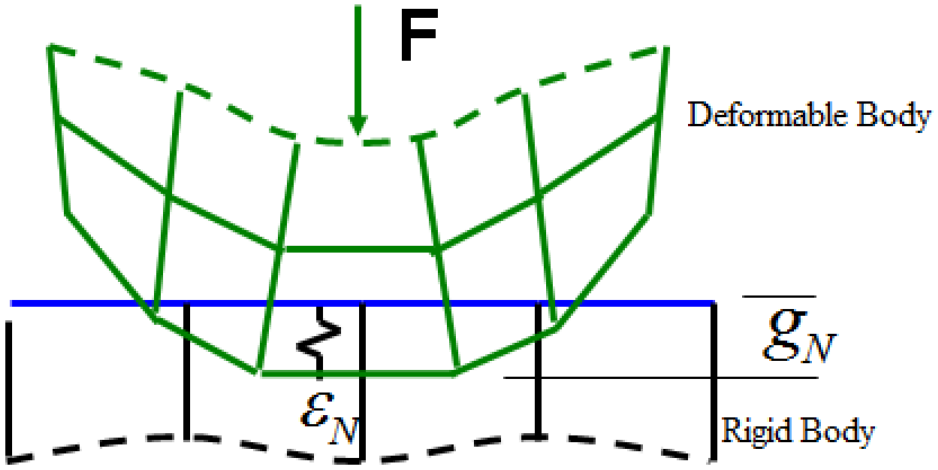

Figure 2.1 – Illustration of the contact problem [19]

2.1.1 Penetration Tolerance

In real world contact problems, ideally, when two solid bodies come into contact, no penetration occurs between the bodies [18]. However, for the mathematical simulation of contact problems there should always be a certain amount of penetration to be able to solve the problem. Penetration can be defined as the sacrifice to be made in order to be able to solve the finite element problems. As long as the amount of the penetration is small enough, the results of the contact problems are assumed to be more realistic. In other words, one should decrease the penetration value in the contact problems as much as possible.

ANSYS calculates a certain amount of the penetration value depending on the sizes of the elements that are in contact and it is possible to set the penetration tolerance factor (FTOLN). Penetration tolerance value is used to satisfy the

compatibility of the contact problem and the tolerance is calculated by the multiplication of the contact penetration factor with the average depth of the each individual contact element in the contact pair. The value of the contact penetration factor is less than 1.0 and it is suggested that it should be less than 0.2 in all of the cases [1]. In a contact problem, even though the convergence criterion is satisfied by the residual forces and the displacement increments of the structure, iterations continue until the penetration criterion is satisfied.

2.1.2 Contact Stiffness Factor

Equation 2.1 also implies that the amount of the penetration becomes zero when the contact stiffness approaches to infinity. However, mathematical simulation may not be possible when contact stiffness is very large.

Contact stiffness is basically the stiffness between two contacting bodies as shown in Figure 2.1. Contact stiffness determines the interpenetration status of the bodies and higher values of contact stiffness are known to result in more accurate solutions. As shown in Figure 2.1 without the presence of contact stiffness, bodies would interpenetrate and contact problem would not be illustrated realistically. In ANSYS, contact stiffness is calculated automatically according to material and elemental stiffness in the contact region and it is simply multiplied with the contact stiffness factor value that the user chooses. However, too large values of contact stiffness values are known to lead to ill-conditioning of the global stiffness matrix, which results in convergence difficulties [20]. Moreover, the loads are not transferred across the contacting bodies correctly. Effect of contact stiffness value on the accuracy and the convergence of finite element solution is unquestionable and it is important to choose the value of the contact stiffness factor that is suitable for the specific problem so that the solution can be robust and accurate.

2.2 Experimental Background

There are numerous experimental studies in the literature investigating the structural behavior of bolted flange connections under various load cases. In this study, strain data of eight-bolt unstiffened steel flange-plate connection splicing two circular hollow sections under pure bending is used for the validation of finite element analysis performed. The experimental setup is shown in Figure 2.2. Eight M24 high strength bolts with grade 8.8S are used and material properties of the bolts are said to be provided by the manufacturer [17]. Full penetration welds are applied in between the steel tube and the end plates for the experimental setup. Four point loading condition is implemented and the two jack loading points are right at the middle of two tubes in order to achieve pure bending condition. Specimens are loaded up to 180 kN as seen in Figure 2.3. Geometrical details, dimensions of the specimens are provided in detail by Wang et al [17].

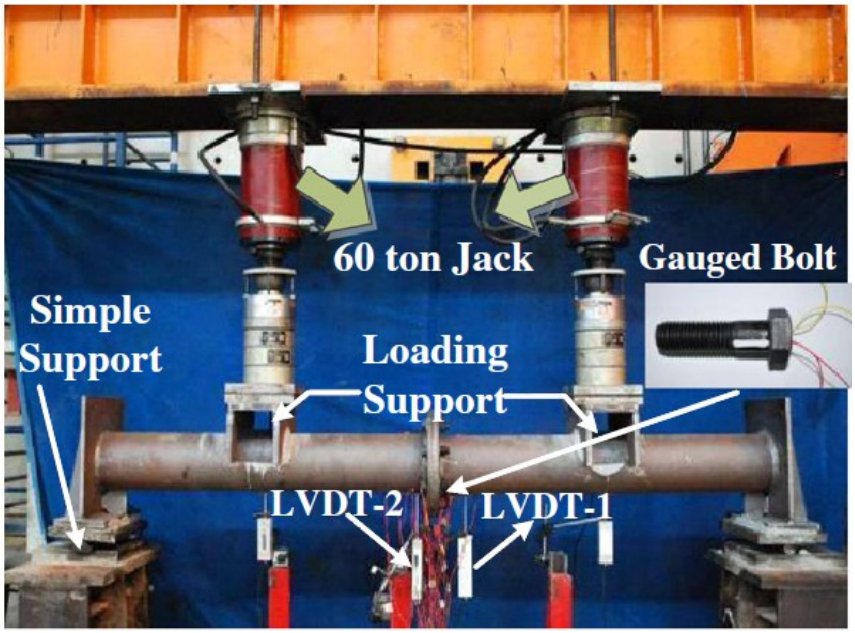

Figure 2.2 – Experimental setup for eight-bolt unstiffened steel flange-plate connection splicing two circular hollow sections under pure bending [17]

Two strain gages are used and placed perpendicular to the radial direction of the circular hollow sections as shown in Figure 2.3. Figure 2.3 also shows the applied load versus average strain readings of the two strain gages. Strain gages are placed at equal distances between the two bolts.

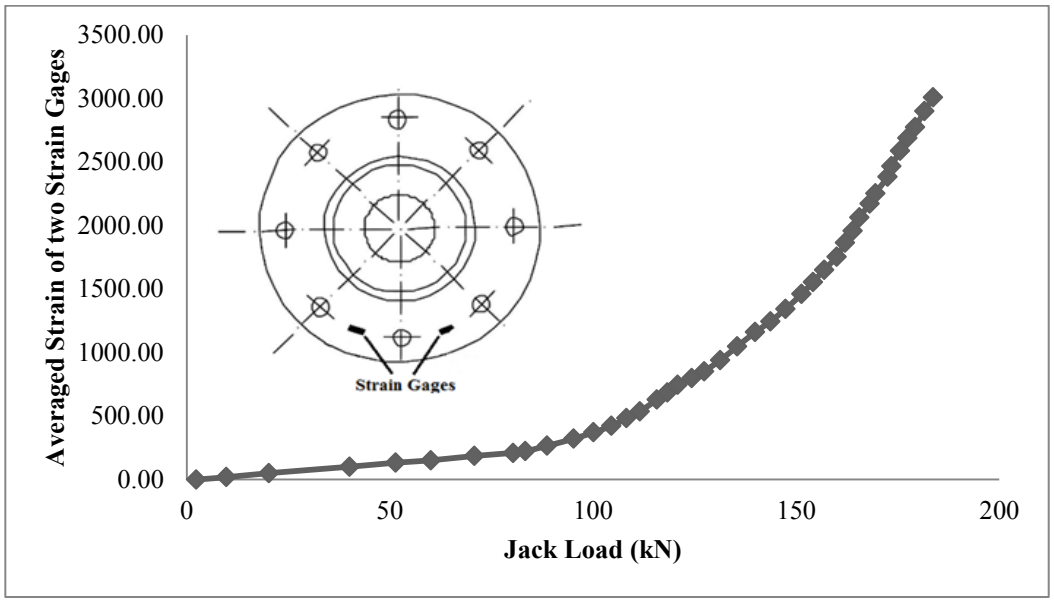

Figure 2.3 – Experimental results and strain gage locations [17]

2.3 Finite Element Model

ANSYS 12.1 is used to create the three dimensional FE model of the bolted flange connection of the circular hollow sections. 20 node SOLID95 type 3D elements are used in the finite element model. Contact regions (bolts, end plates) are modeled with smaller elements in order to obtain better results. There are 33289 elements with 145981 nodes, 26635 elements with 117257 nodes for fine and coarse mesh types (see Figure 2.4), respectively. Standard surface-to-surface contact definition is used between the nut and the end plates, between the bolt and the bolt hole wall and between the end plates. Bolt is modeled as a one piece solid assuming that there is no separation of nut and the bolt. Pretension of the bolt is

applied to the cylindrical shank in order to preserve symmetry of the preload. When the symmetry of the preload section is lost, extra loads like moment occurs and the simulation becomes unrealistic. Contact algorithms, penetration tolerance and contact stiffness values for all of the contact pairs are changed simultaneously before each run and results of finite element analysis are compared with the available experimental results [17]. Two different finite element models are used for the sensitivity analyses to be able to investigate the results for the coarse and the fine mesh structures which are shown in Figure 2.4.

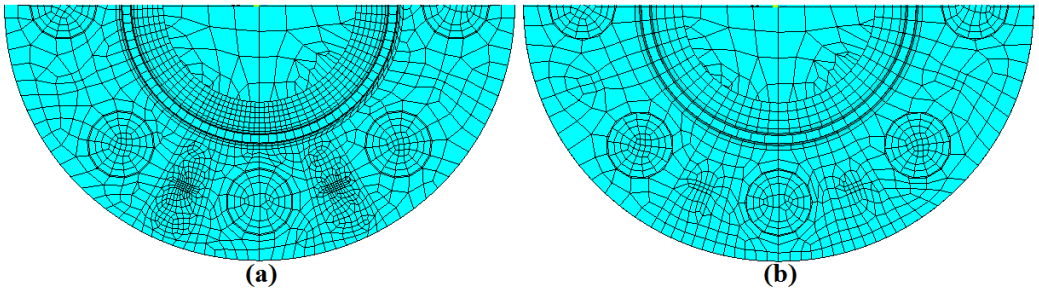

Figure 2.4 – Fine and coarse mesh structures

For the fine mesh structure, nodes on opposing end plate surfaces coincide with each other (see Figure 2.5 – Mesh structure at contact zone for the fine and coarse mesh) and elements are smaller compared to the coarse mesh structure. For the coarse mesh structure, element size of only one end plate is increased leaving the other end plates' mesh structure fine to observe the effects on the solution accuracy and run time when the symmetric mesh structure is not present. For the coarse mesh case, meshes on the end plates do not coincide with each other.

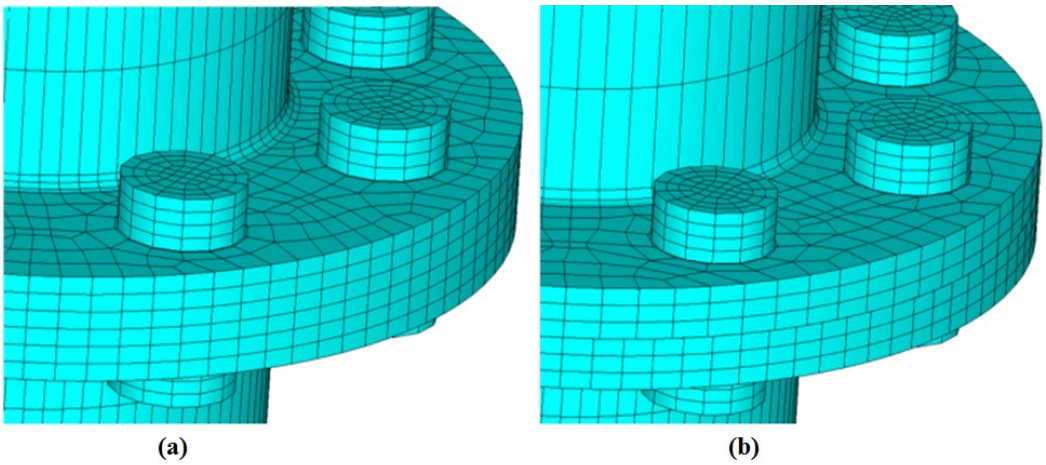

Figure 2.5 – Mesh structure at contact zone for the fine and coarse mesh types

Two different load cases, 50 kN and 75 kN, are used because otherwise results may be deceptive for the validation purposes when one load case is used only. Model is simply supported at the LHS and clamped at the RHS and loading points are at 0.5 m from the supported ends of the 2 m long beam to acquire the pure bending condition. Loading point and boundary conditions are shown in Figure 2.6. The preload of all of the bolts is taken as 125 kN [17].

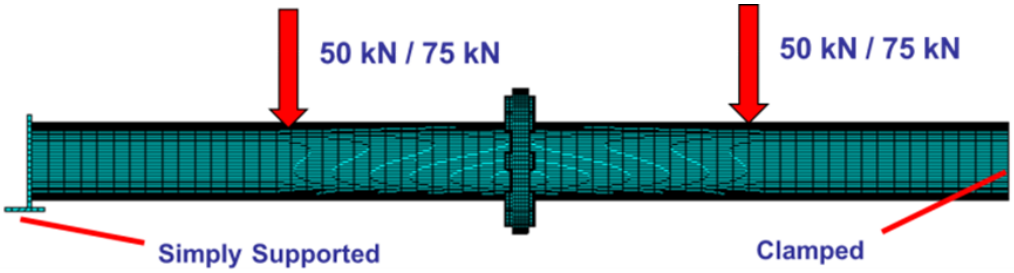

Figure 2.6 – Global finite element model and loading conditions

Strain gage locations are modeled with fine mesh structure for both of the FE models. Axial strain values of the nodes attached to the areas shown in Figure 2.7

are averaged for each solution separately by creating a result coordinate system in line with areas that simulate the strain gages as shown in Figure 2.8. Black coordinate in Figure 2.8 is the x-axis and the results are taken in x-direction.

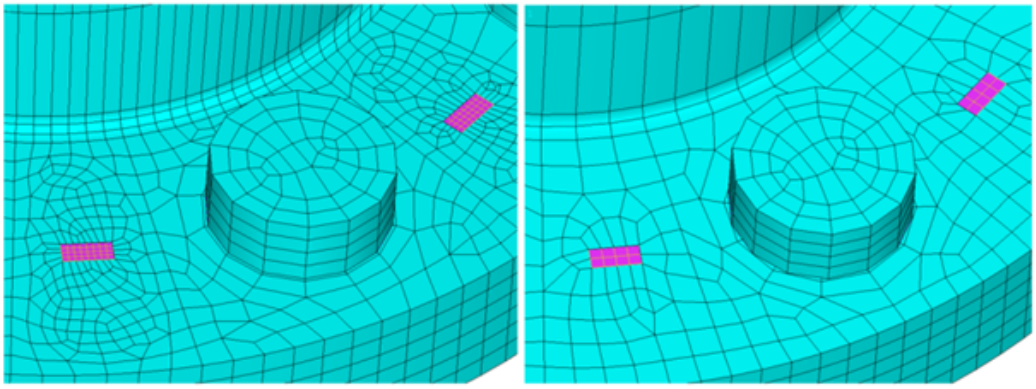

Figure 2.7 – Strain gage locations in the fine and the coarse finite element models

Figure 2.8 – Strain gages and result coordinate systems

Piecewise linear constitutive material models are provided for the end plates, circular hollow sections (CHS) and the bolts and Figure 2.9 illustrates the material models with yield plateau for the circular hollow sections, end plates and high strength bolts [17]. Strain value at the yield plateau is assumed as 0.0226 [21]. Young modulus, yield strength, ultimate strength and ultimate strain values of each material are presented in Table 2.1. In Table 2.1, E is the modulus of

elasticity, f_y is the yield strength, f_u is the ultimate tensile strength and ε_u is the ultimate strain. For the elastic analyses Young's modulus and Poisson's ratio are used for material models only.

Table 2.1 – Material properties of CHS, end plate and high strength bolts

	E (MPa)	f_y (MPa)	f_u(MPa)	ε_u
CHS	212000	380	524	0.137
End plate	206000	290	530	0.290
High strength bolts	201000	660	800	0.136

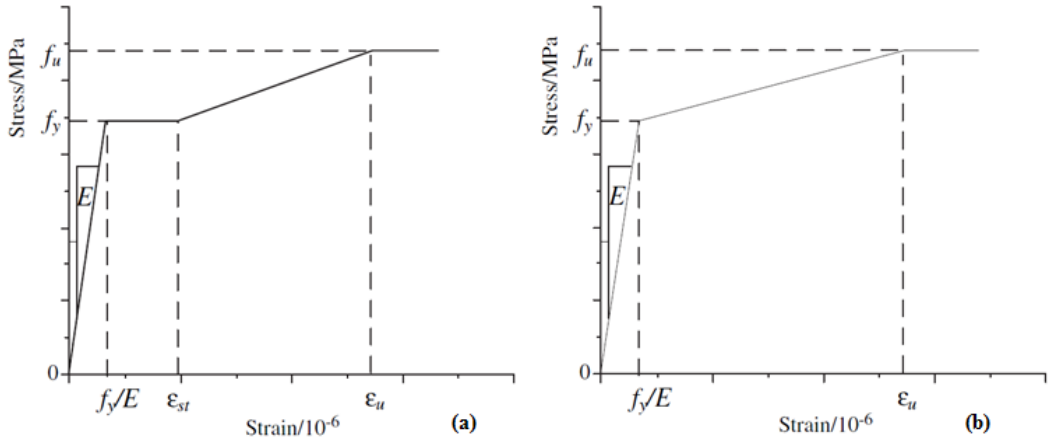

Figure 2.9 – Material models for the CHS, the end plate and the high strength bolts [17]

For the CHS and the end plates constitutive relation (a) and for the high strength bolts constitutive relation (b) in Figure 2.9 are implemented [16].

Surface-to-surface contact is used between the nut and the end plates, between the bolt and the bolt hole wall and between the end plates. For all of the contacts standard contact definition of ANSYS APDL is implemented. Contact regions are illustrated in Figure 2.10. Although there is a gap between the bolt and the bolt

hole, the contact is defined because there is possibility of interaction at that region.

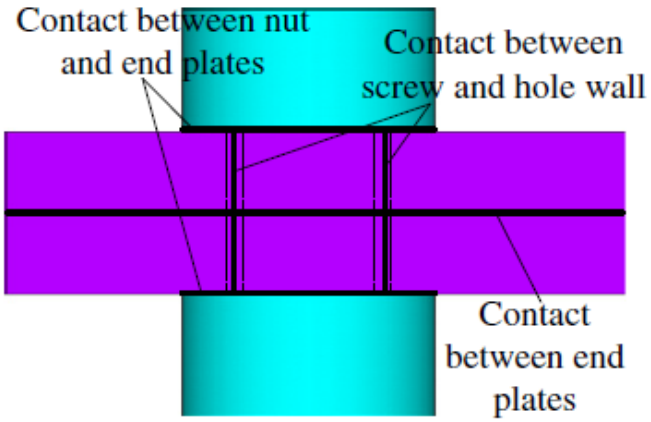

Figure 2.10 - Contact definitions that are used in finite element analysis [17]

Contact stiffness factor, penetration tolerance factor, friction coefficient, mesh type and load cases are chosen as variables for the analysis. In Table 2.2, parameters and modeling details that are changed for the parametric study are shown. In addition to some sensitivity analysis for coefficient of friction and contact stiffness factor, each combination in Table 2.2 is analyzed so there are more than 200 analyses performed.

Table 2.2 - Parameters that are changed throughout the analysis

Algorithm	**Contact Stiffness Factor**	**Penetration Tolerance Factor**	**Load Case**	**Mesh Structure**
Augmented Lagrange	2	0.2	50 kN	Fine
Pure Penalty	1.5	0.15	75 kN	Coarse
	1	0.1		
	0.75	0.05		
	0.5	0.025		

2.4 Results

Each contact parameter is compared separately in the following sections. Absolute value version of the general percent error, which is given in equation 2.2, is used to calculate the error for each combination. Experimental result for both 50 and 75 kN load cases is extracted from available data (see Figure 2.3) for the 50 kN and 75 kN jack loads and error calculations are performed according to corresponding load case.

$$\%\ Error = \frac{|FE_{result} - Experimental_{result}|}{|Experimental_{result}|} x100 \qquad 2.2$$

When the friction is present in the nonlinear contact analysis, coefficient of friction is the major input and it is known to have significant effect on the stress and strain distributions. Coefficient of friction value 0.74 is given as the dry coefficient of friction between steel and steel [21]. However, it is also known that coefficient of friction value depends on many parameters like lubrication, surface roughness and temperature so it is decided to make a sensitivity analysis to determine the friction coefficient to be used in the contact analysis. Three analyses with three different friction coefficient values are run by keeping other parameters constant (Augmented Lagrange, FKN=1, FTOLN=0.1). Figure 2.11 shows the percent difference between the strain values obtained in the analyses and the experimental strain readings. Following the sensitivity study related to the use of different friction coefficients, it is decided to continue with the friction coefficient value of 0.74 since it gave the most accurate result among three as shown in Figure 2.11.

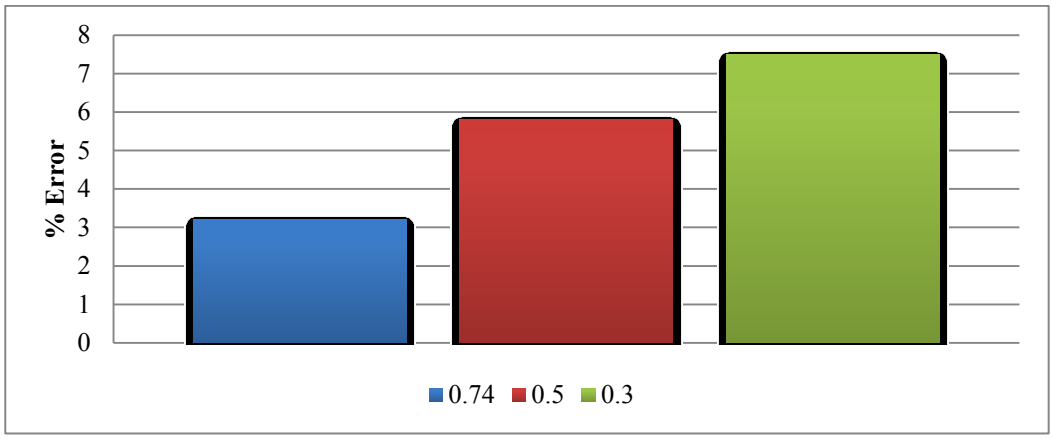

Figure 2.11 - Comparison of various friction coefficient values in terms of accuracy for Augmented Lagrange, Fine Mesh Structure, 75 kN load case

2.4.1 Variation of percent error in strain calculation with respect to the penetration tolerance

Decreasing the penetration tolerance is known to increase the accuracy and decrease the convergence rate. In Figure 2.12, % Error vs. Penetration tolerance factor graph is shown for the Pure Penalty algorithm, fine mesh case and the 75 kN load case.

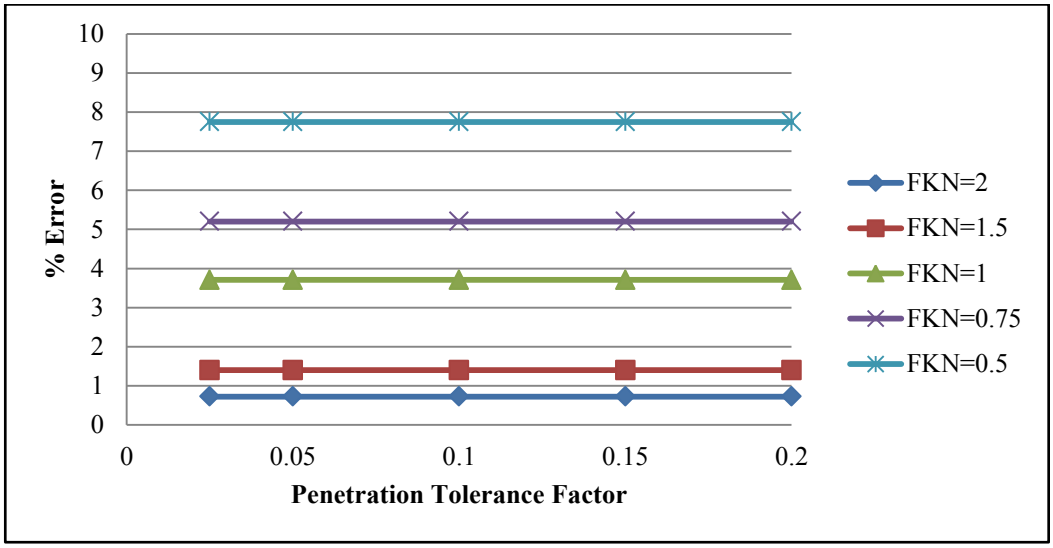

Figure 2.12 - % Error vs. penetration tolerance factor (Augmented Lagrange, Fine Mesh Structure, 75 kN)

From Figure 2.12, it is seen that, when the algorithm, mesh structure and load case are fixed and only the penetration tolerance factor is changed the results are same in terms of accuracy contrary to the theory and common knowledge. For the particular structure analyzed, it is concluded that penetration tolerance factor has insignificant effect on the strain results for the investigated range.

2.4.2 Variation of the solution time with respect to the penetration tolerance

Figure 2.13 gives the variation of the solution time with the penetration tolerance. It is seen that when the other contact parameters and modeling properties are fixed, increasing penetration tolerance factor does not have an apparent effect on the solution time. However, in some cases it is observed that solution time decreases with increasing penetration tolerance factors as shown in Figure 2.13. Contact stiffness factor 2 and penetration tolerance factor value 0.2 resulted in the shortest solution time. In the thesis, very high penetration tolerance factor values are not used because it is assumed that increasing penetration tolerance factor too much may cause unrealistic results. However, using a penetration tolerance factor that is close to 1 is suggested as the accuracy and solution time are not affected for the analysis. When penetration tolerance factor of 1 is chosen by the user, finite element solution uses the default penetration tolerance value calculated by ANSYS. ANSYS uses the element sizes and material stiffness values around the contact regions to calculate the penetration tolerance value and the calculated value is multiplied by the penetration tolerance factor that the user chooses.

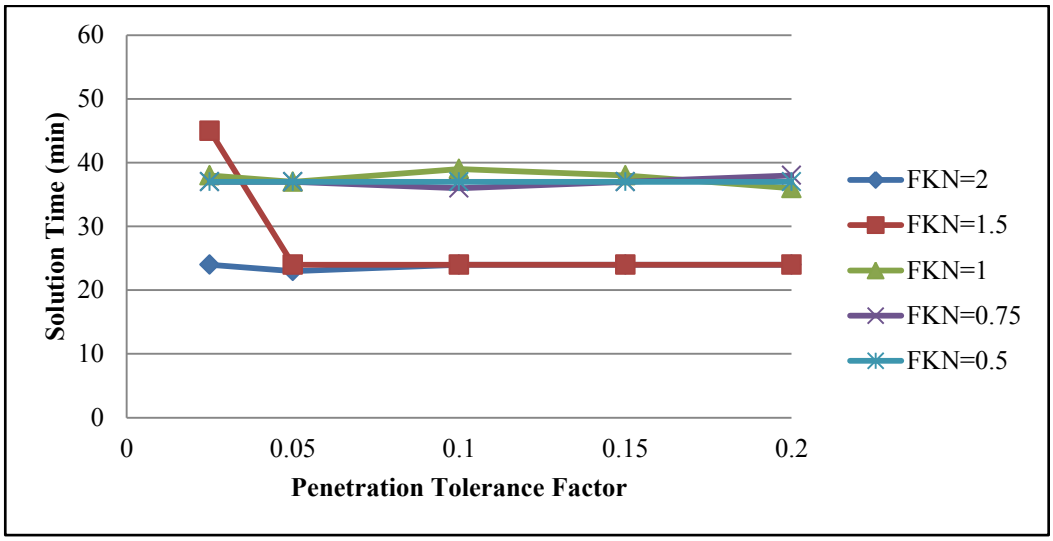

Figure 2.13 - Solution Time vs. Penetration tolerance factor (Augmented Lagrange, Fine Mesh Structure, 75 kN)

2.4.3 Variation of the percent error in strain calculation with respect to the algorithm

Algorithm type is one of the input parameters that a user can choose for nonlinear contact analysis. ANSYS has five algorithms available for contact definitions. For this study four of these algorithms are considered because these algorithms are known to be able to simulate standard contact. ANSYS uses Augmented Lagrange as the default contact algorithm and the other algorithms are Pure Penalty, Pure Lagrange and Lagrange & Penalty methods. For the Lagrange & Penalty method, it is known that two algorithms are used in combination according to the behavior of the structure in the tangential and the normal directions. For some contact problems, Pure Lagrange and Lagrange & Penalty methods are more likely to exhibit to ill-convergence in the contact analyses [7]. In the present study, four of these methods are used separately to study the effect of the contact algorithm on the accuracy. It is observed that the Augmented Lagrange and Pure Penalty methods produced close strain values compared to the experimental data [16]. After several runs to acquire better results for Pure Lagrange and Lagrange & Penalty methods, it is decided to continue the sensitivity analysis using the

Augmented Lagrange and the Pure Penalty methods because the results for Pure Lagrange and Lagrange & Penalty methods are inaccurate.

The comparison of the Augmented Lagrange and the Pure Penalty methods in terms of percent error is presented in Figure 2.14 and Figure 2.15.

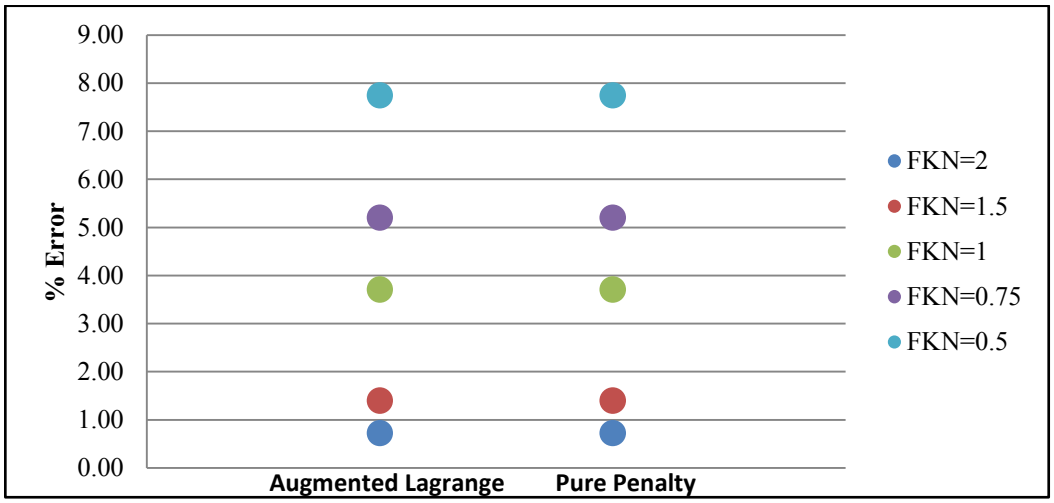

Figure 2.14 - % Error vs. algorithm type (Fine Mesh Structure, 75 kN)

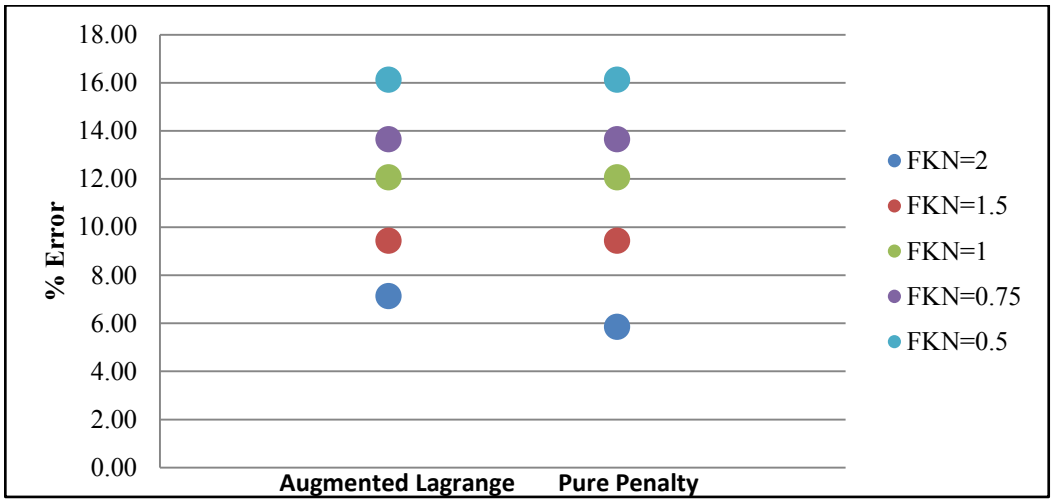

Figure 2.15 - % Error vs. algorithm type (Coarse Mesh Structure, 75 kN)

When Augmented Lagrange and Penalty algorithms are compared, it is seen that there is almost no difference in percent error when the contact stiffness factor and other modeling specifications are the same as seen in Figure 2.14 and Figure 2.15. Augmented Lagrange is a modification of Penalty method [13] and for this contact problem the accuracy is not affected from the algorithm type.

2.4.4 Variation of solution time with respect to algorithm

Figure 2.16 shows the solution times of the Augmented Lagnrage algorithm and the Pure Penalty method. It is seen that there is no drastic change in terms of CPU usage between the two algorithms. In most of the cases solution time for both of the algorithms are same. However, solution time for the Pure Penalty Method is a bit higher for some contact stiffness factor values. It is considered that when the model size increases and fine mesh models are used, Augmented Lagrange algorithm is more preferable due to slightly lower run times.

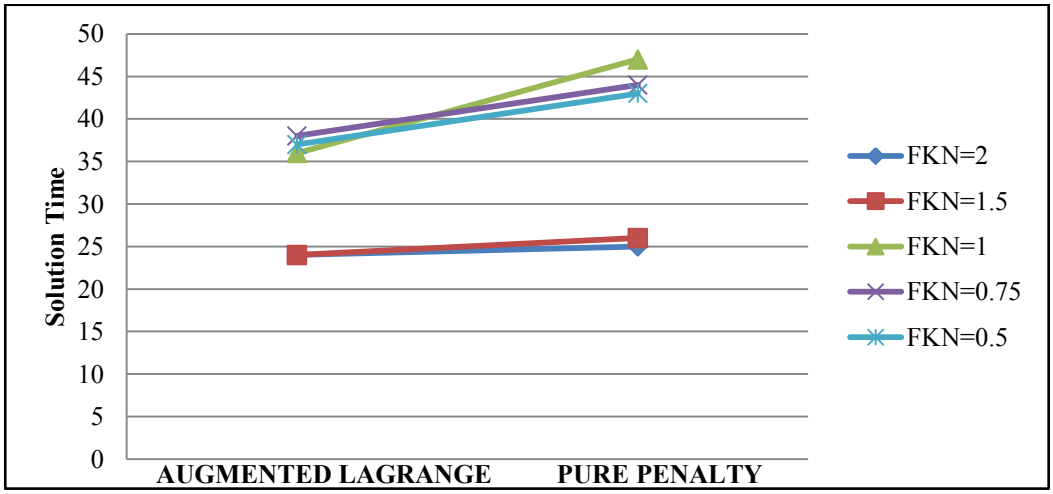

Figure 2.16 - Solution time vs. algorithm type (Fine Mesh Structure, 75 kN)

2.4.5 Variation of percent error in strain calculation with respect to contact stiffness factor

Contact stiffness is known to have an important influence on the accuracy, run time and convergence behavior of the contact problems [13]. ANSYS calculates the contact stiffness value automatically by using the solid element sizes in contact region and material properties of these elements [17] and then updates the contact stiffness value in each iteration by simply multiplying the contact stiffness factor that is chosen by the user with the contact stiffness value calculated by itself. In this section, the results for different contact stiffness factor values are presented. In all analyses, contact algorithm is taken as Augmented Lagrange. Figure 2.17 and Figure 2.18 give the percent difference between the strain readings obtained by the contact analysis and the experimental strain readings. It is observed that in general, higher contact stiffness values give better results in terms of accuracy. However, for the 50 kN load case, the accuracy decreases when the contact stiffness factor is increased to values higher than 1. Hence, there is the possibility that the accuracy may drop when the contact stiffness factor is increased higher than a certain limit. To analyze the effects of contact stiffness factor, further analyses are performed by taking high contact stiffness factor such as 4.

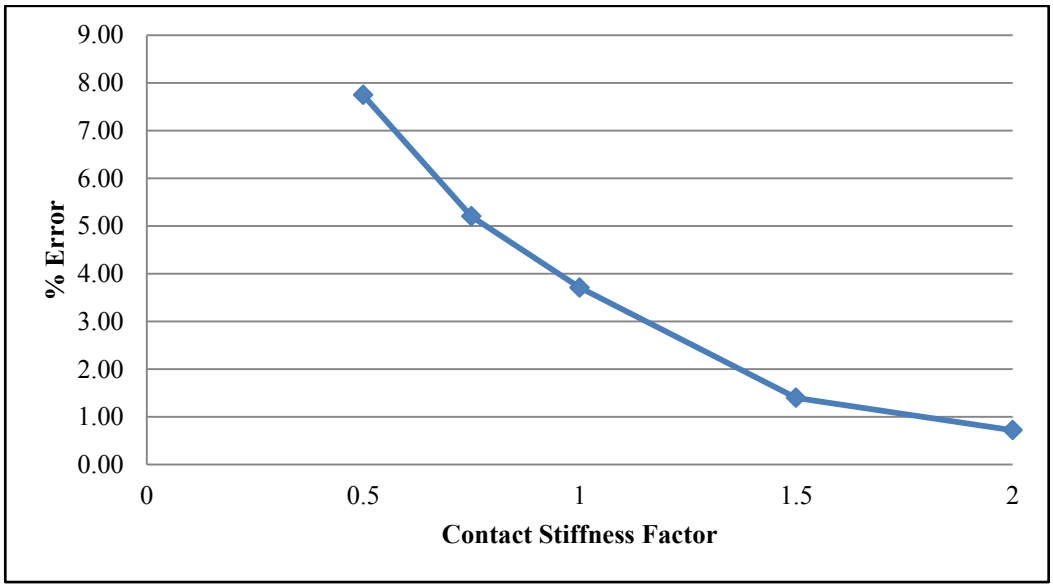

Figure 2.17 - % Error vs. contact stiffness factor (Fine Mesh Structure, 75 kN)

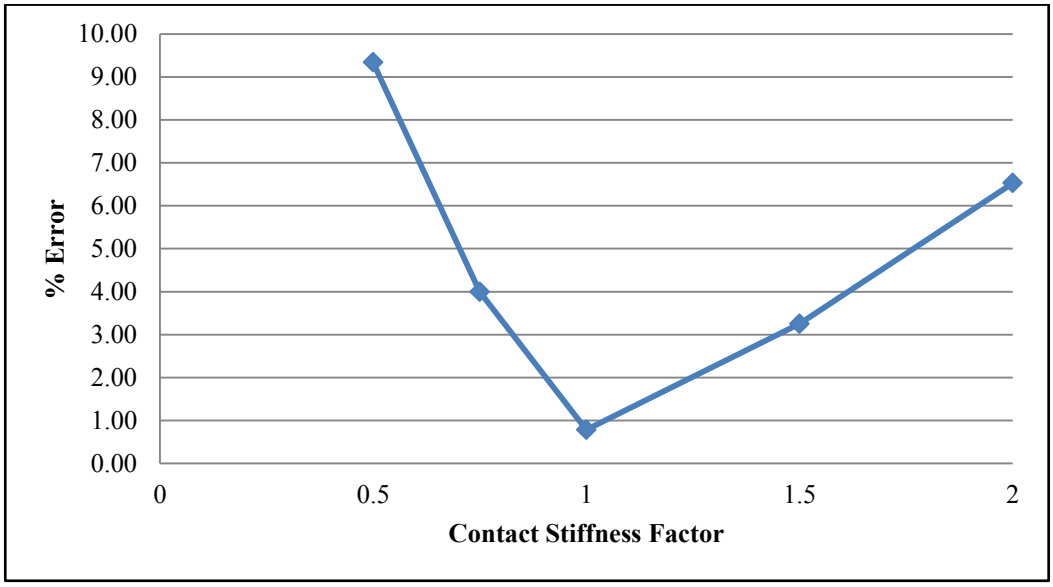

Figure 2.18 - % Error vs. contact stiffness factor (Fine Mesh Structure, 50 kN)

Figure 2.19 shows how the error varies with the contact stiffness factor when the solution algorithm is Augmented Lagrange and the load case is 75 kN. From

Figure 2.19, it is clear that for the particular problem studied, if the contact stiffness factor is increased above 2, the discrepancy between the experimental strain reading and computationally determined strain values increase. One of the reasons for this conclusion might be the insufficiently modeled finite element structure. In other words, elemental stiffness of the elements near contact regions cannot overwhelm the contact stiffness and error increases. Aspect ratio and size of the elements should be compatible with contact stiffness. Another reason might be the numerical problems that arise because of contact stiffness factor.

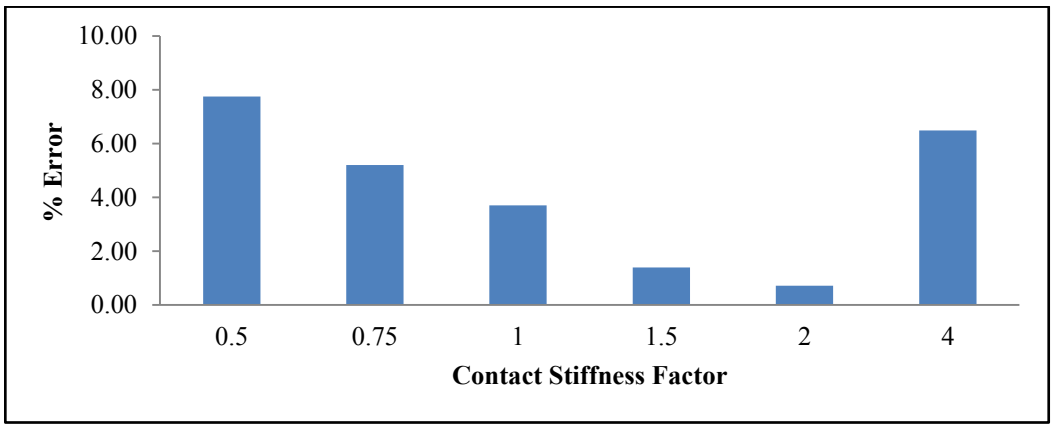

Figure 2.19 - Comparison of various contact stiffness factors in terms of accuracy for the Augmented Lagrange algorithm, fine mesh structure and the 75 kN load case.

2.4.6 Variation of solution time with respect to contact stiffness factor

It is known by experience that, solution time is supposed to increase with increasing contact stiffness factor. However, in some cases higher contact stiffness values resulted in shorter run times for certain set of parameters in contrast to the common knowledge. Variation of the solution time with respect to the contact stiffness factor for different sets of fixed input parameter is given in Figure 2.20.

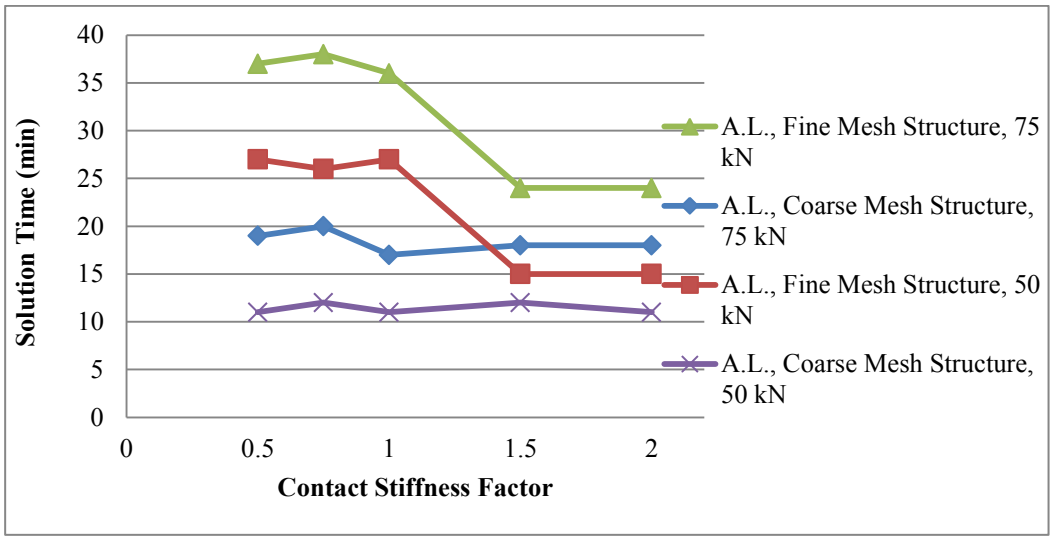

Figure 2.20 – Solution time vs. Contact stiffness factor for different set of inputs

Considering the accuracy and the CPU time of the analyses, it is suggested that sensitivity analyses for contact stiffness factor must be performed with a relatively coarse mesh structure and contact stiffness factor should be decided accordingly because using fine mesh structures during sensitivity analysis leads to very long solution times. It does not always mean that high contact stiffness factor will increase the accuracy or the solution time as the results are highly problem dependent but using 2 is preferable according to the accuracy and the solution time of the analyses for this problem.

2.4.7 Variation of percent error in strain calculation with respect to load case and mesh type

Two different load cases, 50 kN and 75 kN, are used for the analysis of the bolted flange connection for better judgment of the effect of the contact parameters on the run time and on the percent difference of the computational results from the experimental results. Because it is deemed that effects of contact parameters on the accuracy and solution time may vary even in elastic range. For the 50 kN and the 75 kN load cases stress results are checked for preliminary analyses and it is seen that jack loads are in the elastic limits. Jack loads are kept in elastic limits in

order to avoid the convergence and the run time issues associated with the material nonlinearity since there are more than two hundred analyses involved in the parametric study. Variation of percent error in strain calculation, comparing the two load cases and the mesh types are presented in Figure 2.21 and Figure 2.22. Figure 2.21 and Figure 2.22 give the results for both Augmented Lagrange and Pure Penalty methods as there is no difference for the algorithms in terms of accuracy, and also for the fine and coarse mesh models.

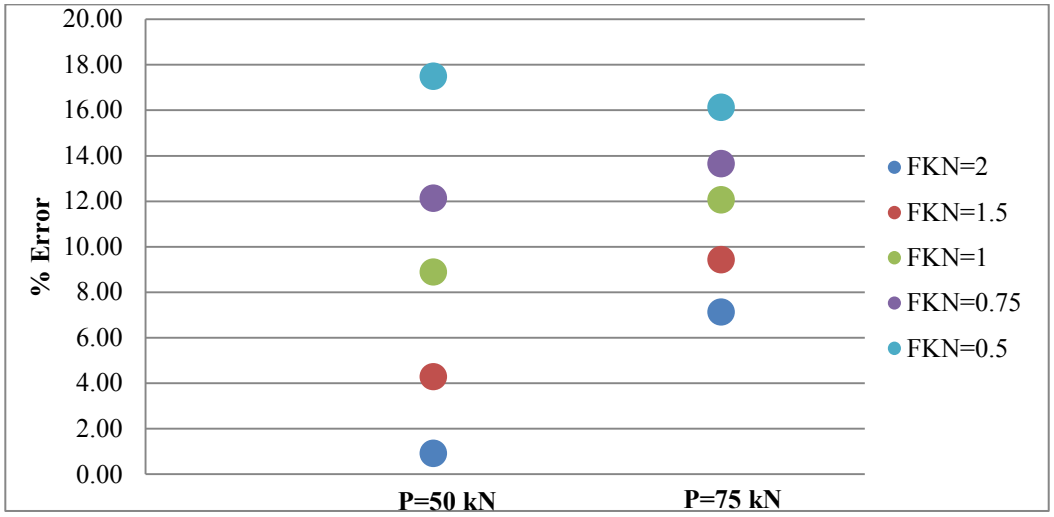

Figure 2.21 - % Error vs. load case (Augmented Lagrange (Pure Penalty), Coarse Mesh Structure)

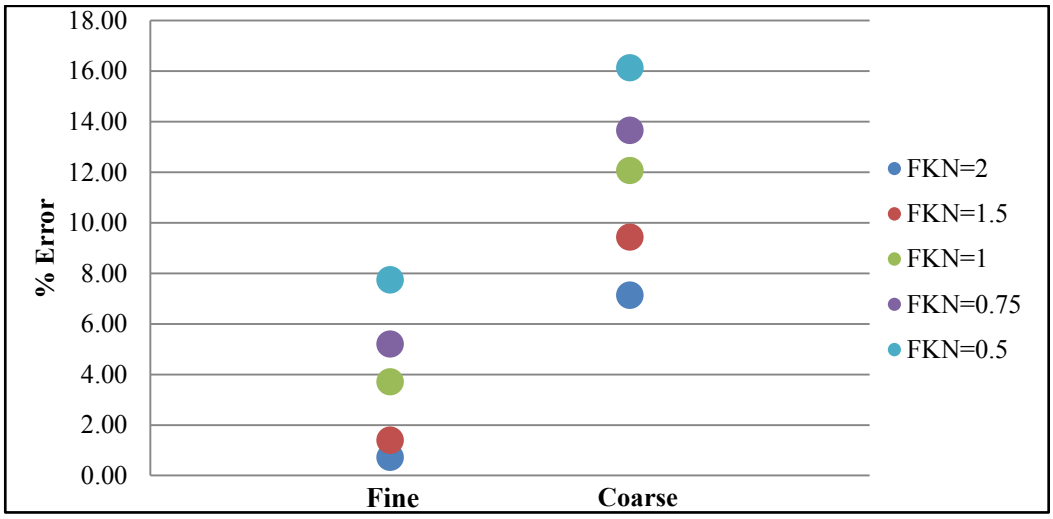

Figure 2.22 - % Error vs. mesh type (75 kN)

Fine mesh finite element model is created using same element sizes on the corresponding surfaces considering the importance of contact detection for the solution of contact problems. Then, mesh for one of the end plates is made coarser and the meshes of the bodies in contact do not match so the effect of the mesh size and matching status of the meshes on the results are observed. For high level of loading conditions with coarse mesh structure, percent error increases and it is observed that contact stiffness factor plays an important role in these cases. Fine mesh structure has a matching mesh structure on the contact regions and has more number of nodes compared to coarse mesh structure. Although it has more number of nodes, it is thought that matching status of the mesh should decrease the solution time, but it is seen that the CPU time is longer for fine mesh structure; thus, it is concluded that number of nodes are more important than the matching status of the models for this structure. On the other hand, coarse mesh structure gave worse results in terms of accuracy for most of the cases, as expected.

2.5 Conclusion for Finite Element Analysis of the Bolted Flange Structure in Elastic Limits

Effects of penetration tolerance factor, contact algorithm, contact stiffness factor, mesh type and the load case on the accuracy and solution time for the nonlinear contact analysis in elastic range are investigated in this chapter. The results showed that some of the common knowledge about effects of contact parameters might be misleading depending on the problem. Initially, the effect of friction coefficient on the accuracy of this problem is investigated and it is concluded that selection of an improper value for coefficient of friction may lead to erroneous results. For the particular problem studied, Augmented Lagrange and Pure Penalty methods are shown to yield almost identical results for most of the cases. Furthermore, it is also stressed that Pure Lagrange and Lagrange & Penalty methods should be used with caution. Penetration tolerance factor is seen to have almost no influence on the results for both of the algorithms and different contact stiffness values. The most important parameter for the nonlinear contact analysis is determined to be the contact stiffness value because the solution time and the solution accuracy are strongly affected with the variation of contact stiffness factor. However, increasing the contact stiffness factor/value too much may lead to ill-conditioned global stiffness matrix, causing inaccurate results [22]. For this specific example, contact stiffness factor 2 has given the best results considering both the accuracy and the solution time of analysis. As a final note, fine mesh structure which has a better matching mesh type results in longer run times indicating that, number of nodes is more significant than the matching status of the meshes on the contacting end plates for this structure. The accuracy obtained by the coarse mesh model is seen to be much lower than the accuracy obtained by the fine mesh model, as expected. In conclusion, Augmented Lagrange method is considered to be one step ahead considering the shorter CPU time for the analyses. Penetration tolerance value can be left as its default value in ANSYS but a carefully chosen contact stiffness factor value is suggested as the results are

highly dependent on the contact stiffness value used in the analyses. To sum up, although there is no major differences for the results of Augmented Lagrange and Pure Penalty methods, shorter solution times encourages the use of Augmented Lagrange method. Fine mesh structure and contact stiffness factor 2 is suggested as the discrepancy between FE results and experimental data is almost 1% for most of the cases. There is almost no effect of penetration tolerance factor on accuracy, thus using higher values for this problem is possible for shorter solution times.

CHAPTER 3

ELASTO-PLASTIC FINITE ELEMENT ANALYSIS OF THE BOLTED FLANGE STRUCTURE

Bolted flange connections should resist extreme load cases when used in gas turbine engines as previously stated. These load cases may cause plastic deformation of the bolted flange connections in some cases. For this reason, results of the plastic contact analysis of the bolted flange connection of the circular hollow sections are compared for different choices of major input parameters of the contact definition in terms of accuracy using ANSYS Workbench. Results are compared with the experimental results available for the structure under pure bending [17] and the input parameters yielding minimal percent error in the results are determined. The objective of this chapter is the determination of the effect of the major contact parameters on the structural response of bolted flange connections which undergoes plastic deformation.

3.1 Experimental Background

Experimental setup in section 2.2 is used for the comparison. For the plastic analysis the specimen is loaded up to 180 kN. Strain data available in Figure 2.3 is used for comparison with the analysis results from 0 to 180 kN.

3.2 Finite Element Model

Plastic analysis might be challenging when material nonlinearity is present along with contact nonlinearity. Therefore, finite element analysis involving material nonlinearity is usually conducted using coarse mesh structures as opposed to the use of fine mesh in elastic analysis. A new finite element model is created in order to perform the analysis in the plastic range and the new mesh structure is shown in Figure 3.1. When compared to Figure 2.4, it is clear that mesh structure for plastic analysis is coarser because of convergence issues.

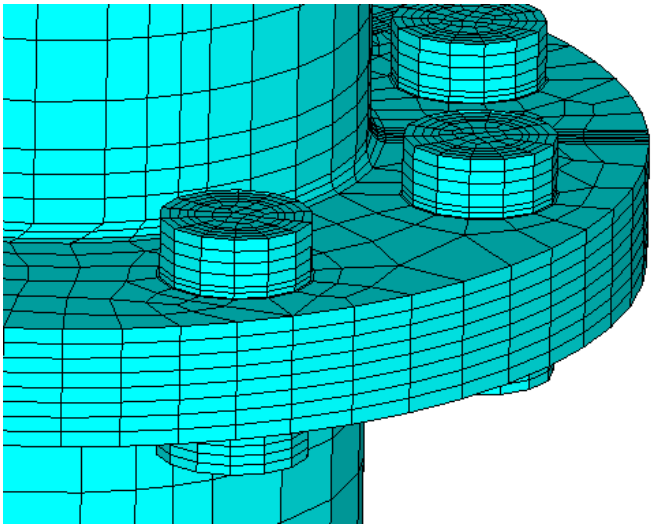

Figure 3.1 – Finite element model for the plastic analyses

New generation 8 node SOLID185 elements of ANSYS are used to create the finite element model in order to reduce the model size. SOLID185 elements are defined by eight nodes and the elements have plasticity, hyper elasticity, stress stiffening, creep, large deflection, and large strain capabilities. There are 41542 elements with 46507 nodes in the entire finite element model.

Strain gage locations are modeled with a finer mesh structure as in elastic analyses. Strain gage locations are shown in Figure 3.2.

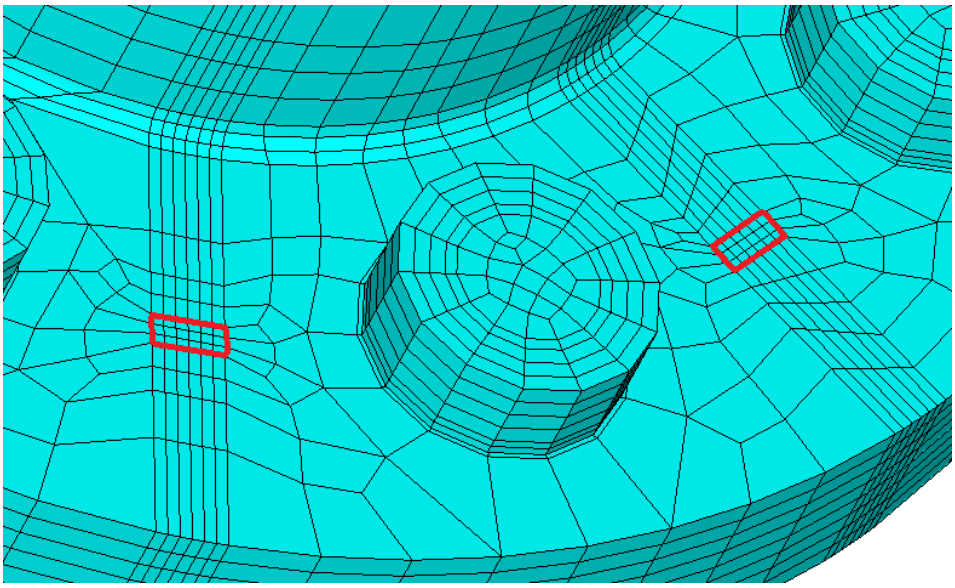

Figure 3.2 - Strain gage locations in the finite element model

A new coordinate system is created in line with the strain gage locations and the axial strain values of the corresponding nodes are averaged to make the comparison with experimental data available [17]. ANSYS APDL's command language is used to create a macro and perform the intermediate steps and acquire the results for each load step. The macro selects the previously created nodal components that represent the strain gages, changes result coordinate system in order to acquire the data in line with strain gages, averages the strain values and writes data to a text file for each load.

Contact algorithm, contact stiffness factor and penetration tolerance factor are changed throughout the analyses to investigate their effect on the strain results when material nonlinearity is also included in the analysis. The details for piecewise linear constitutive material models are given in Figure 2.9 and Table 2.1. The values of the parameters are shown in Table 3.1 and every combination of the parameters is solved resulting in 50 analyses in total. Pure Lagrange and Lagrange & Penalty combination methods are not included in the analyses based on the previous experience.

Table 3.1 - Parameters that are changed throughout the plastic analyses

Algorithm	Contact stiffness factor	Penetration tolerance factor
Augmented Lagrange method	4	0.4
Pure Penalty method	2	0.2
	1	0.1
	0.5	0.05
	0.1	0.01

After several runs to achieve convergence of the contact analysis, it is seen that plastification for this structure starts when the jack load is about 140 kN. Three load steps are implemented for this reason. First load step is the application of preload, 125 kN, second load step is the application of the jack load up to 140 kN and third load step is the application of the jack load from 140 kN to 180 kN. During the analyses, many convergence difficulties are encountered. Several analysis options are altered in order to overcome the convergence difficulty. As the structure is exposed to plastic deformation, it is thought that large deflection effect, which is an analysis option, may have an effect on the accuracy of the solution. However, one disadvantage of this option is the very long solution times and another one is the convergence difficulties that it causes. Firstly, analyses are tried to be performed using large deflection effects included but it is seen that it is almost impossible to finish the solution as the run times increases drastically and solution does not converge when beyond 140 kN load is passed. To overcome the problem, several finite element models are created and finally in one of the finite element models, it was possible to reach 160 kN jack load with large deflections option enabled. It should be noted that each newly created finite element model was coarser compared to previous one. It is observed that there is no effect of large deflection option for this specific problem. The effect of large deflections option on the results is illustrated in Figure 3.3.

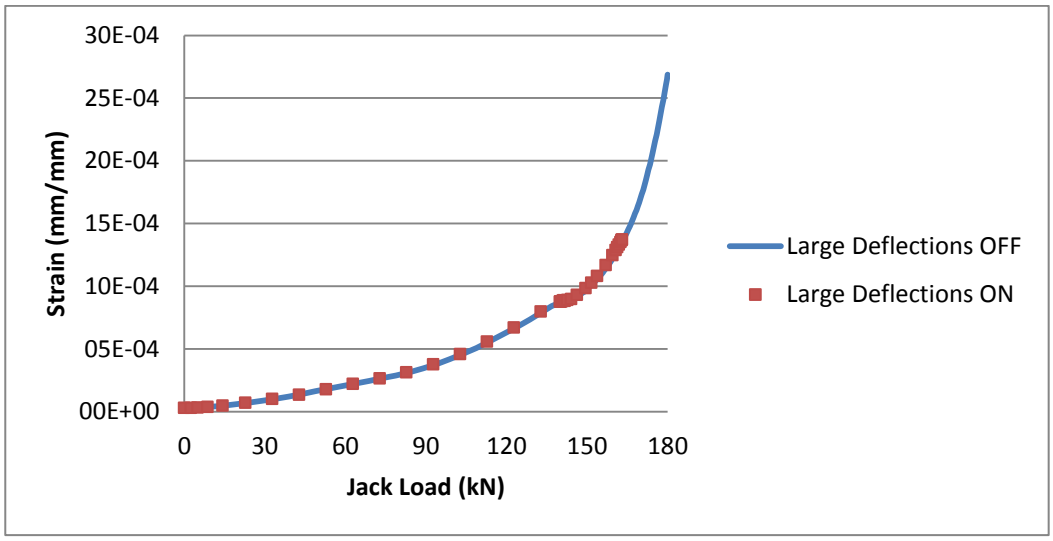

Figure 3.3 - Comparison of analysis setting (large deflections) for the plastic analysis.

It is also known by experience that large deflection command should be included into the analysis when the equivalent strain is over % 2. For this problem, maximum strain that the strain gages read is % 0.3 according to the experimental data [17]. Therefore, it is decided to continue to the analyses excluding the large deflections option.

In the plastic analysis, contact definitions are the same as in the elastic analysis and standard surface-to-surface contact is used between the nut and the end plates, between the bolt and the bolt hole wall and between the end plates as illustrated in Figure 2.10. Same piecewise linear constitutive material models given in Chapter 2 are used for the end plates, circular hallow sections and high strength bolts.

3.3 Results

Error definition in equation 2.2 is not used for the plastic analysis, because the order of the strain results differs depending on the load condition. Variation of strain values with respect to jack load are presented in the following section. The regions with plastic deformation at 180 kN jack load is given in Appendix B.

3.3.1 Comparison of the experimental strain reading with the finite element solution for different contact algorithms

From the previous experience, it was known that Pure Lagrange and Lagrange & Penalty methods could result in convergence problems in non-linear contact analysis; hence, only Augmented Lagrange and Pure Penalty methods are included in the analyses performed in this section. Contact stiffness and penetration tolerance factors are kept constant and chosen as default values 1 and 0.1, respectively, and comparison of different contact algorithms are presented.

The results for the Augmented Lagrange and the Pure Penalty methods are illustrated in Figure 3.4.

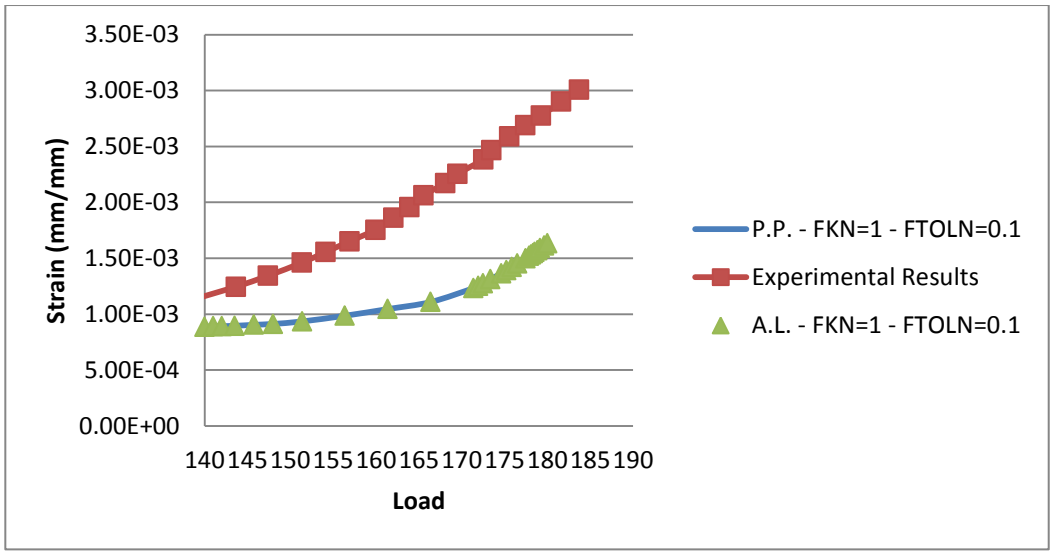

Figure 3.4 - Load vs. strain graph comparing the contact algorithms when FKN=1 and FTOLN=0.1

It is observed that Augmented Lagrange and Pure Penalty methods are similar in terms of accuracy. However, it is also observed during the analyses that Augmented Lagrange method is advantageous because the results are acquired with less number of iterations compared to the Pure Penalty method. Results given in Figure 3.4 show that finite element method underestimates the strain results for both of the contact algorithms. A reason for the discrepancy in the

finite element analysis might be material models. Material models during the analysis are assumed as bilinear constitutive models which do not represent the real material data. It should be noted that in general in the design practice, numerical analyses giving conservative results are preferred, if numerical results do not match with the experimental results.

3.3.2 Comparison of the experimental strain reading with the finite element solution for different contact stiffness factors

Accuracy, run time and convergence behavior of the contact problems are known to be highly dependent on the contact stiffness factor used in the analyses. Five different values of contact stiffness factors are compared using the Augmented Lagrange method and for the penetration tolerance factor value 0.1 in Figure 3.5.

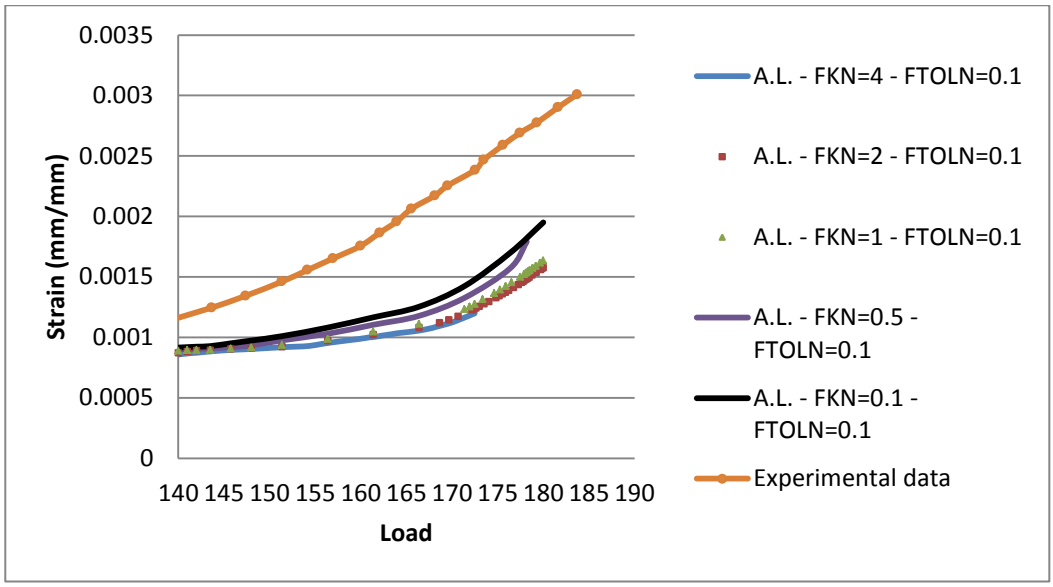

Figure 3.5 - Load vs. strain graph comparing FKN when the contact algorithm is Augmented Lagrange and FTOLN=0.1

It is observed that contact stiffness factor value has a strong influence on the results for this structure. After plastification, lower contact stiffness factor values seem to give more accurate results but still using higher contact stiffness values are suggested because most of the structures are designed in elastic limits. It is

also seen that increasing the contact stiffness factor too much may cause very long solution times and convergence issues arise. Therefore, maximum value of contact stiffness is taken as 2 for this case. It should be noted that for the contact stiffness factor 4, converged solutions could not be obtained till 180 kN.

3.3.3 Comparison of the experimental strain reading with the finite element solution for different penetration tolerance factors

It is known that a decrease in the penetration tolerance factor is supposed to increase the accuracy of the contact analyses. But the results of the elastic analyses showed that there is no effect of penetration tolerance factor on the accuracy of the bolted joint analyses. Using the penetration tolerance values stated in Table 3.1, results presented in Figure 3.6 are obtained.

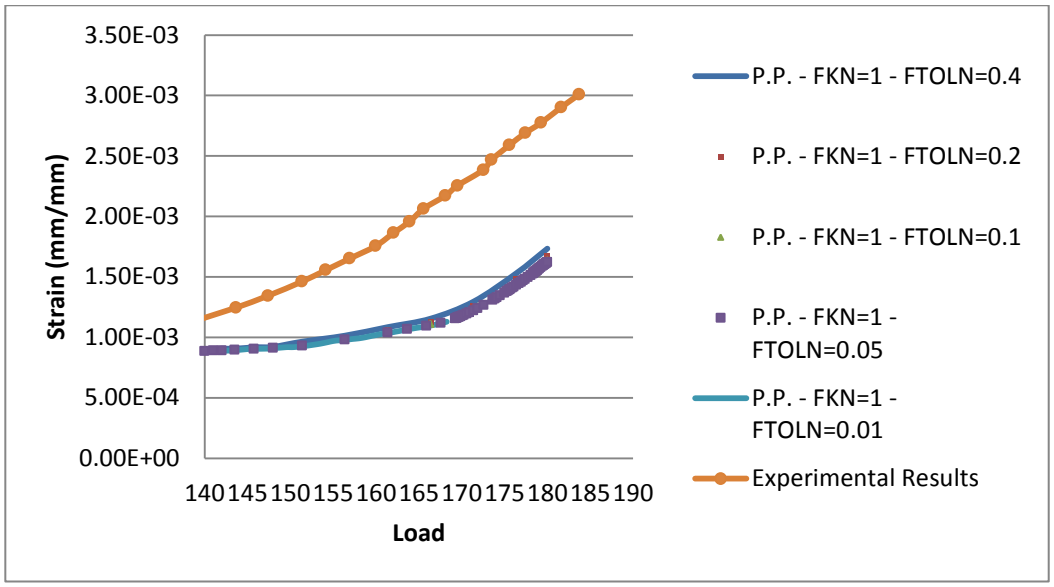

Figure 3.6 - Load vs. strain graph comparing FTOLN for the Pure Penalty contact algorithm and FKN=1

From Figure 3.6 it is seen that, as in the elastic analysis, there is no significant effect of the penetration tolerance factor on the accuracy of the plastic analyses. However, it is observed that number of iterations increases excessively with a decrease in penetration tolerance; thus, the use of high penetration tolerance

factors such as 0.4 is suggested for the least number iterations without compromising the accuracy.

3.4 Conclusion for the Finite Element Analyses of the Bolted Flange Structure in Plastic Limits

In this chapter, effects of the contact algorithm, contact stiffness factor and the penetration tolerance factor on the accuracy and the solution time for the nonlinear contact analysis within the plastic range are investigated. For the contact algorithm, Pure Penalty and Augmented Lagrange algorithms are used and it is seen that contact algorithm does not have much influence on the accuracy. Penetration tolerance factor is found to have almost no effect on the accuracy of this problem for the analyses in the elastic range but for plastic analyses it is seen that there are minor changes in the solution with the variation of the penetration tolerance factor. On the other hand, penetration tolerance factor has a significant effect on the solution time. When lower penetration tolerance factors are used the number cumulative iterations and the solution time increases so using higher penetration tolerance factor values with Augmented Lagrange method is suggested considering their effect on the solution time. On the other hand, contact stiffness factor directly affects both accuracy and the solution time of the analyses. Using too high contact stiffness factor values increases the solution time significantly but the accuracy does not increase in the same manner. For this reason, using a moderately high contact stiffness factor value like 2 is found to be reasonable as in elastic analyses. However, results are inaccurate and unconservative when elastic limit is passed when compared to experimental data. The reason for inaccurate results may be the piecewise linear constitutive material models which are used for bolts, CHS and end plates.

CHAPTER 4

TENSILE TEST OF BOLTED L-BRACKECTS AND VALIDATION WITH FINITE ELEMENT METHOD

4.1 Experiments

4.1.1 Specimens

Symmetrical L-brackets with one bolt are subjected to tensile loading and strain vs. load data is recorded simultaneously using the strain gages and Digital Image Correlation (DIC) method. In order to decide on the geometrical properties of the L-brackets, a number of finite element analyses are performed. In the analyses, material, bolt size, bolt location and thickness of the L-brackets are changed. Two choices for the material type are considered which are steel and aluminum. In order to get reasonable strain results during the DIC measurements it is decided to use aluminum specimens. Using the results of finite element analyses strain gage locations and geometrical specifications of the specimens are determined. Strain gage locations are chosen as close as possible to the bolt to see the effect of contact mechanics during the analyses and the experiments better. Two specimens, A1 and B1, are manufactured from Aluminum 2024 T351 material and bolted with one Grade 8.8 Steel bolt and nut. Three dimensional assembly of the L-bracket is given in Figure 4.1 and the geometrical specifications for specimens A1 and B1 are given in Figure 4.2 and Figure 4.3 and details are given in Table 4.1.

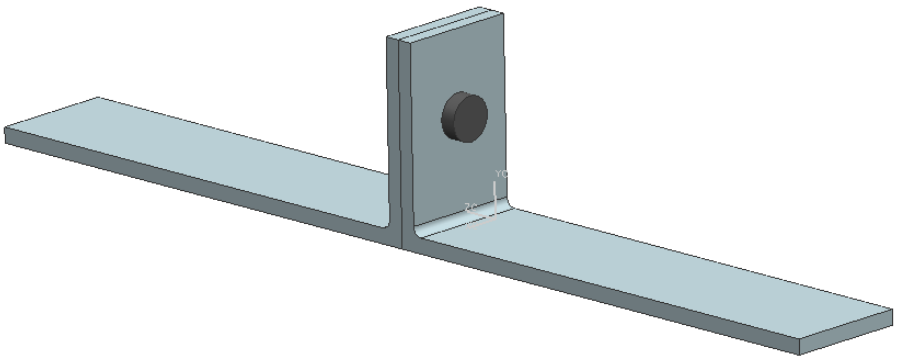

Figure 4.1 – 3D assembly of the L-bracket

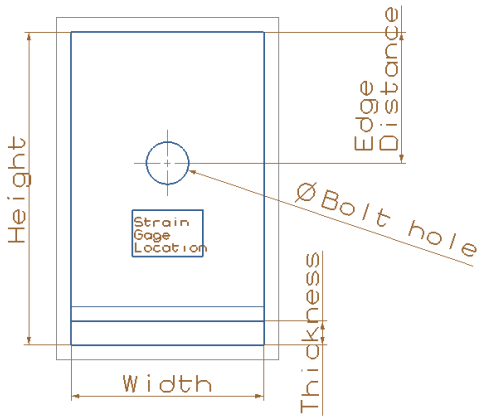

Figure 4.2 – Geometrical specifications of L-brackets

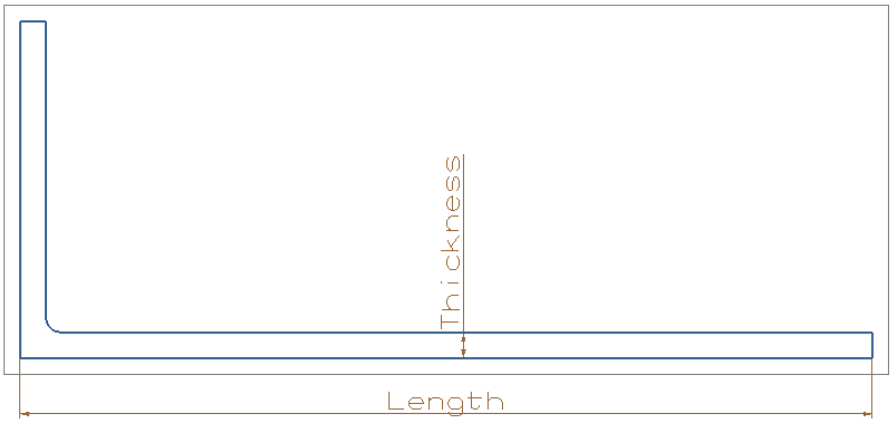

Figure 4.3 – Geometrical specifications of L-brackets

Table 4.1 – Geometrical details of A1 and B1 geometries

	Height	Edge Distance	Thickness	Width	Length
A1	65 mm	19.2 mm	5 mm	40 mm	165 mm
B1	65 mm	31.2 mm	5 mm	40 mm	165mm

When 10 mm thickness is used during finite element analyses it was not possible to observe sufficiently high strain at the strain gage locations. Therefore, for A1 and B1 geometries 5 mm thickness is chosen, because higher thickness reduces the amount of strain at the strain gage locations. Only difference between the specimens is the location of the bolt. For A1 bolt hole edge distance is 19.2 mm and for B1 it is 31.2 mm.

4.1.2 Experimental Setup

Initially, both of the bolts are torqued using a torque meter (see Figure 4.4) around 22 N.m [23]. Torqueing procedure is shown in Figure 4.5.

Figure 4.4 – Torque meter

Figure 4.5 – Torqueing Procedure

After torqueing the bolts strain gages are glued to the previously determined locations. For A1 geometry gluing the strain gages is easier when compared to B1 because there is more space to work on. For specimen A1 strain rosette and for speciemen B1 single strain gage is used considering the practical difficulties. The specimens with strain gages are shown in Figure 4.6.

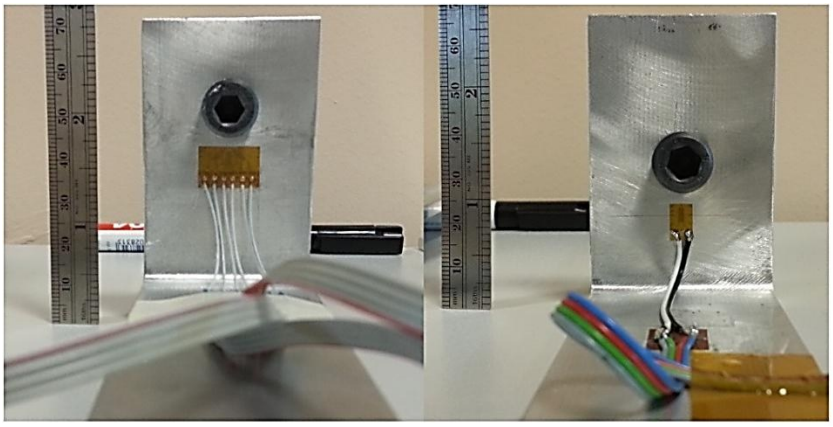

Figure 4.6 – Specimens and the strain gage locations

Strain gages are connected to the data acquisition system and specimens are placed to the grids of 250 kN tensile testing machine along their long edges as

shown in Figure 4.7. According to the testing specification 60mm of the specimens must remain inside the grids at both sides.

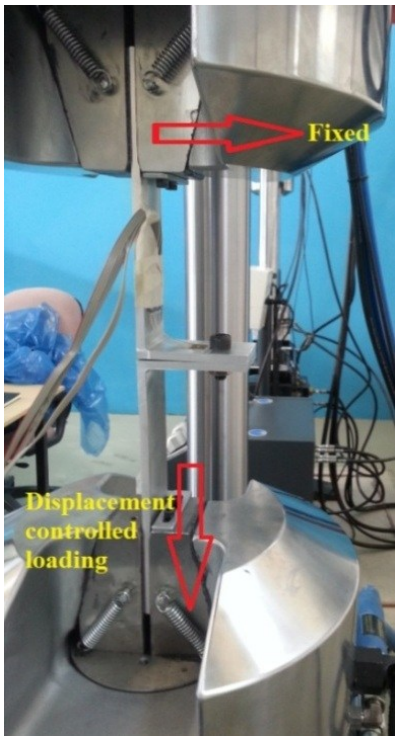

Figure 4.7 – Assembly of test machine and the test specimen

For both of the specimens, the side of the L-bracket with the strain gages is connected to the fixed grip of the testing machine, because there is higher strain at the fixed side of the specimens when the results of finite element analyses are considered.

DIC test setup is shown in Figure 4.8. Specimen is painted with the special DIC paint where the DIC measurements are taken. Specimen is connected to the tensile testing machine, DIC camera is calibrated and measurements are taken simultaneously with the loading

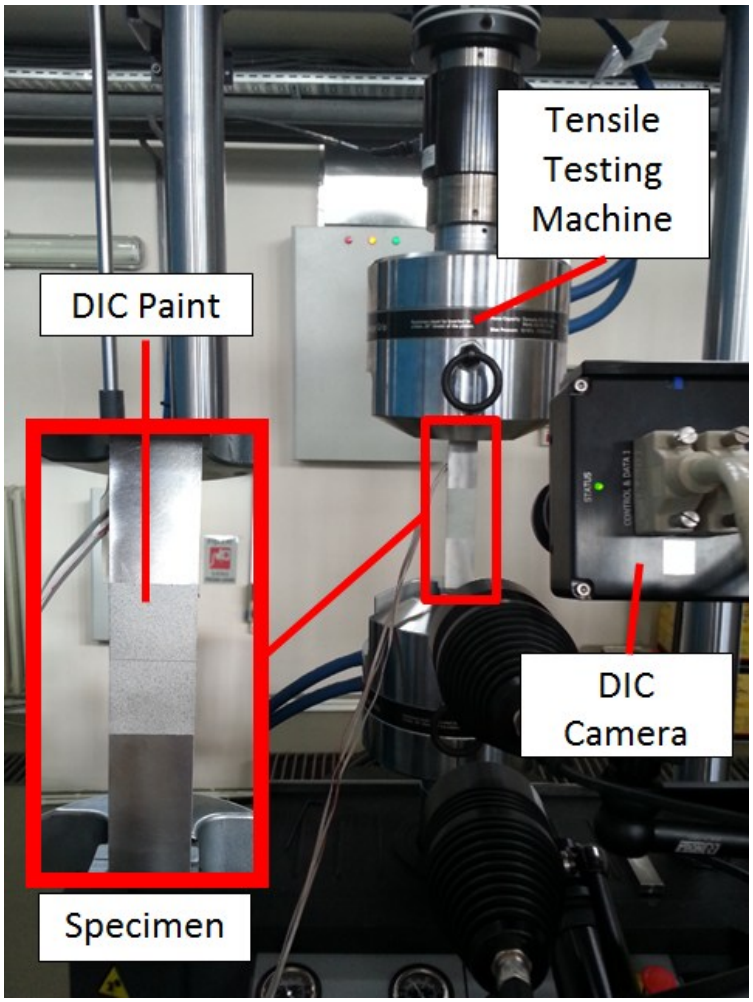

Figure 4.8 – DIC test setup

4.1.3 Experimental Results

Tests are performed in displacement control mode up to 1 kN loading because plastic deformation starts near bolt holes according to the results of finite element analyses. For specimen A1, three tests are conducted and tests 2 and 3 are performed successively. During tests 2 and 3 DIC measurements are also taken for specimen A1. For specimen B1, three tests are performed successively. For both of the specimens, load displacement and load strain graphs for tests 2 and 3 differ from first tests, because there is probably some local plastic deformation.

Displacement vs. load curves, of three tests for both of the specimens are given in Figure 4.9 and Figure 4.10.

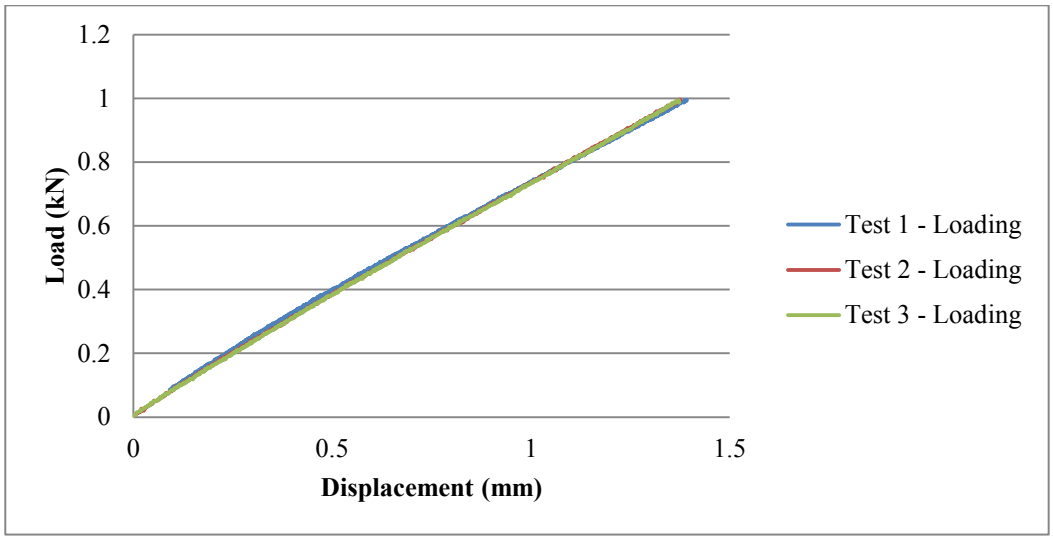

Figure 4.9 – Load vs. displacement comparison for tests during loading for specimen A1

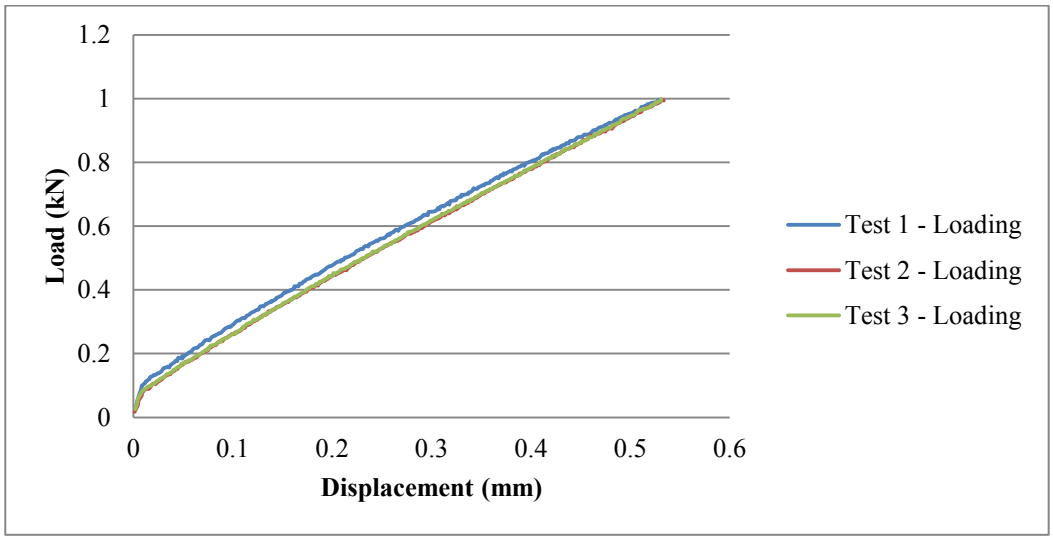

Figure 4.10 - Load vs. displacement comparison for tests during loading for specimen B1

For specimen B1, the difference between tests is clear in the full load and displacement range. Taking a closer look to the load displacement curves, the difference between the tests can also be seen as shown in Figure 4.11 and Figure

4.12. The curves almost perfectly match for the second and the third test, but first tests result in higher load levels for the same amount displacement which indicates plastic deformation.

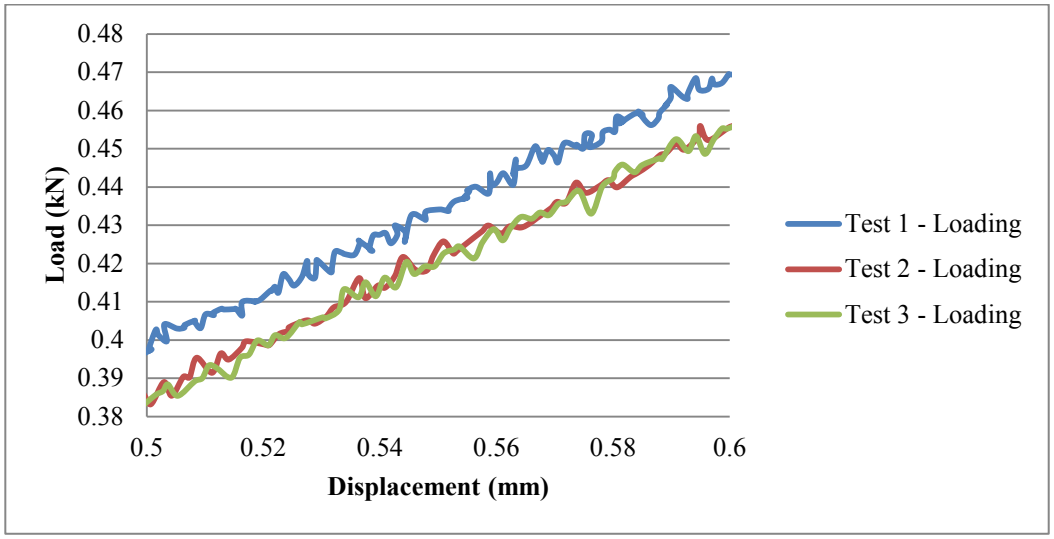

Figure 4.11 – Load vs. displacement comparison between 0.5 - 0.6 mm for tests during loading of specimen A1

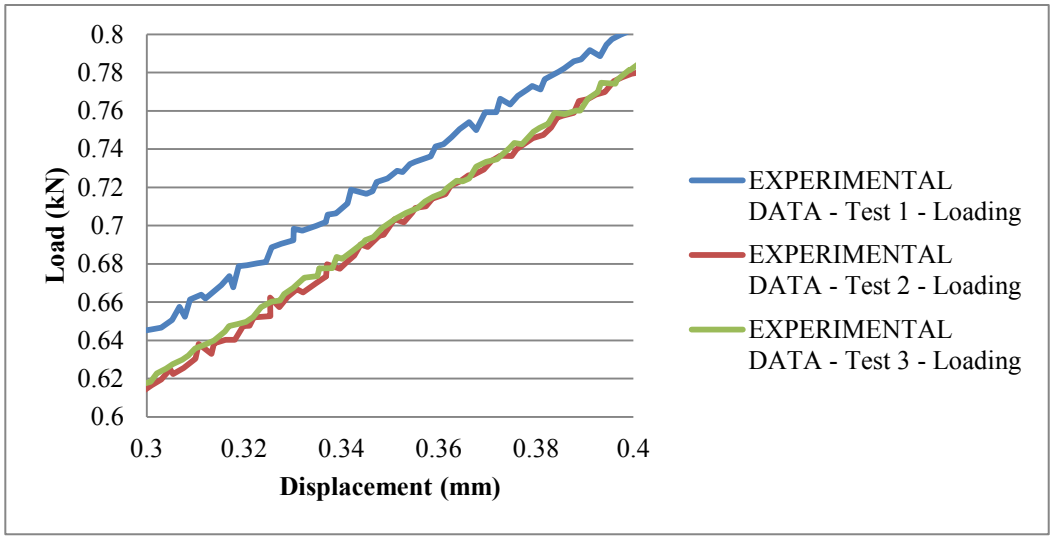

Figure 4.12 - Load vs. displacement comparison between 0.3 - 0.4 mm for tests during loading of specimen B1

In Figure 4.10, there is an obvious slope change in the load displacement curve at low loads and the reason might be a possible contact status change of the contacting bodies. The reason for the slope change is discussed in the Finite Element Analysis section.

4.2 Finite Element Analysis

A number of analyses are performed in order to observe the effects of geometrical specifications on the prying load [24]. Prying load is present due to the contact between the flange and the base plate which is the second flange in this study. Prying load is known to increase the bolt load and may cause the failure of the bolts. It is known that preload increases the prying ratio so as the b/a ratio. Here, a is the edge distance and b is the "height-edge distance" for L-brackets. Three different specimens are analyzed with b/a ratios 1.948, 1.48 and 1.14 in order to observe the effect of b/a ratio on the prying ratio and three specimens are solved with and without preload. Preload value is 14 kN. Prying ratio equation for L sections without preload with different values of t/D ratios are given in equation 4.1 [24]. Here, t is the thickness and D is the bolt diameter.

$$\left(\frac{\mathrm{Q}}{\mathrm{F}}\right)_{L} = \begin{Bmatrix} 2b/a & t/D = 0.3 \\ b/a & t/D = 0.5 \\ 3b/4a & t/D \geq 0.7 \end{Bmatrix} \tag{4.1}$$

When preload is present prying ratio formula is [24]:

$$\left(\frac{\mathrm{Q}}{\mathrm{F}}\right)_{LP} = \begin{Bmatrix} 13b/6a & t/D = 0.3 \\ 11b/10a & t/D = 0.5 \\ 4b/5a & t/D \geq 0.7 \end{Bmatrix} \tag{4.2}$$

For A1 and B1 specimens, t/D ratio is 0.625 so without preload prying ratio is supposed to be between b/a and $0.75 \times b/a$ and with preload prying ratio is supposed to be between $1.1b/a$ and $0.8 \times b/a$. In Figure 4.13 and Figure 4.14, effects of preload and b/a ratio on the prying ratio (Q/F) are shown. It is clear that preload increases the prying ratio drastically but one should note that for higher b/a ratios prying ratio is higher, with or without the presence of preload. However, equations 4.1 and 4.2 are not satisfied and prying ratios are higher. But one should keep in mind that these equations are derived when the L section is fixed to a rigid body [24]. As the boundary conditions are different, results are still satisfactory because general outcomes are the same.

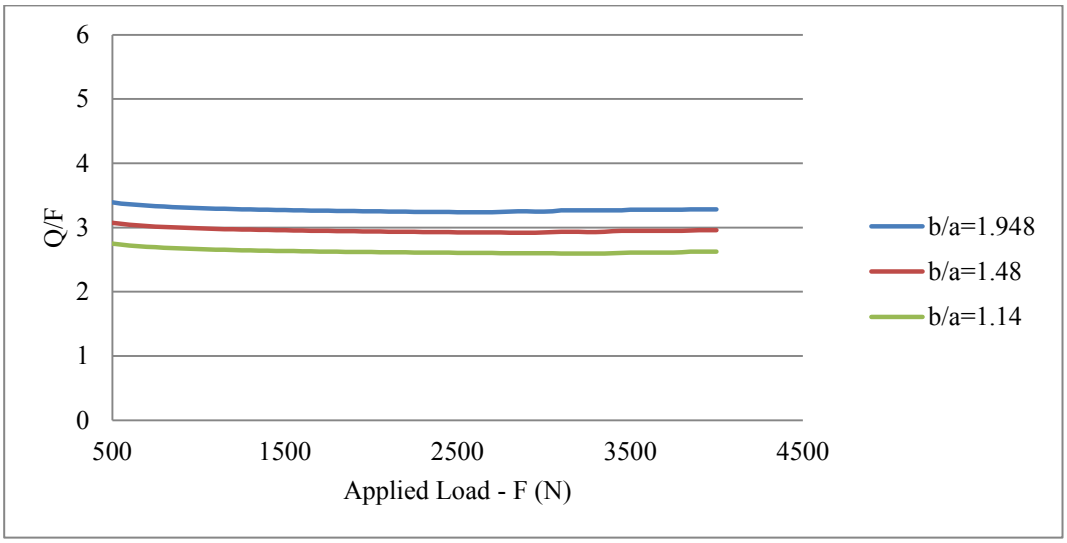

Figure 4.13 – Effect of b/a ratio on prying ratio without preload

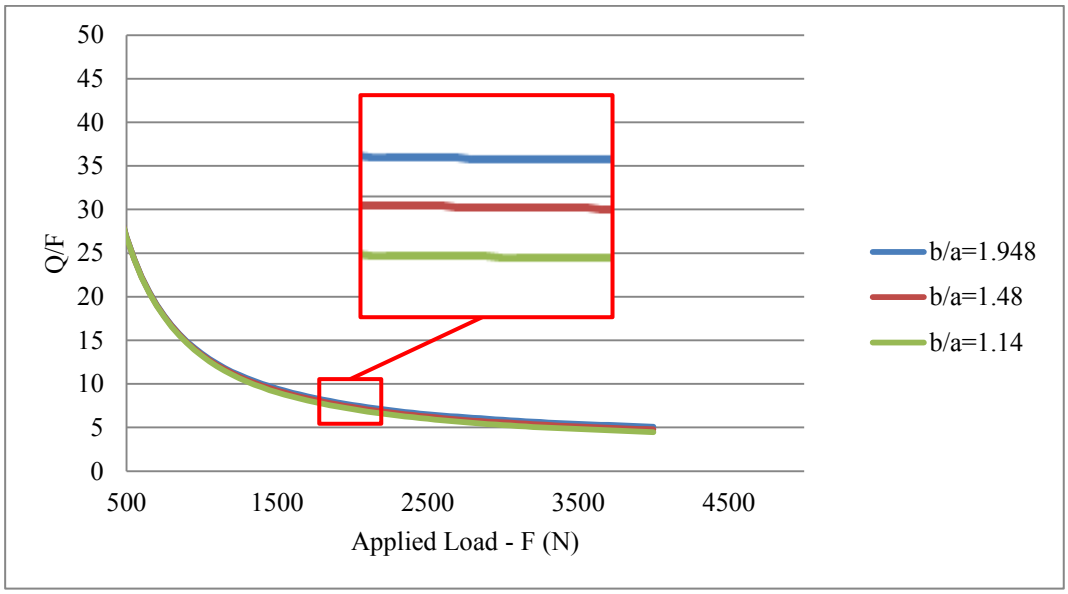

Figure 4.14 - Effect of b/a ratio on prying ratio with preload

Finite element analyses that investigate the effects of major contact parameters on the accuracy of the results for both specimens are performed. It should be noted that finite element analysis is performed with two load cases. First load case is the preload step and the second load case is the loading step. After the preload step there is a certain amount of strain at the strain gage locations due to pretension of the bolts in the finite element analysis. But in the experiments, the strain gages are tared before the loading starts and the strain due to preload is not present before the loading starts. In order to simulate the real world problem for finite element analysis, the strain readings of the finite element analyses at each load step are shifted with the strain data right after preload step and graphs are plotted accordingly. Shifting procedure is illustrated in Appendix C.

One finite element model is prepared for each specimen using SOLID 185 elements of ANSYS considering the mesh convergence which is primarily performed. SOLID185 element type has 8 nodes. There are 56627 elements with 58434 nodes and 51420 elements with 53656 nodes for A1 and B1 specimens respectively. For both of the models strain gage locations are modeled with fine

mesh structure in order get more accurate results. Finite element models for A1 and B1 specimens are shown in Figure 4.15.

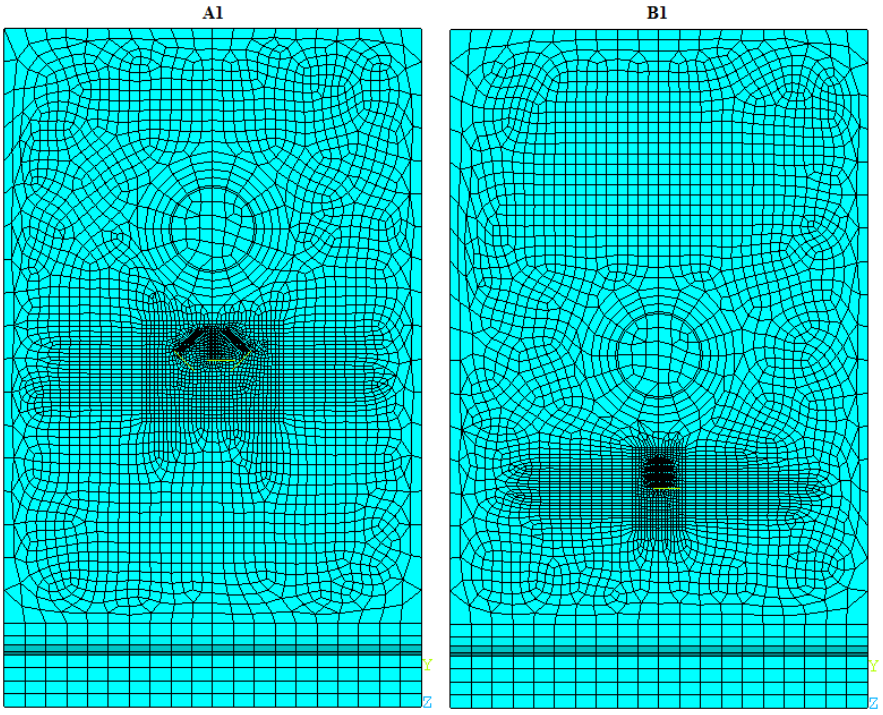

Figure 4.15 – Finite element models of specimens A1 and B1

For specimen A1 strain rosette and for specimen B1 single axis strain gage is used. In Figure 4.16, strain gages on the finite element models are shown.

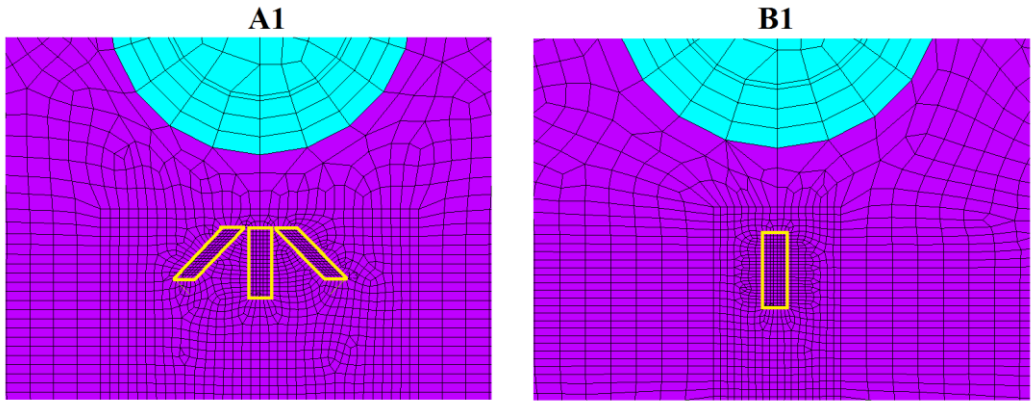

Figure 4.16 – Strain gage locations on specimens A1 and B1

Standard contact definition is used for both specimens. Contact is defined between the two flanges, bolt head and flange, nut and flange, bolt shank and bolt hole as shown in Figure 4.17. Between the two aluminum flanges coefficient of friction is taken as 0.646 and between the bolt and the flanges the friction coefficient is taken as 0.466 [25].

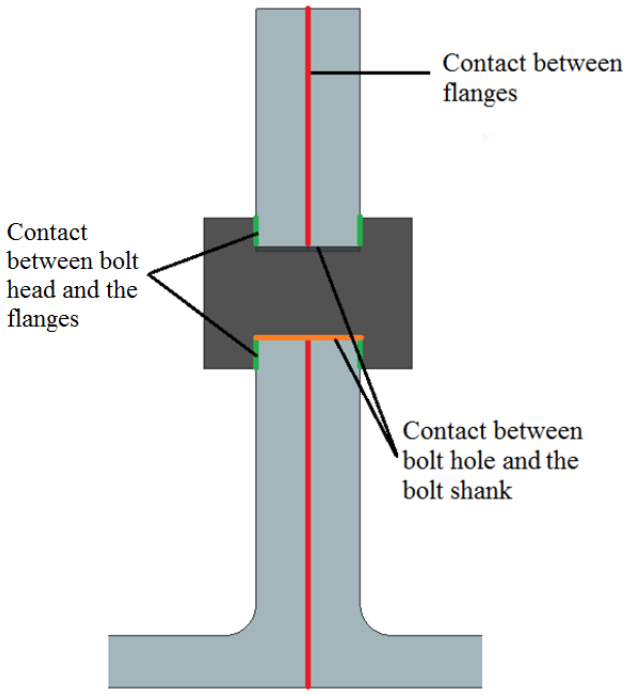

Figure 4.17 – Contact definitions

Isotropic material definition is assumed for all of the materials. For bolts and nuts the elastic modulus is taken as 206 GPa [26] and Poisson's ratio is taken as 0.3 and for flanges the elastic modulus is taken as 72.4 GPa [27] and Poisson's ratio is taken as 0.3.

Bolt preload is calculated as 14kN using empirical relations. Upper edges are 1st and 2nd faces, bottom faces are 3rd and 4th faces. Boundary conditions are shown in Figure 4.18. Specimens are clamped by the grip of the test machine at the bottom of the L-bracket during the tests. Boundary conditions applied at faces 1-4, during the preload and the loading steps are presented in Table 4.2.

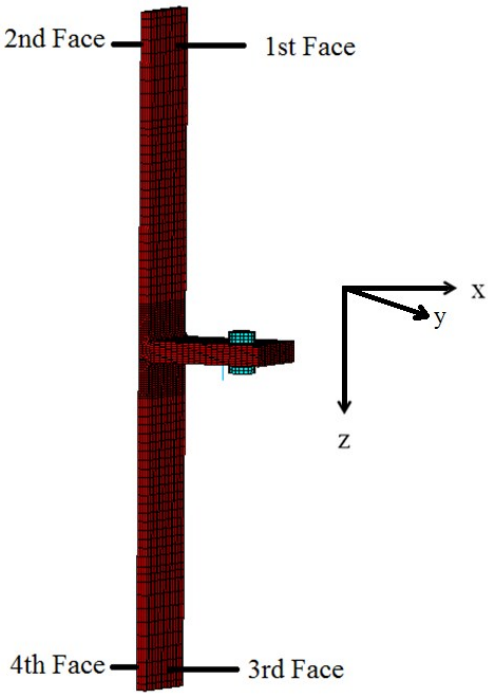

Figure 4.18 – Geometry and coordinate system

Table 4.2 – Boundary conditions for the preload and the loading steps

		Face 1	Face 2	Face 3	Face 4
Preload Step	x	Fixed	Fixed	Free	Free
	y	Fixed	Free	Free	Free
	z	Fixed	Fixed	Free	Free
Loading Step	x	Fixed	Fixed	Fixed	Fixed
	y	Fixed	Free	Fixed	Free
	z	Fixed	Fixed	Displacement Load	Displacement Load

During the preload step, one side of the structure is kept free in order to prevent any reaction forces that can occur during the preload step. The reason for keeping 2^{nd} and 4^{th} faces free in y-direction during both of the steps is to be able to allow structure to deform in the y-direction. If they were fixed Poisson's effects would not be present.

In Table 4.3, the contact parameters that are changed during the parametric study are shown. Parametric study is performed to determine the contact parameters

which account for the closest results to the test results. Pure Lagrange and Lagrange & Penalty combination methods are not included in the analysis because of the possibility of ill-convergence. 50 finite element analyses are performed to cover every combination of the parameters.

Table 4.3 - Parameters that are changed throughout the analysis

Algorithm	**Contact stiffness factor**	**Penetration tolerance factor**
Augmented Lagrange method	4	0.4
Pure Penalty method	2	0.2
	1	0.1
	0.5	0.05
	0.1	0.01

A macro is written using ANSYS design language in order to make 50 analyses and acquire the results with less effort. Macro calls the finite element models, changes the contact parameters in three different do loops (algorithm, contact stiffness factor and penetration tolerance factor), reads the previously created load step files that consists of preload and loading steps, solves the model, averages the strain values in the strain gage directions by using the result coordinate systems generated and writes the average strain values to a text file for each load increment. In Figure 4.19, result coordinate systems and nodal components that represent strain gages are shown with “a”, “b” and “c” are the three strain gages on the strain rosette.

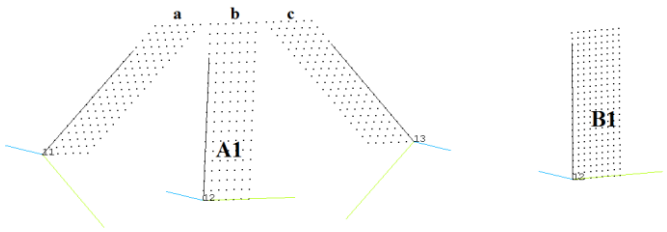

Figure 4.19 – Strain gages and result coordinate systems used for each strain gage location

4.2.1 Results for Specimen A1

Three strain gage readings are recorded for specimen A1 for each test. 45^{o} aligned strain gages “a” and “c” gave similar behavior as the vertical strain gage “b”. Therefore, comparison of the test results with finite element analysis results is made only for strain gage “b”. Moreover, comparison of finite element analyses results is made with test 2 only, because test 2 and 3 gave almost same result.

In Figure 4.20, total displacement vector sum of A1 specimen is shown with 1kN tensile load.

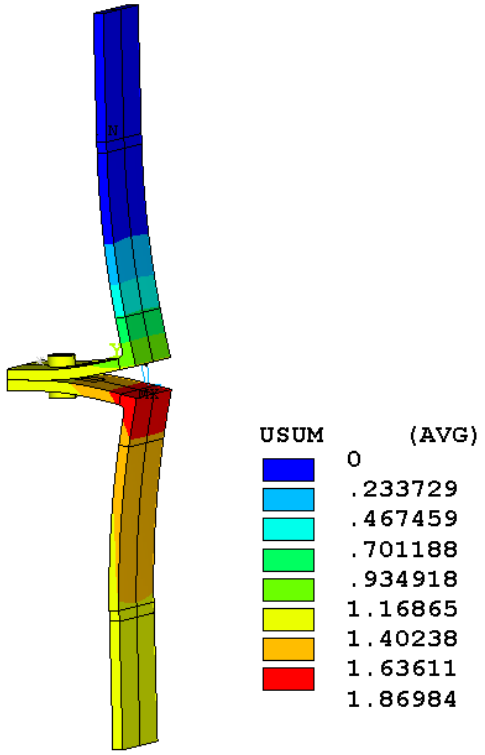

Figure 4.20 – Displacement vector sum of A1 specimen at 1kN tensile load

Comparison of the experimental displacement-load and strain readings with the finite element solution for different contact algorithms

Augmented Lagrange and Pure Penalty contact algorithms are used to understand their effect on the accuracy and the solution time of the problem. In the previous chapters both of the contact algorithms resulted in same results in terms of accuracy in almost every case. For specimen A1, 25 analysis are performed utilizing Augmented Lagrange and Pure Penalty algorithms and it is seen that strain results are exactly the same for both algorithms. To decide on the algorithm to continue the analyses, total number of iterations required for solution is checked. Number of iterations turned out to be same for both algorithms when other contact parameters (contact stiffness factor and penetration tolerance factor) are the same. It can be concluded that, for the specific problem using Augmented Lagrange or Pure Penalty contact algorithms does not change accuracy and solution time. Therefore, in the following results for the effect of contact stiffness factor and the penetration tolerance factor are given for the Augmented Lagrange algorithm.

Comparison of the experimental displacement-load and strain readings with the finite element solution for different contact stiffness factors

It is known from previous chapters that, accuracy and solution time are highly dependent on the contact stiffness factor. In order to understand the effect of contact stiffness factor on the accuracy and the solution time five parameters given in Table 4.3 are used and results of the finite element analysis simulating the tensile test are compared with experimental data of the 2nd test of specimen A1. Analyses are performed for five different values of penetration tolerance factors but results are given different contact stiffness factors when the penetration tolerance factor is 0.1 which is the default value for penetration tolerance in ANSYS APDL. Figure 4.21 shows the load vs. displacement graph for different

contact stiffness factor (FKN). In Figure 4.21, it is clear that general tendency of the finite element results and the experimental data is similar.

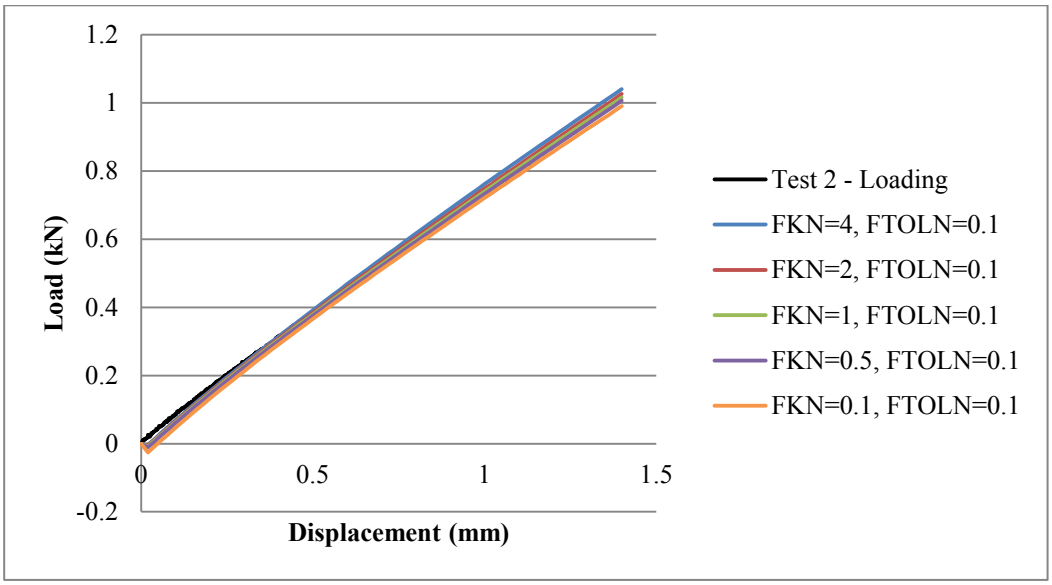

Figure 4.21 - Load vs. displacement graph for different contact stiffness factors (FKN) (Contact algorithm: Augmented Lagrange, Penetration tolerance factor (FTOLN=0.1)

Figure 4.22 shows the zoomed plot of load vs. displacement graph for different contact stiffness factor (FKN). Zooming in to very low loads, it is observed that in the finite element analysis load decreases although the displacement is increased as shown in Figure 4.22. It is also seen that by increasing contact stiffness factor finite element solution gets closer to the test result. But one should also note that total number of iterations also increases with the increase in the contact stiffness factor.

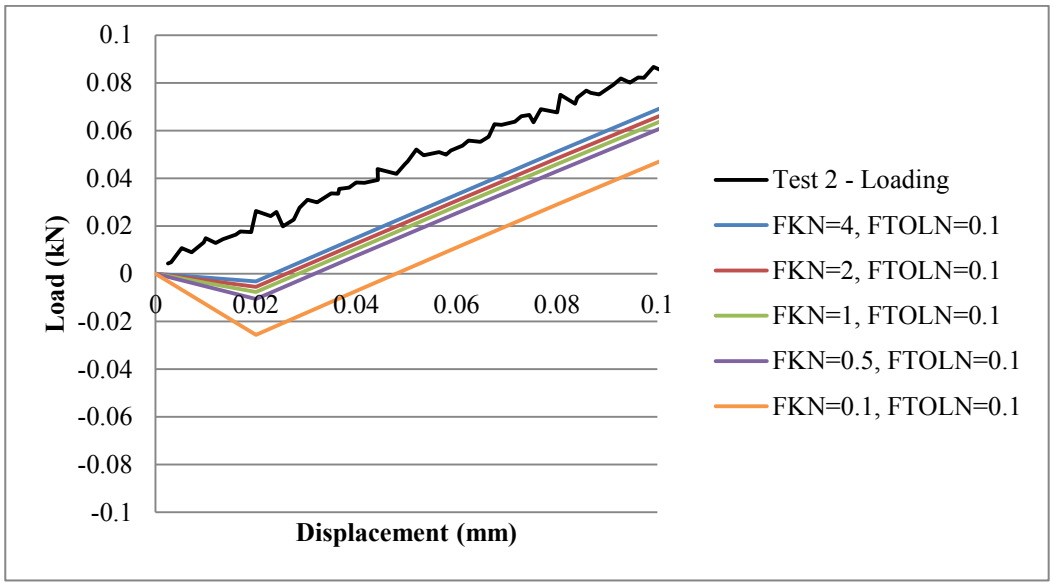

Figure 4.22 – Zoomed plot of load vs. displacement graph for different contact stiffness factors (FKN) (Contact algorithm: Augmented Lagrange, Penetration tolerance factor (FTOLN=0.1)

Investigating the reason for the load drop at the beginning of the load – displacement curve, it is discovered that there is a drastic change of the contact status of the contact region between flanges. The contact status at zero displacement and at the next increment is shown in Figure 4.23. It should be noted that finite element method is an estimation of the real world problems and sudden changes in contact status in the finite element solution affects the resultant curves considerably.

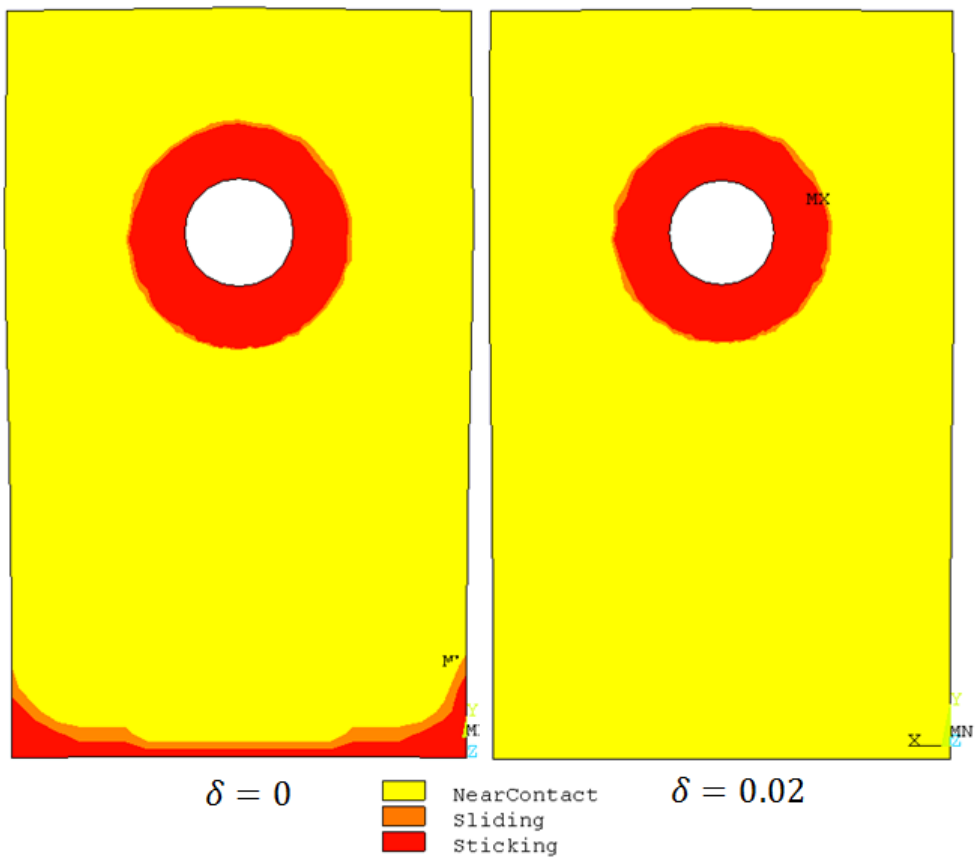

Figure 4.23 – Contact status of contact region between flanges (see Figure 4.17) at zero displacement and 0.02 mm displacement.

In Figure 4.24, comparison of load vs. strain results between the experimental data and finite element solution with different choices of contact stiffness factors is given for strain gage “b”. Because of the contact status change at the beginning of the loading, there are some sudden changes in the load strain curves as well but with the increase in the load (displacement) the results become comparable to the experimental results.

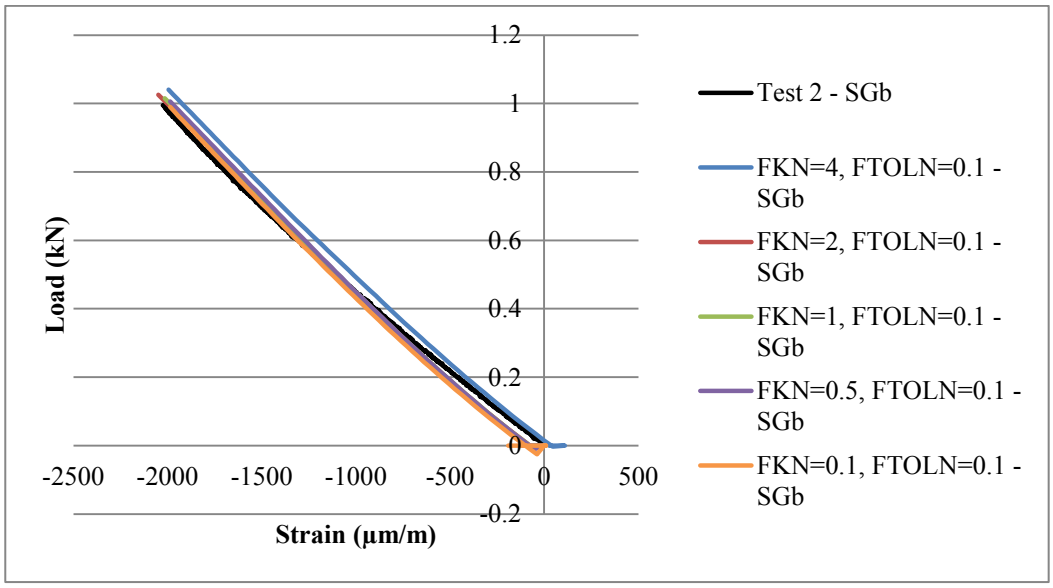

Figure 4.24 - Load vs. strain graph for different contact stiffness factors (FKN) (Contact algorithm: Augmented Lagrange, Penetration tolerance factor (FTOLN)=0.1)

In order to understand the effect of contact stiffness factor on the finite element solution, the zoomed plot is given in Figure 4.25. It is seen that there is good agreement of the finite element solution with the experimental data. When contact stiffness factor (FKN) is 2 or lower, finite element solution predicts conservative strains compared to the test data. For a high contact stiffness factor such as 4, finite element solution underestimates the strain. When both load displacement and load strain curves are considered, using a contact stiffness factor 2 is suggested, because finite element solution utilizing a contact stiffness factor of 2 gives close results to the experimental data.

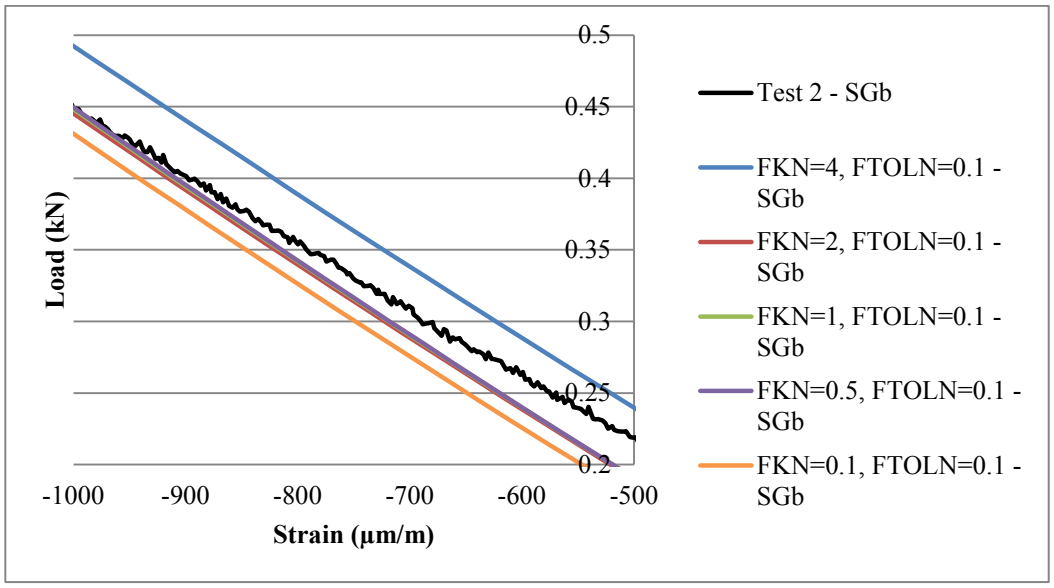

Figure 4.25 – Zoomed load vs. strain graph for different contact stiffness factor (FKN) (Contact algorithm: Augmented Lagrange, Penetration tolerance factor (FTOLN)=0.1)

Comparison of the experimental displacement-load and strain readings with the finite element solution for different penetration tolerance factors

In previous chapters, penetration tolerance factor is found to have no effect on the accuracy of the solution in almost all of the cases. However, the solution time, convergence and total number of iterations of the finite element analysis is affected the by the penetration tolerance factor. Increasing penetration tolerance factor is known to decrease accuracy and the solution time and vice versa. It is also concluded in previous chapters that high penetration tolerance factor does not decrease the accuracy but decreases the solution time and total number of iterations. Therefore, it was suggested that using higher values for the penetration tolerance factor is recommended to decrease the solution times without compromising the accuracy.

For specimen A1, five different penetration tolerance factor values are considered and each one of them is combined with five different values of the contact stiffness factor but the results are given for contact stiffness factor 2.

Figure 4.26 shows the load vs. displacement graph for different penetration tolerance factors (FTOLN).

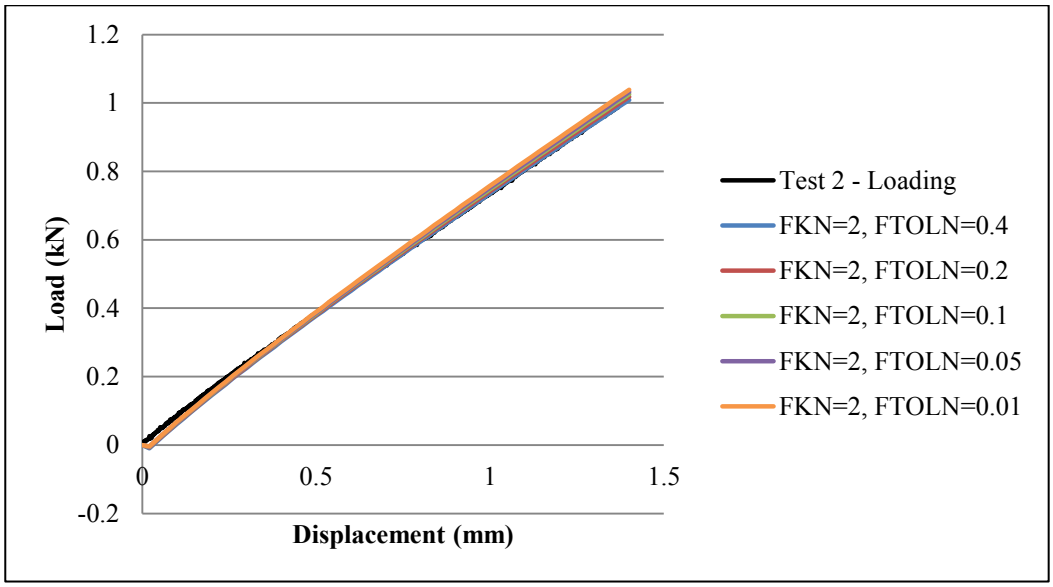

Figure 4.26 - Load vs. displacement graph for different penetration tolerance factors (FTOLN) (Contact algorithm: Augmented Lagrange, Contact stiffness factor (FKN)=2)

Zoomed plot for load-displacement comparison for different choices of penetration tolerance factors is given in Figure 4.27. It is noticed that contrary to the results of previous chapters, penetration tolerance factor affects the results of finite element solution for the L-bracket. Considering the load displacement curve, from Figure 4.27, it can be concluded that, finite element solution obtained utilizing the default value of 0.1 for the penetration tolerance factor, is conservative and compatible with experimental data.

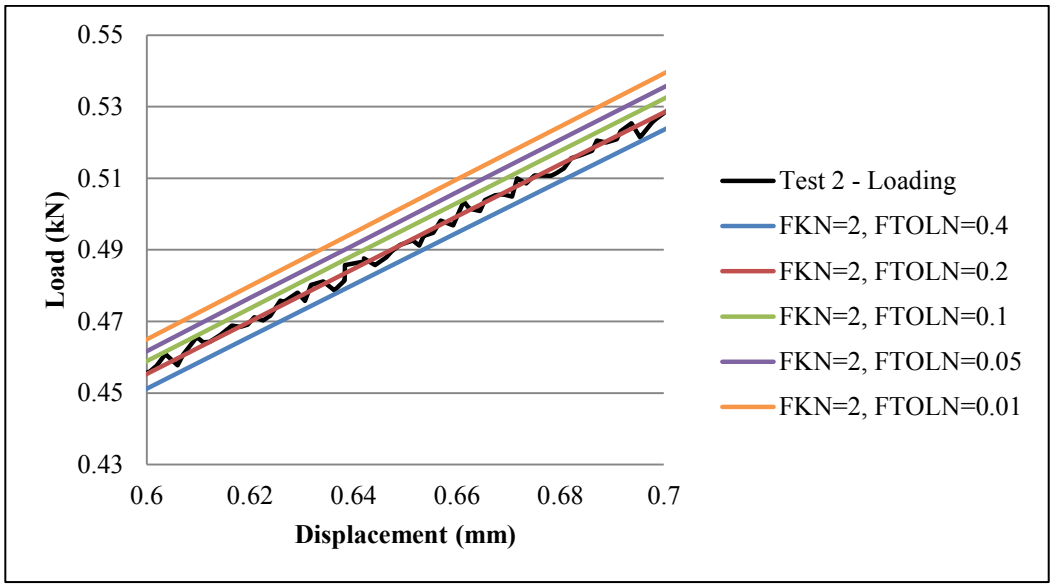

Figure 4.27 – Zoomed load vs. displacement graph for different penetration tolerance factors (FTOLN) (Contact algorithm: Augmented Lagrange, Contact stiffness factor (FKN)=2)

In Figure 4.28 and Figure 4.29, load versus strain graphs for different choices of penetration tolerance factor values are given. Considering the zoomed plot, the results are similar except when penetration tolerance factor is 0.01, which is supposed to give more accurate results. In the design phase, conservative results are expected but when FTOLN is 0.01 the strain results are less conservative and great number of iterations is needed to solve the model. Moreover, the accuracy does not increase with decreasing penetration tolerance factor as much as expected and penetration tolerance factor (FTOLN) 0.1 gives more conservative results with less solution time. Default value for penetration tolerance factor, 0.1, is suggested for this problem.

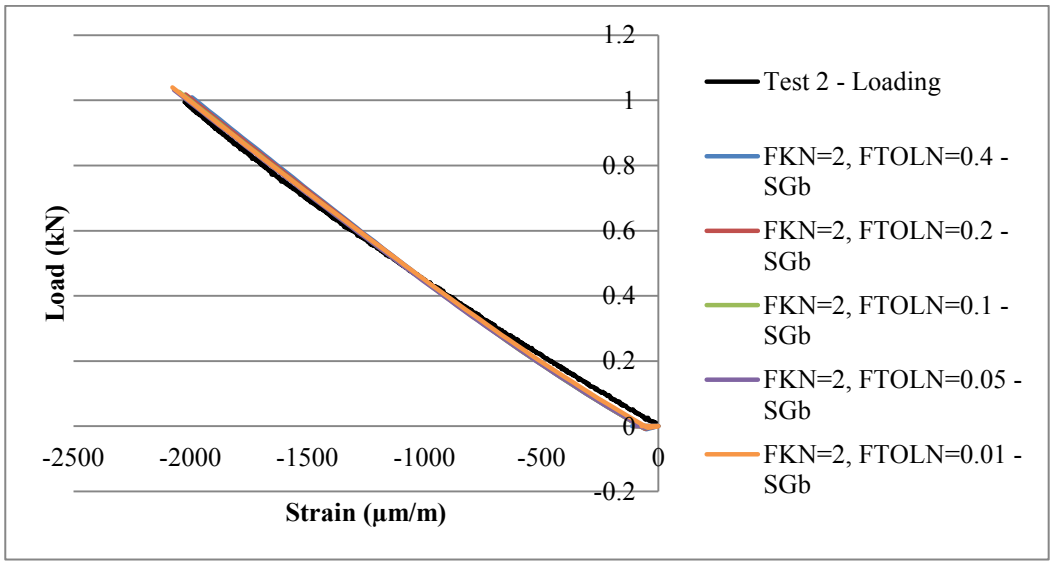

Figure 4.28 - Load vs. strain graph for different penetration tolerance factors (FTOLN) (Contact algorithm: Augmented Lagrange, Contact stiffness factor (FKN)=2)

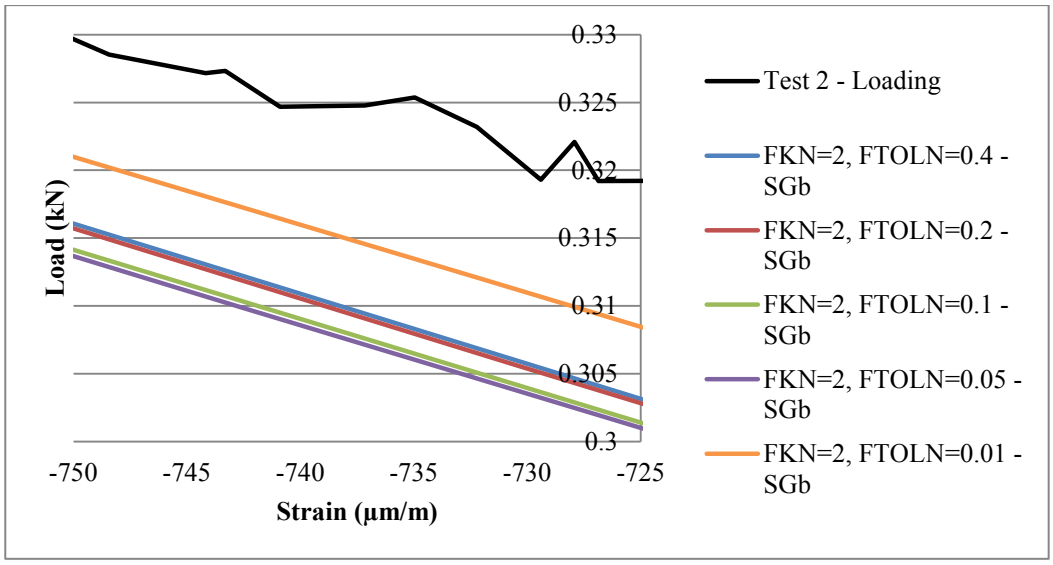

Figure 4.29 – Zoomed load vs. strain graph for different penetration tolerance factors (FTOLN) (Contact algorithm: Augmented Lagrange, Contact stiffness factor (FKN) =1)

Comparison of finite element solution with DIC results

During tests 2 and 3, DIC measurements are taken and comparison of z-displacement (loading direction) between DIC test result and finite element solution is given in Figure 4.30. Figure 4.30 shows that DIC measurements and finite element solution are close in terms of accuracy.

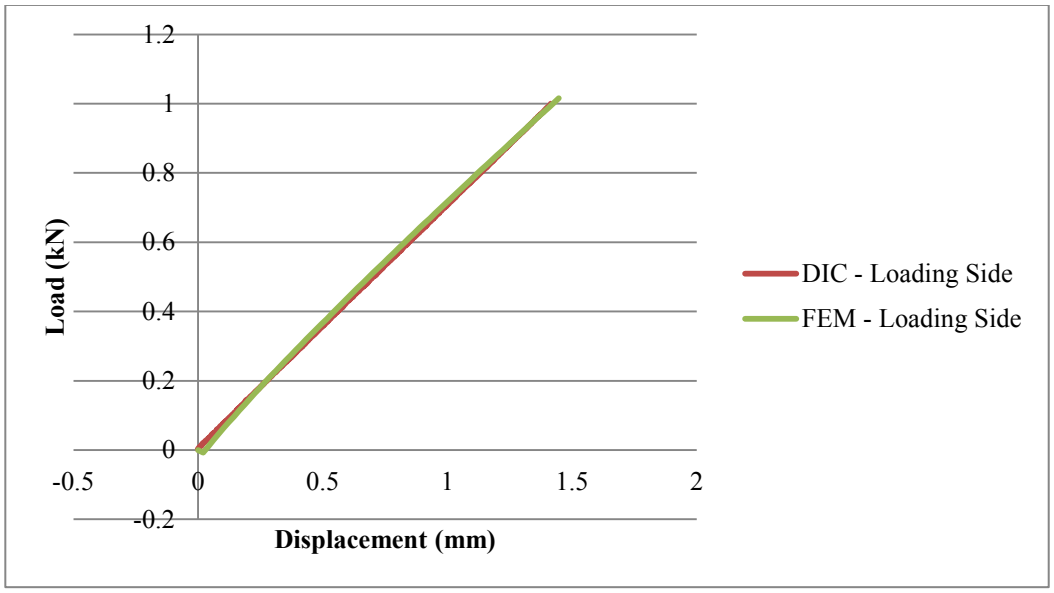

Figure 4.30 - Loading direction displacement comparison of finite element solution with the DIC measurement at the loading side of specimen A1 (Contact algorithm: Augmented Lagrange, FKN=2 and FTOLN=0.1)

DIC method is capable of capturing displacement contours in-plane direction (y-direction) of the specimen because it uses two cameras to take measurements. From the back side of the specimen A1, y-direction displacement results at 1 kN loading are taken using DIC method and results are compared with the finite element solution in Figure 4.31. There is %6 difference between the maximum loading direction displacements obtained by the finite element analysis and DIC measurements.

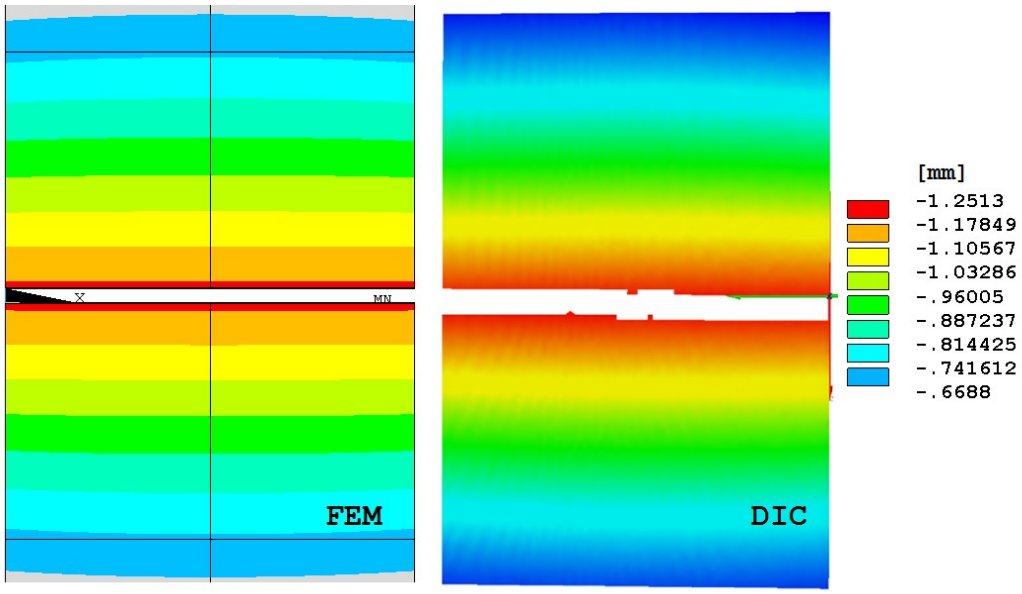

Figure 4.31 – Comparison of y-direction displacements of DIC measurement region (see Figure 4.8) calculated by the finite element solution and measured by DIC

The results are negative in y-direction and 50 times increased scale y-displacement finite element result is shown in Figure 4.32. It is clear that the specimen moves in –y direction when loaded.

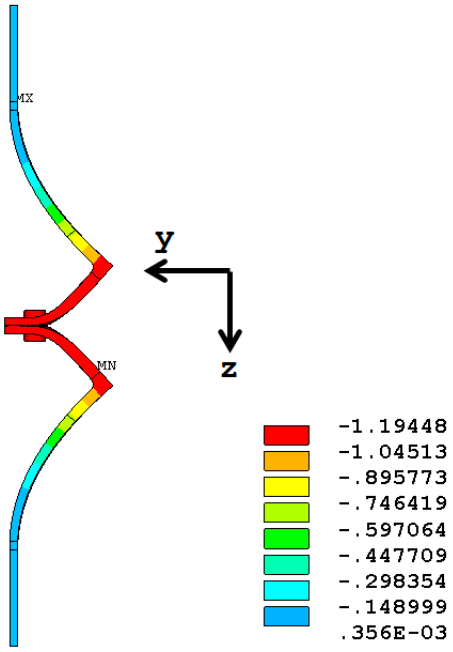

Figure 4.32 – Displacement results of finite element solution in y-direction

4.2.2 Results for Specimen B1

One strain gage is glued to specimen B1 because of the practical difficulties. Tests 2 and 3 produced almost same results so the comparison of the finite element solution with the experimental results is made with Test 2 only.

Total displacement vector sum of B1 specimen with 1kN tensile load is shown in Figure 4.33.

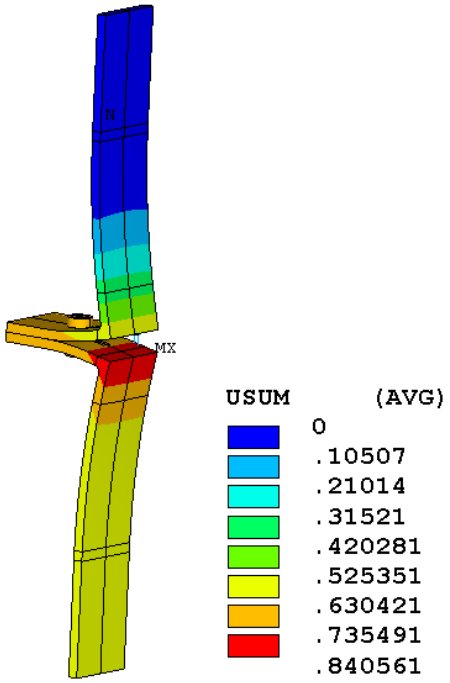

Figure 4.33 – Displacement vector sum of B1 specimen at 1kN tensile load

Comparison of the experimental displacement-load and strain readings with the finite element solution for different contact algorithms

Referring to the results of A1 geometry, Augmented Lagrange algorithm is used for the analysis.

Comparison of the experimental displacement-load and strain readings with the finite element solution for different contact stiffness factors

Five different contact stiffness factors (see Table 4.3) with different choices of contact algorithms and penetration tolerance factors are used during the parametric analysis. Load displacement of the second test and strain data are compared with finite element analysis results. Finite element solution is obtained for a penetration tolerance value of 0.1 and load displacement curves for different

contact stiffness factors are compared with the actuator displacement of the test machine in Figure 4.34.

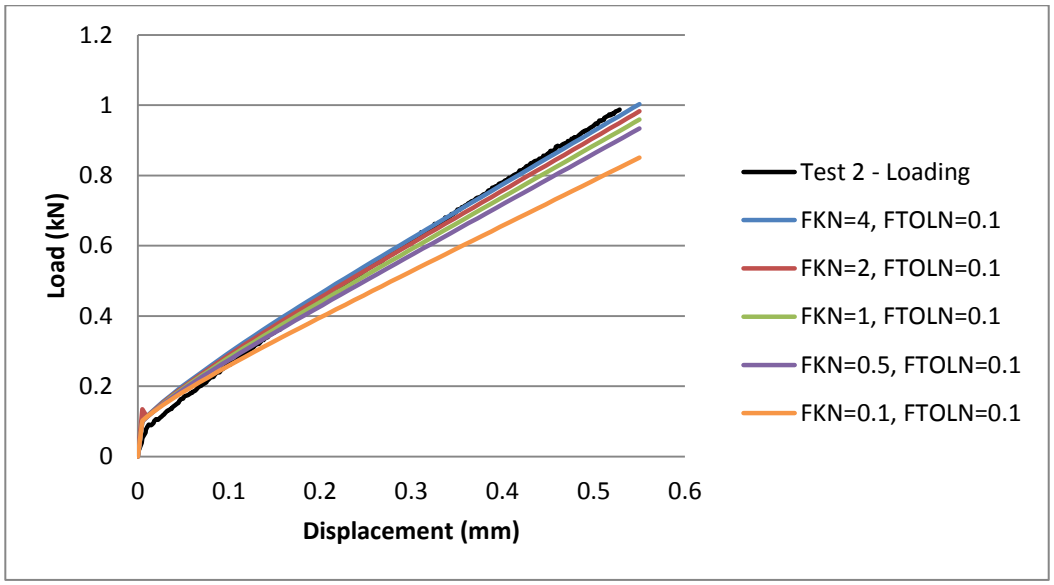

Figure 4.34 - Load vs. displacement graph for different contact stiffness factors (FKN) (Contact algorithm: Augmented Lagrange, Penetration tolerance (FTOLN)=0.1)

For specimen B1, the effect of the contact stiffness factor on the load – displacement curve is more obvious compared to specimen A1. It is seen that using very low contact stiffness factors results in the lower slope of the load displacement curve. It should also be noted that at the initial step of the load application in the test and also in the finite element analysis, slope change occurs in the load displacement curve. Initially, this slope change is attributed to the probable change in contact status both in the test and in the finite element analysis.

However, in finite element results there is no contact status change, but when the gap distances of the flanges are investigated, it is seen that the slope change occurs when the gap contour changes, as shown in Figure 4.35.

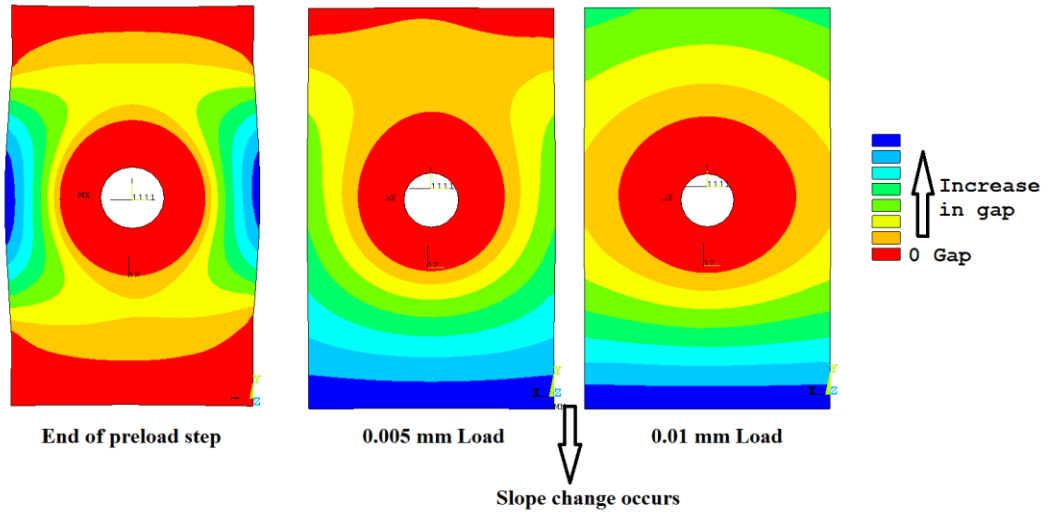

Figure 4.35 – Gap distance contours when the slope change occurs at contact region between flanges (see Figure 4.17)

It is also observed that at the upper edge of the flange gap decreases indicating that as load increases free edge of the flanges close up. This behavior is the main reason of prying effect which causes an increase in the bolt load.

The load – displacement curve is investigated thoroughly by zooming into Figure 4.34. The zoomed plot is shown in Figure 4.36. It is seen that for low contact stiffness factors finite element results result deviate from the test results more. Using a high contact stiffness factor such as 2 or 4 is encouraged considering the agreement that it provides with the test result.

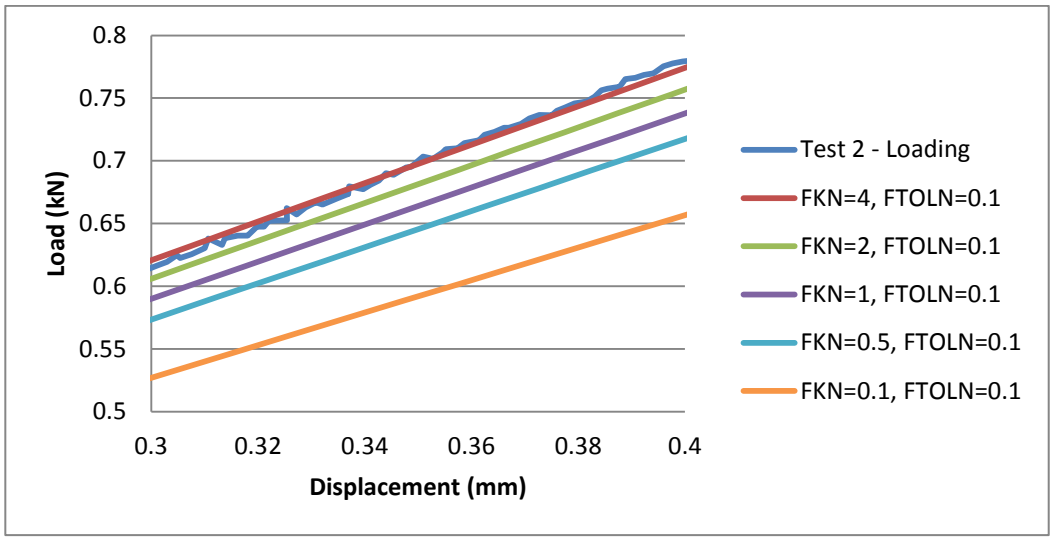

Figure 4.36 - Zoomed load vs. displacement for different contact stiffness factors (FKN) (Contact algorithm: Augmented Lagrange, Penetration tolerance (FTOLN)=0.1)

In Figure 4.37, load vs. strain results are compared for different contact stiffness factors. For specimen B1, strain results are underestimated by the finite element solution for all contact stiffness factors. However, when the contact stiffness factor is 4, slope of the curves of finite element solution and experimental data are closer. For specimen B1, using high contact stiffness factors like 2 can be suggested but the results still are not satisfactory for the stiff specimen B1.

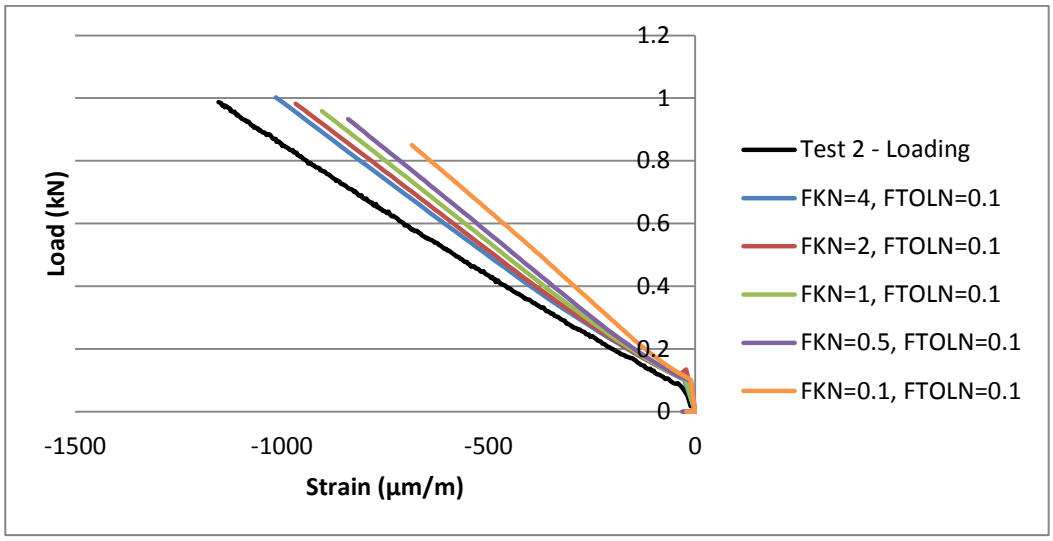

Figure 4.37 - Load vs. strain graph for different contact stiffness factors (FKN) (Contact algorithm: Augmented Lagrange, Penetration tolerance (FTOLN)=0.1)

Comparison of the experimental displacement-load and strain readings with the finite element solution for different penetration tolerance factors

It is seen that penetration tolerance influences the accuracy of the finite element solution for specimen A1. In Figure 4.38, load – displacement curve comparison of finite element solution for varying penetration tolerance factors with the experimental data is given. Figure 4.38 shows that the slopes of the modulus line are different for finite element solutions compared to the slope of the experimental data and it is concluded that penetration tolerance should be chosen as small as possible because for small penetration tolerance values finite element solution approaches to the experimental data. For low penetration tolerance values, the total number of iterations increases but if the accuracy is sought for, one could compromise from solution time.

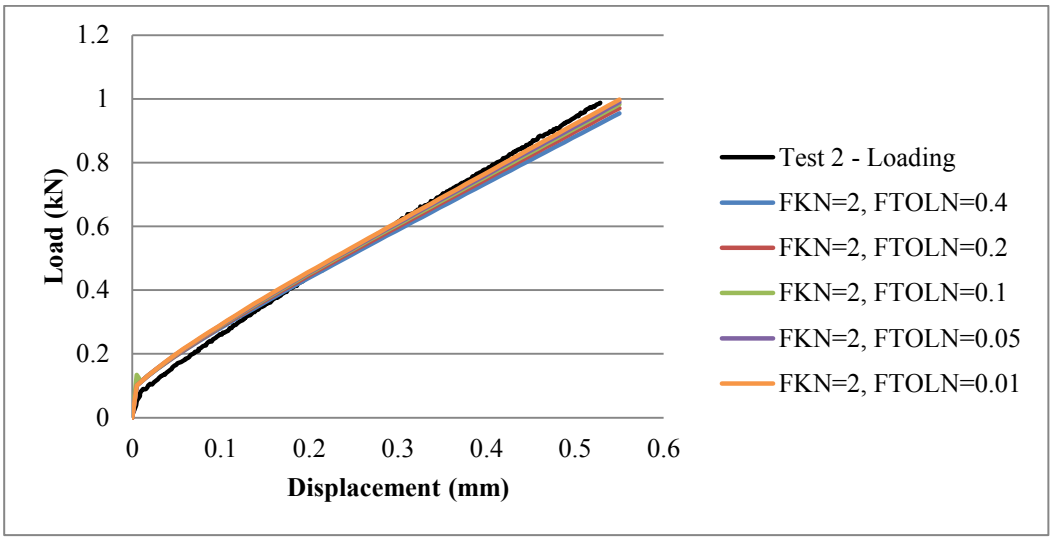

Figure 4.38 - Load vs. displacement graph for different penetration tolerance factors (FTOLN) (contact algorithm: Augmented Lagrange, Contact stiffness factor (FKN)=2)

The effect of penetration tolerance is more clearly seen on the zoomed plot given in Figure 4.39.

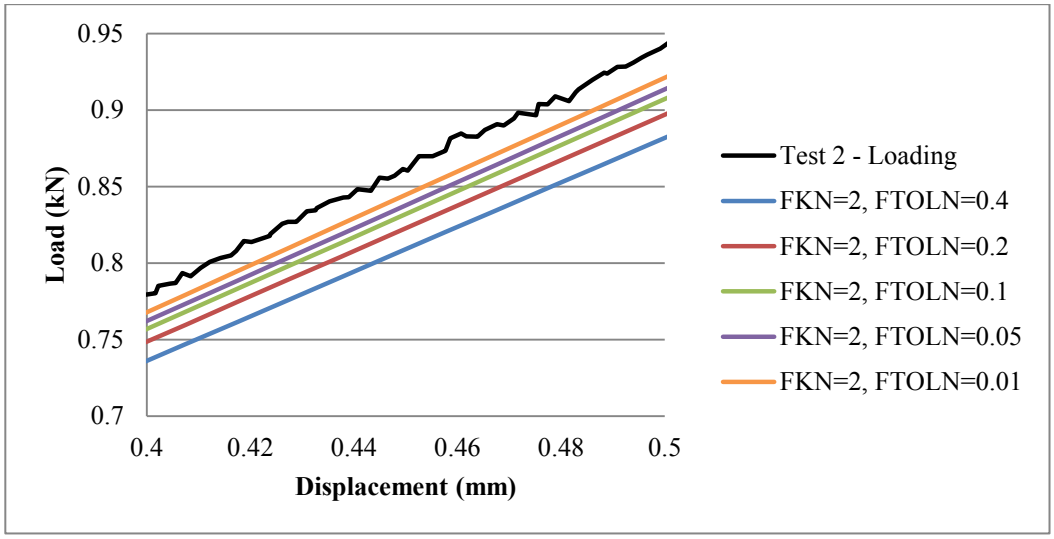

Figure 4.39 – Zoomed load vs. displacement graph for different penetration tolerance factors (FTOLN) (Contact algorithm: Augmented Lagrange, Contact stiffness factor (FKN)=2)

Load vs. strain graph is given Figure 4.40. Again, decrease in penetration tolerance results in more accurate strain values when finite element solution is compared with the experimental data. Finite element solution underestimates the strain in specimen B1.

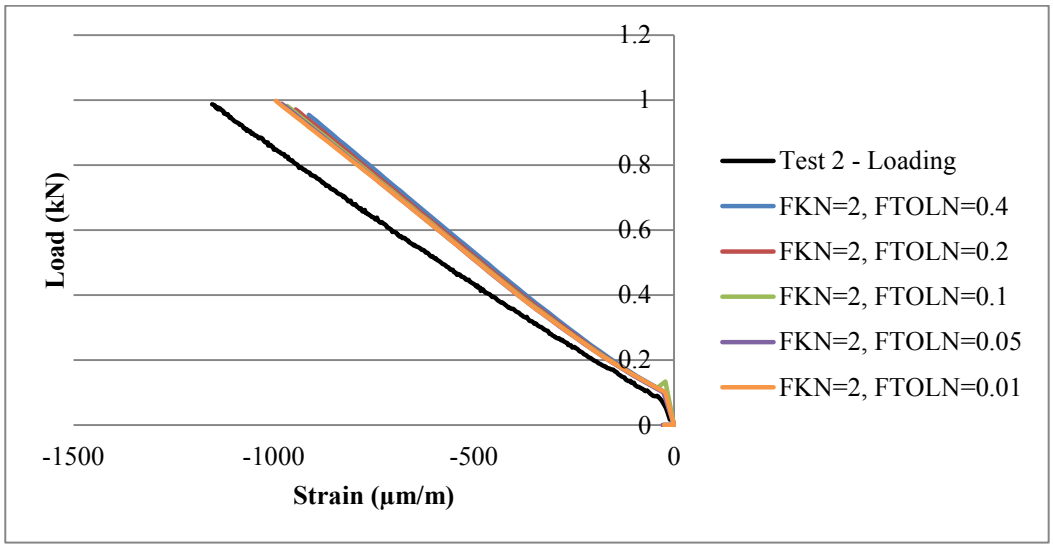

Figure 4.40 - Load vs. strain graph for different penetration tolerance factors (FTOLN) (Contact algorithm: Augmented Lagrange, Contact stiffness factor (FKN)=2)

4.3 Conclusion for Tensile Test of Bolted L-Brackets and Validation with Finite Element Method

In this chapter, tensile testing of two L-brackets is explained and parametric study is made by varying contact algorithms, contact stiffness factors and penetration tolerance factors. Load-displacement and load-strain curves with suggested contact parameters are given in Appendix D for A1 and B1 specimen. For specimen A1, DIC results are also compared with the results of finite element analysis. Specimen A1 is less stiff compared to specimen B1 because the edge distance is smaller. Both specimens are loaded up to 1 kN and strain readings are recorded simultaneously. For specimen B1, there is a slope change in the load – displacement curve and based on the finite element analysis results, it is

concluded that change in the contact status or the gap distance change may cause such a slope change. For both specimens, there is noticeable nonlinearity in the load displacement and load strain curves, and the reason for the nonlinearity is considered to be due to the small changes in the contact status during the loading.

In general, finite element solution and the experimental data have similar tendency but for the stiffer geometry B1, results of finite element analysis is highly dependent on the contact parameters. Contact algorithm does not change either the accuracy or the solution time of the analysis for both specimens. In terms of contact stiffness factor, for specimen A1, contact stiffness factor of 4 results in unconservative strain results. Therefore, for specimen A1, choosing a contact stiffness factor of 1 or 2 should be preferred. For specimen B1, the results seem to be more accurate for contact stiffness factor of 4, but when a contact stiffness factor of 2 is used, the difference in the response is minimal. Therefore, it is recommended that contact stiffness factor of 2 be chosen for specimen B1. In previous analyses of the bolted flange structure with the eight bolts, penetration tolerance is seen to have no effect on the accuracy of the results. But for both of the L-brackets penetration tolerance changes the load displacement and load strain and it is seen that using lower values of penetration tolerance gives more accurate results. Especially for specimen B1, if high values for penetration tolerance is chosen, the results are inaccurate and for more accuracy, penetration tolerance should be small such as 0.01 at the cost of longer solution time. Because friction coefficient value is taken from literature and preload value is calculated with an empirical relation it is thought that either friction coefficient or preload value may be the reason for inaccurate load – strain results for B1 specimen. For this reason, additional analyses for varying preload values and 10% increased and decreased friction coefficient values are performed and results are given in Appendix D. Although there is a little increase in the accuracy for increasing preload values, change in friction coefficient does not affect the accuracy for specimen B1. Thus, further investigation of the reason for the discrepancy between the finite element solution and the experimental data is needed.

CHAPTER 5

DISCUSSIONS AND CONCLUSIONS

In the thesis, effects of contact parameters on the accuracy and solution time of the analysis of bolted flange connections are investigated. For this purpose, two main studies are conducted. In the first study, an eight bolt flange connection, for which experimental strain measurements are available, is analyzed utilizing contact definitions in between all relevant parts. The effect of main contact parameters is investigated by making comparisons of the finite element solution with the experimental findings. In the second study, both finite element analysis and experiments are performed for different bolted connections of L brackets. Again, the effect of main contact parameters is investigated by making comparisons with the experimental data obtained. There are number of contact parameters that are used for the contact analysis and the accuracy and convergence behavior of the results are affected by these parameters significantly. In the literature, there are numerous studies that investigate the structural integrity of bolted flange connections and other structures with contact. Design standards, linear tools or finite element method are used in these studies and it is stated that all of these methods have some sort of drawbacks. Finite element method takes contact and material nonlinearities into account and it is the most widely used method in the structural analysis involving contact. In this thesis, importance of the contact parameters is acknowledged and sensitivity analyses are conducted in order to investigate the effects of the main contact parameters on the accuracy and solution time of the analyses. Contact stiffness factor, penetration tolerance factor and contact algorithm are selected as focus areas in the thesis. In real world

problems, when two bodies are in contact there is no penetration [18]. However, in order to solve the contact problems mathematically, there has to be a certain amount of allowable penetration and penetration tolerance is the amount of penetration that is required for contact problems to be solved mathematically. On the other hand, contact stiffness factor can be resembled to the stiffness of a spring that holds the contacting bodies together. The value for the contact stiffness is calculated by the finite element software and updated by the contact stiffness factor that is determined by the user. Contact stiffness factor is supposed to be as high possible for accuracy but high contact stiffness factor may lead to ill-conditioned global stiffness matrix causing convergence difficulties [20]. In the literature, there are some misleading studies about the choice of contact stiffness factor values stating that it should be between 0.1 and 1 [8, 9, 11, 12], but in this thesis finite element results are compared with experimental data and it is shown that contact stiffness factor should be above 1 depending on the problem.

Mathematical simulation of the contact mechanics is given for a simple mass-spring model with and without friction. Minimization of total potential energy of the system is used in order to derive the equations related to contact mechanics and the mathematical difficulties that can be encountered to solve for the load displacement curves of the problems are stated. Kinematically linear contact problems are explained mathematically for the Signorini, contact with rigid obstacle, problem. After introducing a general potential energy functional; Lagrange (multiplier), Penalty and Augmented Lagrange methods are explained. One should note that these are the main algorithms that can be chosen in most finite element software for contact analysis. For Lagrange algorithm the solution can be directly obtained for such a simple problem; however, it should be added that for a real world problem there are many constraints that are known a priori and iterative solutions are required when Lagrange method is used. For the Penalty method, Penalty parameter should be chosen carefully because the accuracy and the solution time strongly depend on this parameter. Using higher Penalty parameter values gives more accurate results, however for complicated

contact problems convergence may not be acquired for such high Penalty parameter values. For the Augmented Lagrange method, that the solution is simpler since there is no need to choose a parameter as in the Penalty method [14]. Finally, mathematical explanation of contact problems with friction is given for the Penalty and the augmented Lagrange algorithms. When friction is present, solution becomes more complicated for both of the algorithms because there are additional terms in the equations due to tangential forces.

Strain data of experimental study of an eight-bolt unstiffened flange-plate steel connection splicing two circular hollow sections that is exposed to pure bending is compared with elastic finite element analysis by varying contact parameters, load cases and mesh types. It is observed that there is no effect of penetration tolerance factor on the accuracy of the results but the solution time increases when low penetration tolerance factors are used. As there is no change in accuracy, it is concluded that higher penetration tolerance factor values can be used due to lower solution times that can be obtained with higher penetration tolerance factors. For the sensitivity analysis, four of the most popular contact algorithms of ANSYS contact menu are used. However, it is observed that for Pure Lagrange and Lagrange & Penalty combination methods the solution ill-converges and percent error between finite element and experimental data increases drastically. Hence, it is decided to continue with the augmented Lagrange and Pure Penalty methods. It is observed that both of the algorithms resulted in the same accuracy except a few combinations of contact parameters (different contact stiffness and penetration tolerance factors). But for the augmented Lagrange method, solution time is lower compared to the Penalty method; therefore, the use of Augmented Lagrange algorithm is suggested. Finally, the effect of contact stiffness factor is investigated on the accuracy and solution time and it is seen that contact stiffness factor is the most important parameter that affects both the accuracy and the solution time. Higher contact stiffness factor values resulted in more accurate solution but at the cost of solution time. It is also noted that increasing contact stiffness factor too much may also decrease the accuracy. A moderately high contact stiffness factor 2

is suggested. On the other hand, for high load levels which almost cause plastic deformation, contact stiffness factor should be chosen carefully because the results might be erroneous. Finally, it is concluded that fine mesh structure gives more accurate solutions and there is no clear effect of better matching mesh structure on the solution time. It is noted that total number of nodes is more important than the matching status of the mesh structure.

Plastic analysis of bolted flange connections is a challenging task. There is nonlinear material data and contact nonlinearity included in the analysis and reaching to a converged solution is not easy. After generating several finite element models and several trials, convergence after the start of plastic deformation is obtained. It is seen that slope of the load strain graph degenerates and finite element method underestimates the strain values. Lower contact stiffness factors resulted in better estimation in contrary to the theory. However, using high contact stiffness factor values are suggested because almost every machinery is designed to stay in elastic limits.

Two L-brackets with different bolt location are subjected to tensile testing. Three tests are conducted for both of the specimens and it is seen that for 2^{nd} and 3^{rd} tests load deflection and load strain curves are close and different from 1^{st} tests. Different behavior in the second and third tests is attributed to the plastic deformation that occurs during 1^{st} tests. Finite element analysis estimates the structural response of the specimens accurately but the sudden changes in the contact status causes unexpected changes in the load displacement curves at low load levels. A visible slope change is detected for B1 specimen, which is stiffer compared to A1, at a very low load and similar behavior is also obtained by the finite element analysis. It is seen that the contact algorithm does not have any effect on either accuracy or on the solution time of the analyses. Contact stiffness factor affects the results for both of the specimens, but using too high contact stiffness factors such as 4 is not suggested because of the inaccurate results. It is concluded that contact factor of 2 is the optimum value that should be used for

both specimens. Penetration tolerance factor is found the have significant effect on the accuracy and on the solution time. Especially for stiffer specimen B1, penetration tolerance should be chosen as small as possible compromising from the solution time.

In conclusion, finite element method can lead to erroneous results when the contact parameters are not chosen carefully. Especially, contact stiffness factor has a strong effect on the accuracy and the run time of the analysis. Use of contact stiffness factor values more than 1, like 2, but not too high is suggested because the results may degenerate when higher contact stiffness factor values are used. Augmented Lagrange and Penalty methods give similar results in terms of accuracy, but augmented Lagrange method is faster in some cases so it is better use augmented Lagrange method during nonlinear contact analysis. Penetration tolerance factor may affect both the accuracy and the solution time and using higher values shortens the solution time in some cases without affecting the accuracy. A sensitivity analysis should be performed with high penetration tolerance factor values such as 0.2 and 0.4. If there is change in accuracy of the finite element solution, small penetration tolerance factor values should be used if the high accuracy is sought for. Using smaller values of penetration tolerance factor values increases the solution time considerably but one can tolerate long solution times for accuracy. If there is no change in the accuracy with the changing penetration tolerance factor, using penetration tolerance factor values close to 1 is suggested.

In the thesis, effects of contact parameters on the accuracy and the solution time of three different bolted joint connections are examined. In the future, this work may be extended by choosing different types of connection structures such as dovetail, fir tree and lug joint. For dovetails and fir trees slipping on the contact regions is dominant and tangential stiffness factor plays an important role for such analysis. In addition to contact algorithm, contact stiffness factor and penetration tolerance factor, tangential stiffness factor may also be included in the sensitivity

analysis if such structures are chosen to be analyzed. Material properties of the aluminum may be determined experimentally and finite element analysis may be performed with this data. When the gas turbine engines are considered nonlinear contact analysis with temperature effects may also be accounted for. In the present study, strain distribution after the preload of the bolted joints are omitted but the effect of preload on the structures may be determined experimentally and compared with the finite element solution. Moreover, experimental studies can be conducted in order to determine the prying effect on the bolt and validated with the finite element analysis. In addition, material type can be changed and contact analysis may be performed for composite structures by assuming linear elastic material type or by including the viscoelastic material behavior of the resin.

REFERENCES

[1] ANSYS, *Contact Technology Guide,* Canonsburg: ANSYS, Inc., 2009.

[2] Abid, M., Nash, D.H., "A parametric study of metal-to-metal contact flanges with optimized geometry for safe stress and no-leak conditions". International Journal of Pressure Vessels and Piping, 81, 2004, pp. 67–74.

[3] Vishwanath, V. H., Sanjay, S.J., Math, V.B., "The Study Of The Behavior Of Bolted Flanges With Gaskets". International Journal of Engineering Research & Technology, Vol. 2 (5), 2013, pp. 135-137.

[4] Baker, J.C., "Analysis of Bolting in Flanged Connections". MSc Thesis, Graduate Faculty of Rensselaer Polytechnic Institute, 2009.

[5] Guizzo, A.C., "Experimental Behavior of Bolted Joints".Fluid Sealing Association Technical Symposium, 1998.

[6] Auricchio, F., Sacco, E., "Augmented Lagrangian Finite-Elements for Plate Contact Problems".International Journal for Numerical Methods in Engineering, Vol. 39, 1996.

[7] Stefancu, A.I., Melenciuc, S.C., Budescu, M., "Penalty Based Algorithms for Frictional Contact Problems". Bulletin of the Polytechnic Institute of Iasi, 61(3), 2011, pp. 119-129.

[8] de Jesus, A. M. P., da Silva, A. L. L., Correia, J. A. F. O., "Fatigue of riveted and bolted joints made of puddle iron—A numerical approach", Journal of Constructional Steel Research, Vol. 102, 2014, pp. 164-177

[9] Liao, X., Wang, G. G., “on-linear dimensional variation analysis for sheet metal assemblies by contact modeling”, Journal of Finite Elements in Analysis, Vol. 44 (1-2), 2007, pp. 34-44

[10] Lanoue, F., “Finite element analysis and contact modelling considerations of interference fits for fretting fatigue strength calculations”, Journal of Simulation Modelling Practice and Theory, Vol. 17, 2009, pp. 1587-1602.

[11] Diaz, J. J. d. C., Nieto, P. J. G., Biempica, C. B., Rougeot, G. F., “Non-linear analysis of unbolted base plates by the FEM and experimental validation”, Journal of Thin-Walled Structures, Vol. 44, 2006, pp. 529-541

[12] Santos, C. L., de Jesus, A. M. P., Morais, J. J. L., Lousada, J. L. P. C., “Quasi-static mechanical behaviour of a double-shear single dowel wood connection”, Journal of Construction and Building Materials, Vol. 23, 2009, pp. 171-182.

[13] Wriggers, P., Computational Contact Mechanics, Springer, 2nd Ed., 2006.

[14] Laursen, T. A., Computational Contact and Impact Mechanics, Springer, 2nd Ed., 2002.

[15] Wu, H. C., Continuum Mechanics and Plasticity, CRC Press, 2004.

[16] Ionescu, I. R., “Slip-dependent friction in dynamic elasticity”, Journal of Nonlinear Analysis,: Theory, Methods & Applications, Vol. 53, 2003, pp. 375-390.

[17] Wang, Y. Q., Zong, L., Shi, Y. J., “Bending behavior and design model of bolted flange-plate connection”, Journal of Constructional Steel Research, Vol. 84, 2013, pp. 1-16.

[18] Imaoka, S., “Contact Analysis Tips”, Ansys.net, 2009

[19] M. D. Group, Nonlinear Contact Analysis Techniques using ANSYS, Ansys INC.

[20] ANSYS, Structural Analysis Guide, Ansys, Inc., 1999.

[21] Wenlong, S., "Experimental and theoretical study on semi-rigid beam-to-column composite joints with flush end-plate connection" Shanghai: Tongji University, 2006. (in Chinese)

[22] Tegola, A. L., Mera, W., "Influence of friction on the constraints with degrees of freedom on the seismic behavior of steel structures", STESSA 2012, Chile.

[23] Zhao, A.H., Xin, X.J., Pei, Z.J., "Implicit and Explicit Finite Element Simulation of Soft-Pad Grinding of Silicon Wafers". International LS-DYNA Users Conference, 2004.

[24] Bonnick, A., Newbold, D., A Practical Approach to Motor Vehicle Engineering and Maintenance, Elsevier/Butterworth-Heinemann, 2011.

[25] Atasoy, M., "Determination of Prying Load on Bolted Connections", MSc Thesis, Middle East Technical University, 2012

[26] Tracton, A. A., Coatings Technology: Fundamentals, Testing, and Processing Techniques, CRC Press, 2006.

[27] Huang, Y., Deng, H. Z., Jin, X. H., "Experimental research on large-scale flange joints of steel transmission poles", Proceedings of Tubular Structures XII, Shanghai, China, 2008, pp. 615-621

[28] Warminski, J., Lenci, S., Cartmell, M.P., Rega, G.,Wiercigroch, M., Nonlinear Dynamic Phenomena in Mechanics, Springer, 2012.

APPENDIX A

ADDITIONAL RESULTS FOR FINITE ELEMENT ANALYSES OF THE BOLTED FLANGE STRUCTURE IN ELASTIC LIMITS

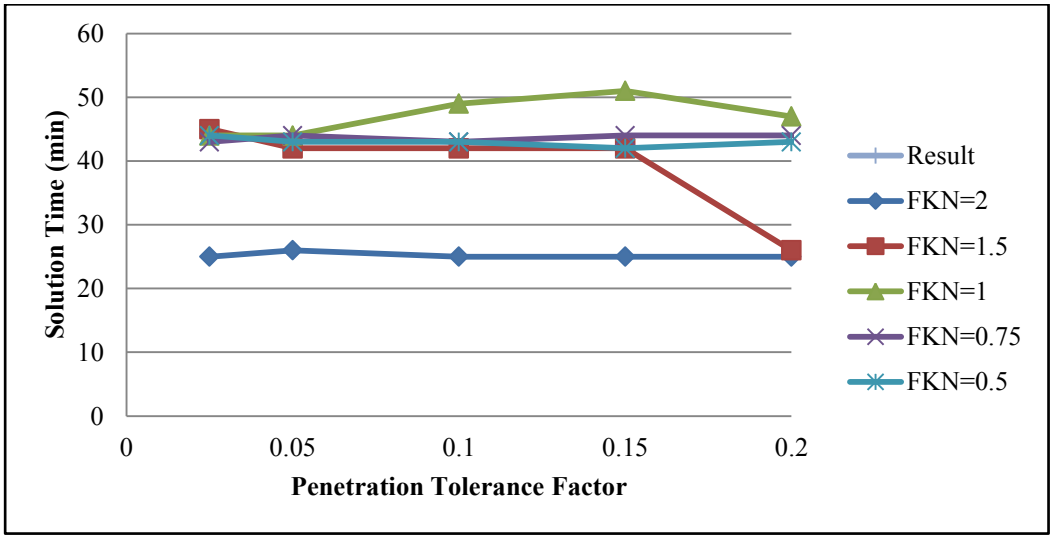

Figure A.1 - Solution time vs. penetration tolerance factor (Pure Penalty, Fine Mesh Structure, 75 kN)

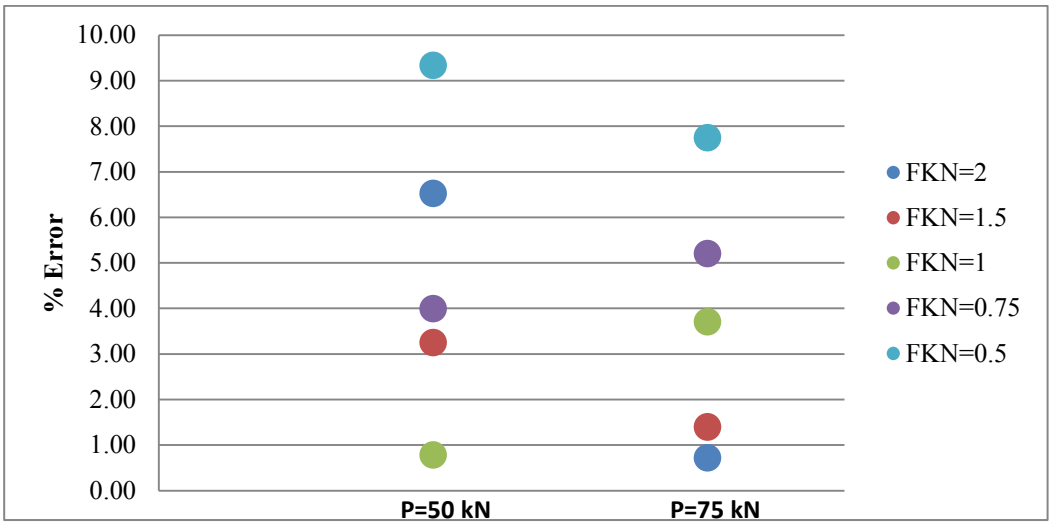

Figure A.2 - % Error vs. load case (Augmented Lagrange (Pure Penalty), Fine Mesh Structure)

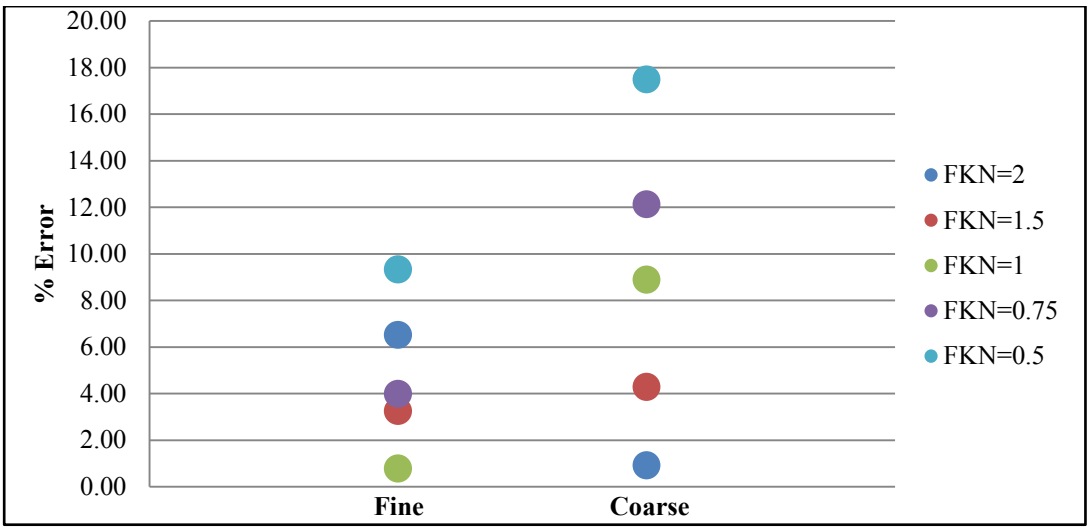

Figure A.3 - % Error vs. mesh type (50 kN)

APPENDIX B

ADDITIONAL RESULTS FOR ELASTO-PLASTIC ANALYSIS OF BOLTED FLANGE STRUCTURE

A.1 Plastic Deformation Regions

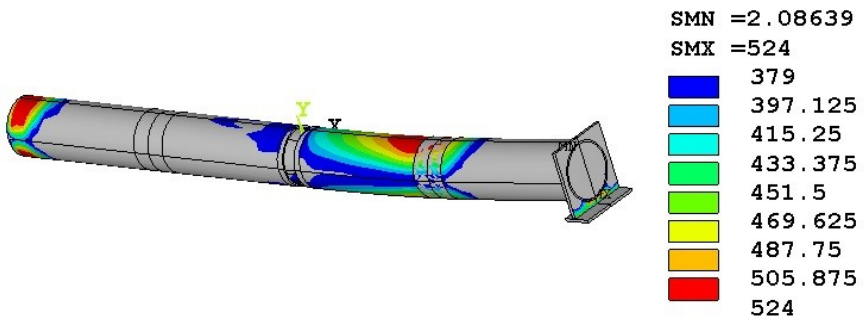

Figure B.1 –Plastic deformation regions for circular hallow sections at 180 kN jack load

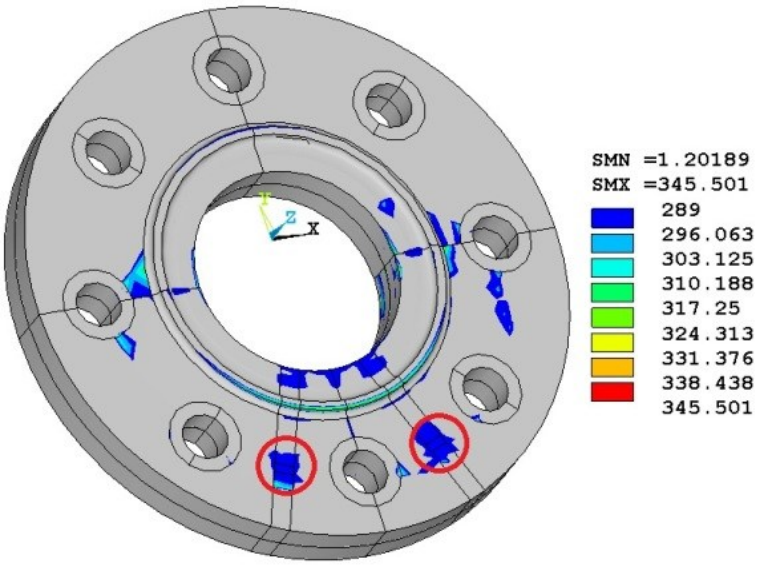

Figure B.2 - Plastic deformation regions for end plates at 180 kN jack load

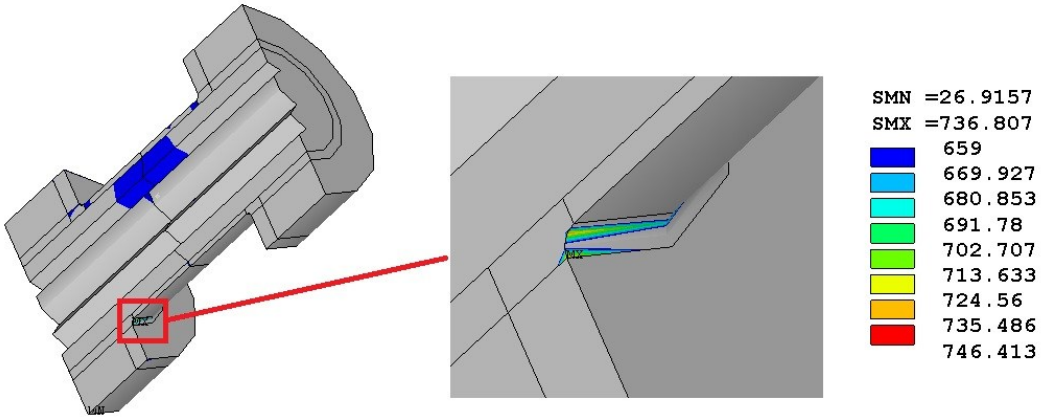

Figure B.3 - Plastic deformation regions for a sample bolt at 180 kN jack load

A.2 Comparison of Finite Element Analysis with Elastic and Multi-linear Material Data

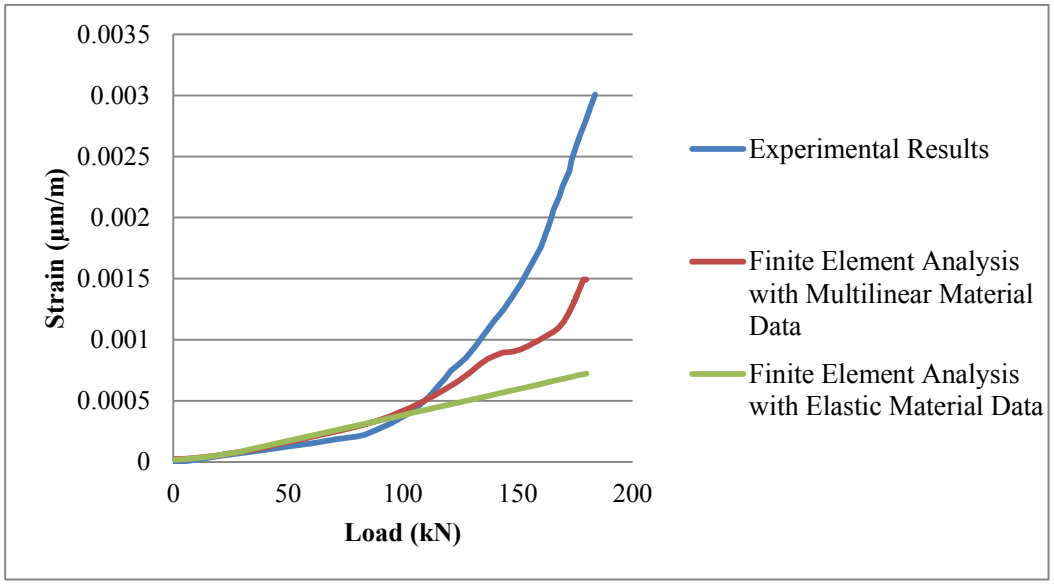

Figure B.4 – Comparison of material models on the accuracy

APPENDIX C

ANSYS APDL MACRO FOR SENSITIVITY ANALYSIS

! Previously saved finite element model is opened (Procedure is same for B1 specimen) except that the components and load step files are created separately

resume,a1,db

fini

! Contact stiffness, penetration tolerance factor and algorithm arrays are defined and created

/prep7

**dim,afkn,array,5*

**dim,aftoln,array,5*

**dim,aalgo,array,2*

afkn(1)=4

afkn(2)=2

afkn(3)=1

afkn(4)=.5

afkn(5)=.1

aftoln(1)=.4

aftoln(2)=.2

aftoln(3)=.1

aftoln(4)=.05

aftoln(5)=.01

aalgo(1)=0 ! Augmented Lagrange

aalgo(2)=1 ! Penalty

fini

save

! Do loops that change contact parameters are started

**do,i,1,2*

**do,j,1,5*

**do,k,1,5*

alls

fini

! File name is changed and previously created load step files (preload and loading) are renamed

/filename,a1_%i%%j%%k%

/COPY, a1, s01,, a1_%i%%j%%k%, s01,

/COPY, a1, s02,, a1_%i%%j%%k%, s02,

fini

/prep7

! Algorithm, contact stiffness factor and penetration tolerance factors are changed

keyopt,54,2,aalgo(i)

keyopt,56,2,aalgo(i)

keyopt,58,2,aalgo(i)

keyopt,60,2,aalgo(i)

/COM, CONTACT PAIR PROPERTIES - START

RMODIF,54,3,afkn(j)

RMODIF,56,3,afkn(j)

RMODIF,58,3,afkn(j)

RMODIF,60,3,afkn(j)

/COM, CONTACT PAIR PROPERTIES - END

/COM, CONTACT PAIR PROPERTIES - START

RMODIF,54,4,aftoln(k)

RMODIF,56,4,aftoln(k)

RMODIF,58,4,aftoln(k)

RMODIF,60,4,aftoln(k)

/COM, CONTACT PAIR PROPERTIES - END

! Model is solved

/solu

lssolve,1,2

! Postprocessing procedure

/post1

SET,, ,,, ,1

**get,nofset,active,,set,nset*

**do,l,1,nofset*

SET,, ,,, ,l

! Previously created nodal components that define the strain gages is selected, strain in x direction according to previously created result coordinate system is summed and averaged for each load step (loading condition)

alls

cmsel,s,sga

rsys,11

**Get,totnode1,NODE,0,count*

*Get,minnode,NODE,0,NUM,MIN

*Get,maxnode,NODE,0,NUM,Max

*Get,strain1,Node,minnode,EPEL,X

total1=strain1

*do,m,2,totnode1

*Get,n,NODE,minnode,NXTH

*Get,strain1,Node,n,EPEL,X

total1=total1+strain1

minnode=n

*enddo

ave1=(total1/totnode1)*1000000

alls

cmsel,s,sgb

rsys,12

*Get,totnode2,NODE,0,count

*Get,minnode,NODE,0,NUM,MIN

*Get,maxnode,NODE,0,NUM,Max

*Get,strain2,Node,minnode,EPEL,X

total2=strain2

*do,m,2,totnode2

*Get,n,NODE,minnode,NXTH

*Get,strain2,Node,n,EPEL,X

total2=total2+strain2

minnode=n

*enddo

ave2=(total2/totnode2)*1000000

alls

cmsel,s,sgc

rsys,13

*Get,totnode3,NODE,0,count

*Get,minnode,NODE,0,NUM,MIN

*Get,maxnode,NODE,0,NUM,Max

*Get,strain3,Node,minnode,EPEL,X

total3=strain3

*do,m,2,totnode3

*Get,n,NODE,minnode,NXTH

*Get,strain3,Node,n,EPEL,X

total3=total3+strain3

minnode=n

**enddo*

*ave3=(total3/totnode3)*1000000*

! Strain results are written to the file

**cfopen,A1_SG_Results%i%%j%%k%,txt,,append*

**VWRITE,ave1,ave2,ave3*

(E14.6,2x,E14.6,2x,E14.6)

**CFCLOS*

! Nodal component from which the reaction force will be extracted is selected reaction force calculated

alls

cmsel,s,dispnode

cmsel,s,dispelem

rsys,0

**get,thetime,active,0,set,time ! The time of that load step*

*appdisp=(thetime-1)*1.4 ! The applied load value at that load step*

**get,loads,active,,set,lstp*

*get,subs,active,,set,sbst

fsum ! This command is included otherwise fsum value is not updated.

*get,reacforce,fsum,,item,fz !Reaction force of the selected nodes and elements, (probably the fixed end)

reacforce=reacforce/1000

! Reaction force and applied load (displacement) at the load increment is written to the file

*cfopen,A1_DispvsLoad_%i%%j%%k%,txt,,append

*VWRITE,appdisp,reacforce,,,,

(f13.4,2x,f13.4,2x)

*CFCLOS

alls

*enddo

*enddo

*enddo

*enddo

finish

APPENDIX D

POSTPROCESSING DETAILS AND ADDITIONAL RESULTS FOR L-BRACKET SPECIMENS

D.1 Shifting Procedure

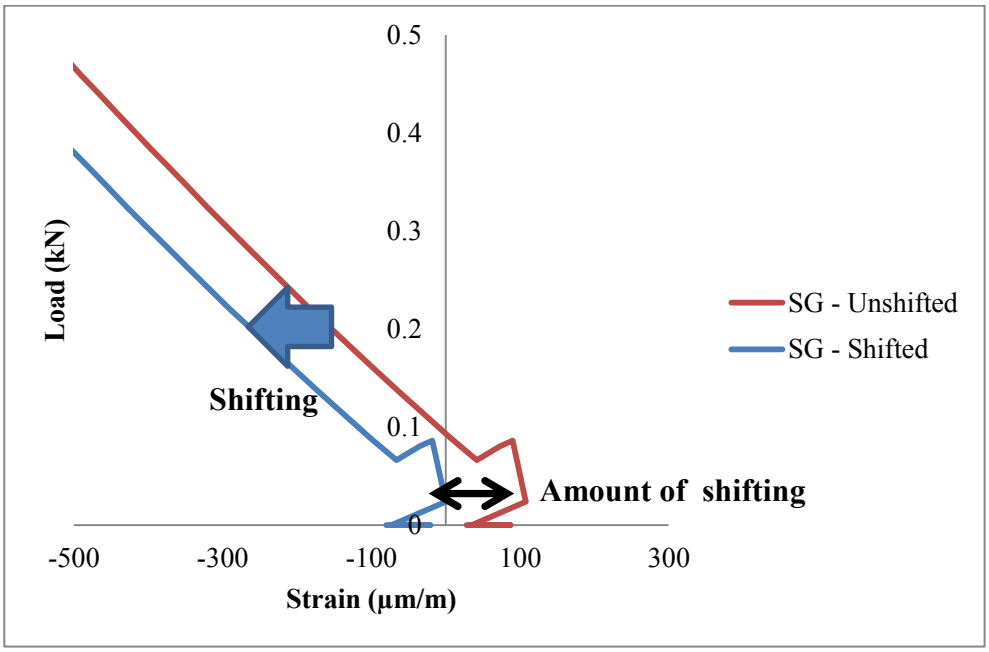

Figure D.1 – Shifting of finite element analysis results

D.2 Comparison of Finite Element Solution with Experimental Data for Specimen A1 with Appropriate Choice of Contact Parameters

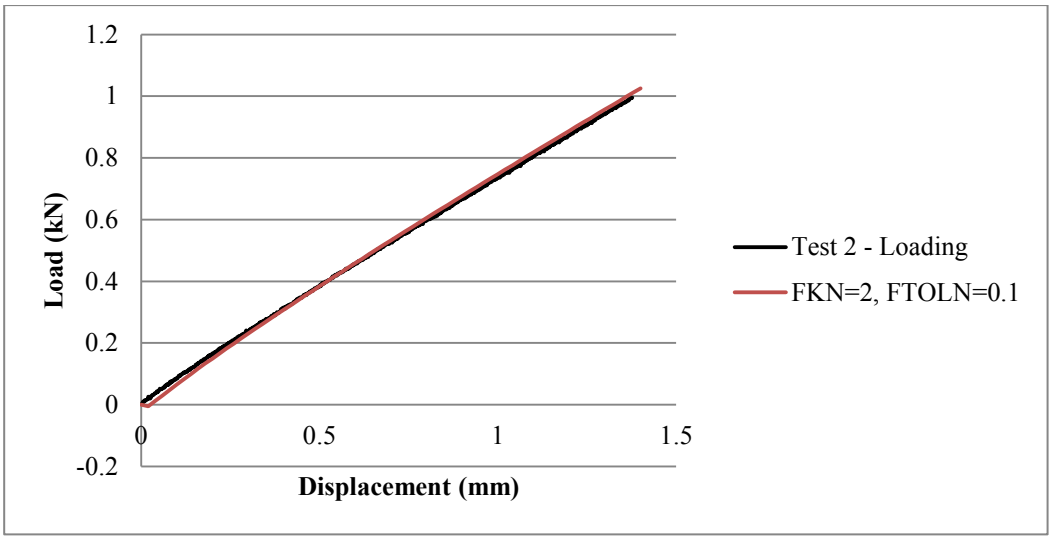

Figure D.2 - Load vs. displacement comparison for test data and contact stiffness factor FKN=2 (Contact algorithm: Augmented Lagrange, Penetration tolerance factor (FTOLN=0.1))

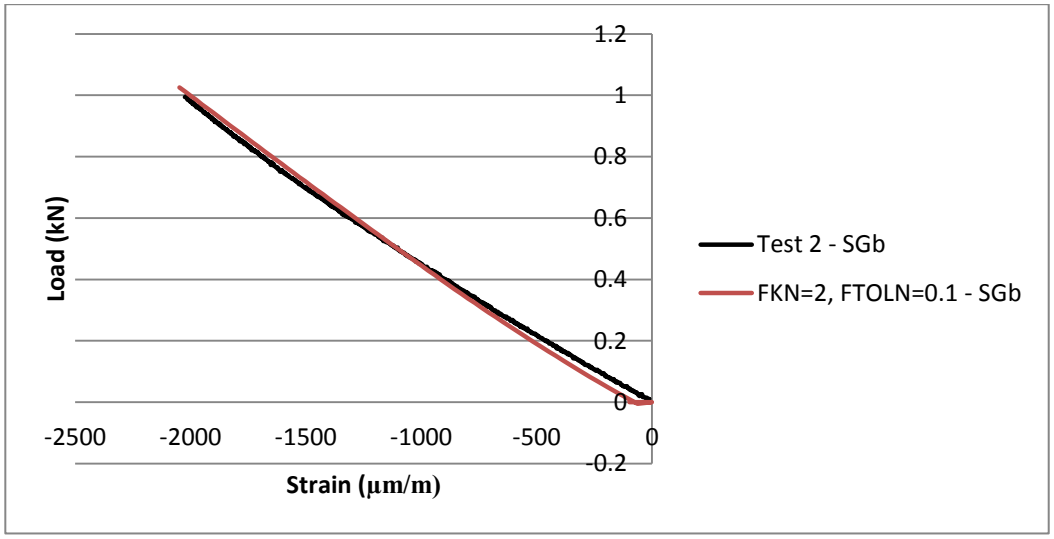

Figure D.3 - Load vs. strain comparison for test data and contact stiffness factor FKN=2 (Contact algorithm: Augmented Lagrange, Penetration tolerance factor (FTOLN=0.1))

D.3 Comparison of Finite Element Solution with Experimental Data for Specimen B1 with Appropriate Choice of Contact Parameters

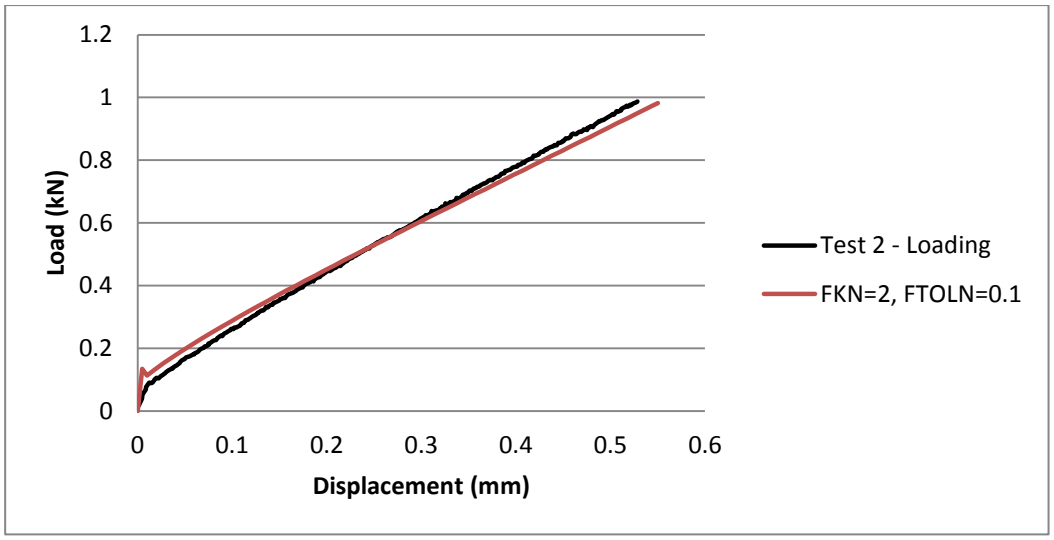

Figure D.4 - Load vs. displacement comparison for test data and contact stiffness factor FKN=2 (Contact algorithm: Augmented Lagrange, Penetration tolerance (FTOLN)=0.1)

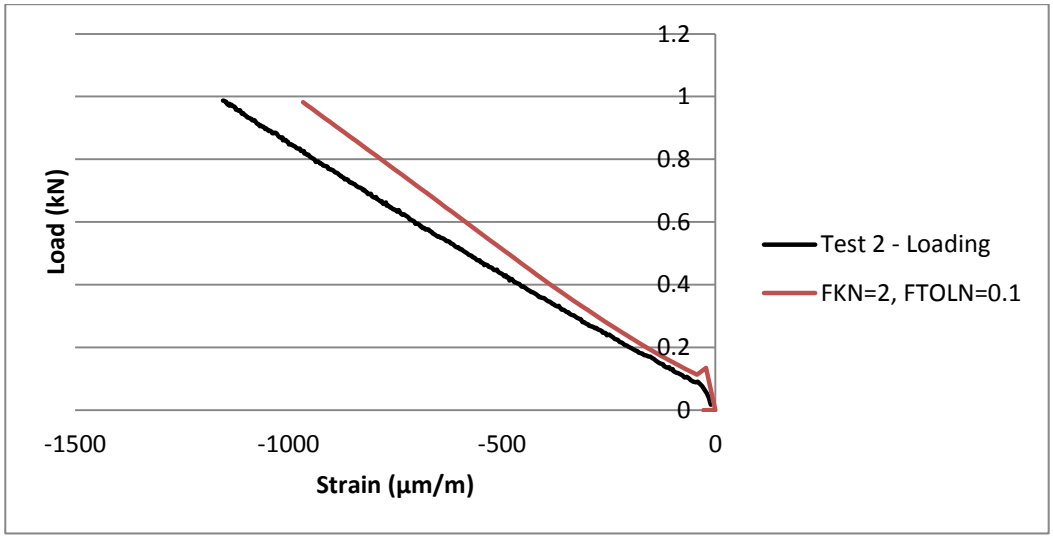

Figure D.5 - Load vs. strain comparison for test data and contact stiffness factor FKN=2 (Contact algorithm: Augmented Lagrange, Penetration tolerance (FTOLN)=0.1)

D.4 Additional Analyses for Specimen B1

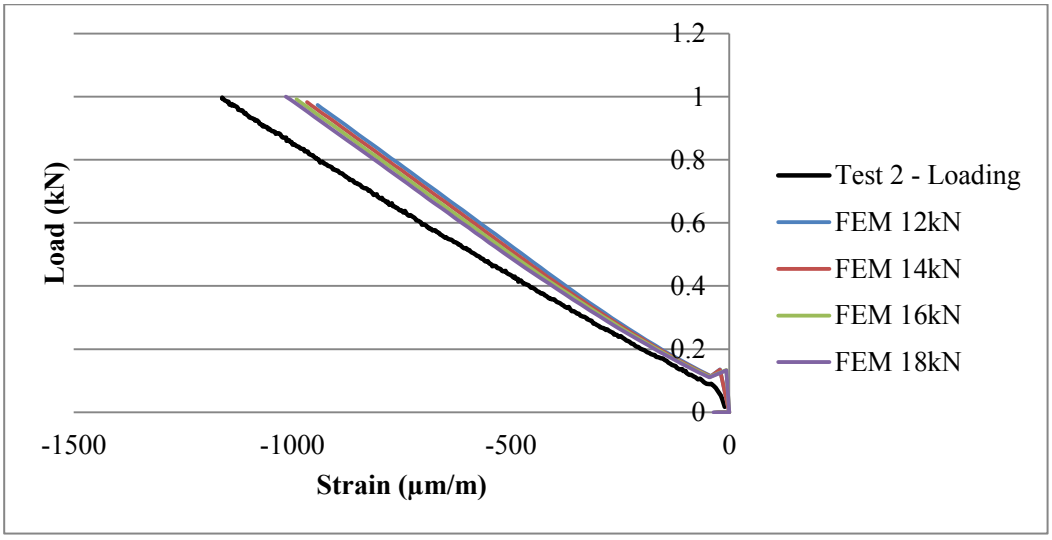

Figure D.6 - Load vs. strain comparison for test data and varying preload values (Contact stiffness factor (FKN)=2, Contact algorithm: Augmented Lagrange, Penetration tolerance (FTOLN)=0.1)

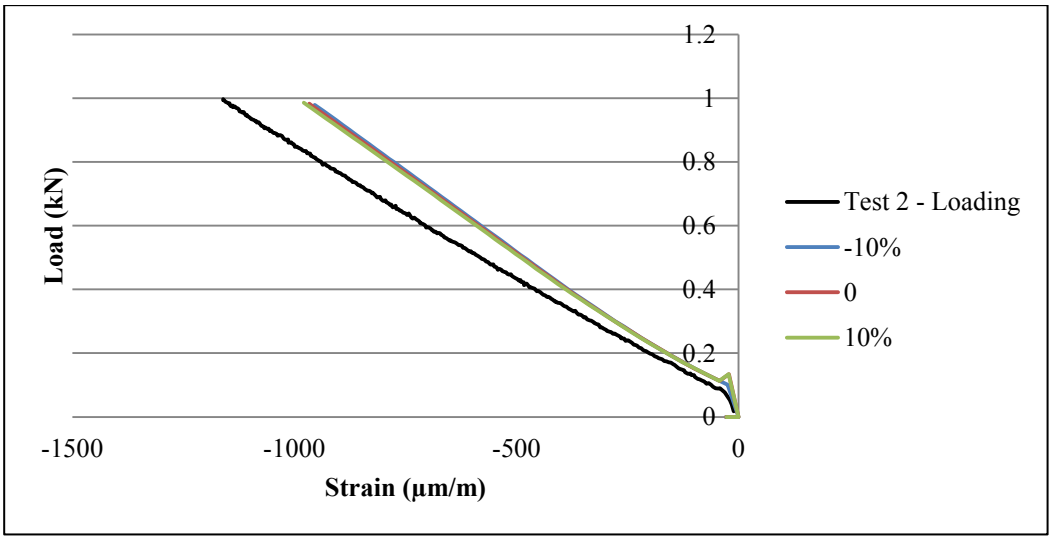

Figure D.7 - Load vs. strain comparison for test data and varying coefficient of friction values (Contact stiffness factor (FKN)=2, Contact algorithm: Augmented Lagrange, Penetration tolerance (FTOLN)=0.1)